Effectiveness of Organic Carbon Cover Systems on Sulfide-rich Tailings

by

Mason Kirk McAlary

A thesis
presented to the University of Waterloo
in the fulfillment of the
thesis requirement for the degree of
Master of Science
in
Earth Sciences (Water)

Waterloo, Ontario, Canada, 2021

Author's Declaration

This thesis consists of material all of which I authored or co-authored: see Statement of Contributions included in the thesis. This is a true copy of the thesis, including any required final revisions, as accepted by my examiners.

I understand that my thesis may be made electronically available to the public.

Statement of Contributions

Dr. Eva Pakostova was a postdoctoral fellow who assisted in the collection of samples and completion of microbiological analyses, such as most probable number (MPN) and next-generation (NGS) 16S rRNA sequencing. I have attached a manuscript of her paper in Appendix C and refer to the background and results of her research in Chapter 2 of this thesis.

Abstract

Acid mine drainage (AMD) occurs when sulfide minerals oxidize; generating low pH water and the release of dissolved metals. This phenomena is of primary concern in the mining industry, where the future loading of dissolved metals from inactive mine sites could continue for decades to centuries, with recent estimates of total liability related to AMD remediation exceeding $10 billion in Canada alone (Mining Watch Canada, 2017). Traditionally, remediation of AMD generally is focused on collection and treatment of water from surface-water bodies (i.e., ponds, ditches and streams) and treatment through pH neutralization using lime (CaO). While this approach improves water quality, it represents a recurring cost for the mining companies who need to continue operating these systems after mine closure. Due to this reality, numerous approaches have been developed over the past few decades to passively mitigate and remediate AMD by limiting the supply of O_2 and water to tailings rich in sulfide minerals. These passive approaches can be done through the use of: 1) cover systems by limiting $O_{2(g)}$ diffusion and/or $O_{2(g)}$ consumption; and 2) waters covers by limiting $O_{2(g)}$ diffusion. Examples of option 1) include biosolids, wood-waste, peat, compost, geosynthetic clay liners (GCL), covers with capillary barrier effects (CCBEs), and monolayer covers with an elevated water table; while an example of option 2) is subaqueous tailings disposal.

The performance of a cover system, consisting of a 0.5 m layer of biosolids fertilizer and municipal compost underlain by a ~ 2 m layer of thickened desulfurized tailings (DST), was studied. Six locations were investigated, including four locations with a 2-layer cover system, one location with a 1-layer cover of DST only, and one location without any cover system. The DST layer had been in place for up to 12 years and the organic cover components in place between 5 and 8 years. Results demonstrated that the cover system was able to consume all

atmospheric $O_{2(g)}$ prior to the base of the cover system, resulting in improved water quality when compared to the location without a cover system. Comparison between the locations with a 2-layer cover system and the location with a 1-layer cover revealed that the current geochemical conditions were similar, except that the organic layer consumes a portion of incoming $O_{2(g)}$ and leaches alkalinity to the shallow porewater; thus improving the acid-neutralizing capacity. This research shows that cover systems which use an organic layer over top of a low sulfur (S) thickened tailings layer with an elevated water table can limit oxidation of the tailings and neutralize acidity. However, in order for the organic carbon portion of this cover system to operate as an effective O_2 barrier in the long-term, occasional replenishment of organic material is required.

Acknowledgements

I would like to acknowledge my supervisor, Dr. Carol Ptacek, for her advice regarding both my thesis and future career prospects. To my committee members Dr. David Blowes for his guidance and critical commentary; Dr. Bruno Bussière for his help with O_2 flux determinations; and Dr. Walter Illman for his support and encouragement.

Funding for this project was provided by the Natural Sciences and Engineering Research Council of Canada Strategic Project Grant program (NETGP 479708-15).

I would like to thank the Glencore team of Stephanie Marshall, Samantha McGarry, Rob Mellow, and Joe Fyfe for their knowledge of the study site, patience in answering all of my questions, and willingness to supply data whenever I requested it. Thanks to Jeff Bain for assisting in project planning, field work, and for teaching me about mine waste; and to Dr. Eva Pakostova for sharing her insight into the microbiology of the cover system and for being so approachable. Thank you to former co-op students Morgan de Kroon, Graydon King, McKenna Jackson, Cindy Li, Sana Ahmad, Corey Zanatta, and Nikki Bell for their assistance with field work, laboratory activities and figure development. To former graduate students Brent Verbuyst and Joanne Angai, your friendship has been immensely appreciated. Thanks are also required to Joy Hu, Laura Groza and Sara Fellin for their hard work analyzing samples in the laboratory.

Lastly, I would like to acknowledge the importance of my family in the completion of this thesis. I am very grateful to my parents, Mike and Colomba, and my brother, Taylor, for teaching me how to work hard and be proud of your accomplishments and to my Uncle Todd for his guidance throughout this project. Finally, my sincerest thanks to my girlfriend, Kylie, and her parents, Brian and Colleen, who supported me at every step and love me unconditionally.

Dedication

For Mr. Brian. You always knew that I could do it.

Table of Contents

Table of Contents

List of Figures

List of Tables

List of Abbreviations

AMD	Acid Mine Drainage
aIOM	Acidophilic Fe Oxidizing Bacteria
Al	Aluminum
aSOB	Acidophilic S Oxidizing Bacteria
C	Carbon
Co	Cobalt
Cu	Copper
E/C	Electrical Conductivity
Fe	Iron
GCL	Geosynthetic Clay Liner
nHET	Neutrophilic Heterotrophs
Ni	Nickel
nIOM	Neutrophilic Fe-Oxidizing Microorganisms
nSOB	Neutrophilic S-Oxidizing Bacteria
Pb	Lead
S	Sulfur
SO_4	Sulfate
nIRB	Neutrophilic Fe Reducing Bacteria
nSRB	Neutrophilic SO_4 Reducing Bacteria
T	Temperature
VWC	Volumetric Water Content
XRF	X-ray Fluorescence
Zn	Zinc

Chapter 1

Introduction

The generation of acid mine drainage (AMD) and release of dissolved metals is a significant concern in the mining industry. According to Moncur (2005), sulfide oxidation and subsequent AMD can cause future loading of dissolved metals, SO_4 and acid from inactive mine sites for decades to centuries and recent estimates of total liability related to AMD remediation exceed $10 billion in Canada alone (Mining Watch Canada, 2017). The goal of the research presented herein is to assess the effectiveness of mine waste covers at reducing AMD from sulfide tailings and guide future improvements in cover designs.

Metal mining takes place predominantly in sulfide [S^{2-}] ore bodies, through the recovery of metals from sulfide minerals of interest, such as chalcopyrite [$CuFeS_2$] and pentlandite [$(Ni,Fe)_9S_8$]. The ore is extracted from the subsurface, pulverized and concentrated using chemical reactions. The processing of the ore produces a concentrated product and a large amount (sometimes greater than 90% of the ore) of fine-grained waste material called tailings or gangue, which contain the primary sulfide minerals of pyrite [FeS_2] and pyrrhotite [$Fe_{(1-x)}S$] (Blowes et al., 2014). This material is generally pumped from the mill as a slurry (containing greater than 50% water by volume [v/v]) to tailings storage facilities (such as in tailings ponds or impoundments) for long term storage and management. These tailings slurries are transported by way of a pipeline to the tailings impoundment and may be stored subaerially or subaqueously.

After tailings deposition ceases, tailings stored subaerially will, in time, desaturate. This decrease in the moisture content causes an increase in the rate of $O_{2(g)}$ diffusion from the atmosphere into the shallow tailings. When sulfide minerals are exposed to $O_{2(g)}$ in the presence

of moisture, they react to produce SO_4 and acidity (Blowes et al., 2014) through reactions similar to that shown in Equation 1.1. The Fe^{2+} released to infiltrating pore waters may then oxidize to ferric iron (Fe^{3+}) through Equation 1.2, if exposure to $O_{2(g)}$ continues. This ferric iron can then produce more SO_4 and acidity through Equation 1.3.

(1.1) $$FeS_{2(s)} + \frac{7}{2}O_{2(g)} + H_2O_{(l)} + \rightarrow Fe^{2+}_{(aq)} + 2SO^{2-}_{4(aq)} + 2H^{+}_{(aq)}$$

(1.2) $$Fe^{2+}_{(aq)} + \frac{1}{4}O_{2(g)} + H^{+}_{(aq)} + \rightarrow Fe^{3+}_{(aq)} + \frac{1}{2}H_2O_{(l)}$$

(1.3) $$FeS_{2(s)} + 14Fe^{3+}_{(aq)} + 8H_2O_{(l)} \rightarrow 15Fe^{2+}_{(aq)} + 2SO^{2-}_{4(aq)} + 16H^{+}_{(aq)}$$

It is known that the rate of iron-sulfide oxidation can be greatly accelerated in the presence of Fe and S-oxidizing microorganisms (Baker and Banfield, 2003; Johnson and Hallberg, 2003). Neutrophilic S-oxidizing microorganisms (nSOM) and Fe-oxidizing microorganisms (nIOM) are often detected in neutral-pH mine wastes (e.g. Blowes et al. 1998), while acidophilic species dominate in acidic mine wastes (Johnson and Hallberg, 2003; Johnson, 1998) of which *Acidithiobacillus ferrooxidans* is the most widely studied. Other sulfide minerals found in tailings storage facilities, such as sphalerite [(Zn,Fe)S], bornite [Cu_5FeS_4], arsenopyrite [FeAsS] and galena [PbS] have various resistances to oxidation, and the composition of the tailings porewater is profoundly affected by the redox conditions and mineralogy of the tailings (Jambor, 1994).

Acid generated during the oxidation of pyrite, pyrrhotite and other sulfide minerals is neutralized to varying degrees by the dissolution of (in the following order) carbonates, (oxy)hydroxides, and silicate minerals (Lindsay, 2015) which can lead to significant declines in

the concentrations of dissolved metals released from mine wastes and increases in porewater pH along the flow path (Blowes et al. 2014). An example of a neutralization reaction using calcium carbonate can be found in Equation 1.4.

(1.4) $$CaCO_{3(s)} + H^{+}_{(aq)} \leftrightarrow Ca^{2+}_{(aq)} + HCO^{-}_{3(aq)}$$

The primary minerals are those that are extracted from the orebody for mineral processing. During mineral processing and waste disposal, oxidation of the primary sulfide assemblage can occur and form secondary minerals (Blowes et al. 2014). Tertiary minerals are those that form when a sample of the tailings is extracted from its storage facility (Jambor and Blowes, 1998). These are important to note because the primary minerals evolve into secondary and tertiary minerals as the ore is extracted and processed.

Examples of secondary minerals include (oxy)hydroxides and sulfates (which vary in solubility). The most common secondary phases of (oxy)hydroxides in sulfide tailings disposal sites include goethite [α-FeOOH] (Equation 1.5) and ferrihydrite [Fe_2O_3•$0.5H_2O$]; which is metastable and transforms to goethite or hematite [α-Fe_2O3] over time (Jambor and Dutrizac, 1998; Waychunas et al., 2005). The most common secondary phases of SO_4 minerals include gypsum [$CaSO_4$•$2H_2O$] and jarosite [$KFe_3(SO_4)_2(OH)_6$] (Equation 1.6), of which gypsum is more soluble (Gunsinger, 2006). Typical geochemistry and hydrology of a decommissioned mine tailings impoundment can be found in Figure 1.1.

(1.5) $$Fe^{3+}_{(aq)} + 2H_2O_{(l)} \leftrightarrow \alpha - FeOOH_{(s)} + 3H^{+}_{(aq)}$$

(1.6) $$K^{+}_{(aq)} + 3Fe^{3+}_{(aq)} + 2SO^{2-}_{4(aq)}6H_2O_{(l)} \leftrightarrow KFe_3(SO_4)_2(OH)_{6(s)} + 6H^{+}_{(aq)}$$

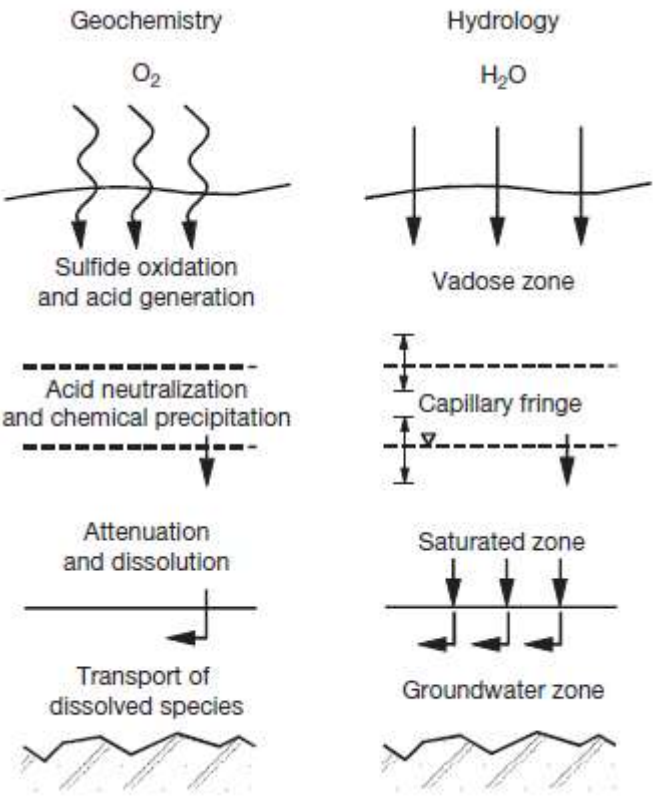

Figure 1.1: Schematic diagram of the hydrology and geochemistry of a decommissioned mine-tailings impoundment. Reproduced with permission from Blowes DW and Ptacek CJ (1994).

In the left column, $O_{2(g)}$ oxidizes sulfide minerals, generating acid. This acid is then neutralized by the dissolution of carbonate minerals and the precipitation of secondary minerals. Based on these reactions, select elements will be released, while others will be attenuated; affecting the transport of elements in the groundwater. In the right column, precipitation infiltrates into the subsurface, creating a partially-saturated vadose zone with a tension-saturated layer, as well as a saturated groundwater zone.

Reactions 1.5 and 1.6 result in low pH water, which enhances the solubility of many heavy metals, which can have adverse consequences for surrounding flora and fauna. Covers are a strategy to reduce AMD by either restricting $O_{2(g)}$ influx (through fine-grained material with a high moisture content) or consume $O_{2(g)}$ (through aerobic degradation of organic materials by microbes). This research includes monitoring of both types of covers to assess their performance

toward limiting sulfide oxidation. This chapter provides essential background information on the various types of remediation strategies that currently exist to mitigate AMD along with their benefits/drawbacks.

1.1 Background

1.1.1 Mitigation and Remediation Approaches

Numerous approaches have been developed over the past few decades to mitigate and remediate AMD. Mitigation approaches have generally focused on minimizing the production of AMD by limiting the supply of $O_{2(g)}$ and water to tailings rich in sulfide minerals. Examples of these approaches include various types of cover systems (which either consume $O_{2(g)}$ or limit its transport) or water covers. Remediation of AMD after it is produced generally focuses on collection and treatment of water from surface-water bodies (i.e., ponds, ditches and streams) and treatment through pH neutralization using lime, precipitation as a ferric hydroxide sludge, and then storage (Blowes et al. 2014).

A common example of a water cover that has been used with success is subaqueous disposal of tailings. This approach involves depositing the wastes in natural water bodies (such as lakes or oceans) or in constructed impoundments that maintain a water cover (Pederson et al. 1993) and has been found to be one of the most promising and cost-effective methods to reduce or prevent acid mine drainage from tailings (MEND, 2001; INAP 2017). The performance of water covers relies on lowering the $O_{2(g)}$ diffusion coefficient for free air (D_a; $\sim 1.8\times10^{-5}$ m^2/s), which is almost 10,000 times larger than that of water (D_w; $\sim 2.5\times10^{-9}$ m^2/s) (Scharer et al. 1993). This, combined with a relatively low (8-13 mg L^{-1}) solubility of $O_{2(g)}$ in water (Blowes et al. 2014), means that the exposure of sulfide minerals to $O_{2(g)}$ is limited in this setting. However, locating a suitable water body has been shown to be challenging, as there are federal regulations

regarding disposal, such as Canada's *Metal and Diamond Mining Effluent Regulations* (MDMER, 2002/2020), authorized under the *Fisheries Act*. On a global scale, submarine tailings disposal (STD) is outlawed in jurisdictions that follow the *London Protocol* (Dold, 2014). One option is to avoid using natural water bodies by constructing an engineered water cover using dykes, however their long-term stability is of significant concern (Aubertin et al., 1997). Another challenge is that the deposition of these tailings must take place before any significant oxidation can occur, as oxidized tailings have been shown to undergo reductive dissolution when placed subaqueously, releasing heavy metals into the porewater and requiring treatment of the seepage (MEND, 2000).

Covers composed of synthetic materials have been emplaced at various mine-waste sites to prevent ingress of both $O_{2(g)}$ and water. Traditional geosynthetic clay liners (GCLs) are composed of bentonite that is encased between two geotextiles or attached to a single geomembrane and held together by needle-punching, stitching, and/or gluing with an adhesive (Shackelford et al. 2010). A cover system that includes geosynthetic materials has been installed at the Kam Kotia mine; a closed Cu/Zn mine located in Timmins, Ontario. This cover system includes an uppermost, vegetated soil layer, underlain by a protective layer of sand, a clay moisture-retaining layer, a GCL, and a capillary-break layer of cushion sand and crushed waste-rock (Pakostova et al. 2020). While GCLs are known to have low hydraulic conductivities (10^{-11} m s^{-1}) the permeation of fluids with high ionic strength (such as mine process water and leachate) can be orders or magnitude higher (Shackelford et al. 2010). Also, installing GCLs can be expensive, costing upwards of $250,000 per hectare and only having a warranty of 20-30 years (Renken et al., 2005).

Another mitigation approach is to use single-or multi layer cover systems, composed partially or wholly of fine-grained material. The goal of these cover systems is to maintain conditions of near-saturation above the water table, thus limiting $O_{2(g)}$ diffusion. Covers with capillary barrier effects (CCBEs) are one such example, generally consisting of a saturated, fine-textured material placed between underlying and overlying coarse-textured materials and can maintain an average water saturation > 85% (MEND, 2004a; Hotton et al., 2020). Another example is a monolayer cover along with an elevated water table. Desulfurized tailings (DST) have been shown to be a suitable material for use in the construction of monolayer covers (Bussière et al. 2004, 2007; Demers et al. 2009; Dobchuk et al. 2013) and this method has been shown to have the potential to reduce acid generation and metal loading in the reactive tailings below the cover by limiting the oxygen flux at the base of the cover (Demers et al., 2008; Éthier et al., 2018; Rey et al., 2020). In addition, the small sulfide content in the DST can contribute to a further decrease in the oxygen flux to the reactive tailings, however, the use of DST can sometimes lead to concentrations of metals and sulfate in the pore water of this layer that exceed environmental criteria, particularly in regard to metals that are mobile at neutral pH conditions (Bussière et al. 2021). In terms of geotechnical considerations, the deposition of DST can be completed using a thickened tailings method; increasing the solids content of discharge tailings from 30% to 45% which has been shown to increase the geotechnical stability of the impoundment (since no retaining dykes have to be built) along with the improved in-situ density and homogeneity of these tailings. However, if these tailings become dry, these fine-grained materials are susceptible to wind-driven erosion, causing fugitive tailings and related human-health impacts.

1.1.2 Organic Carbon Covers

The use of organic material as a passive treatment for AMD has been studied since the 1990's and has been shown to have the potential to:

1) block $O_{2(g)}$ ingress by acting as a physical barrier;
2) consume $O_{2(g)}$ through decomposition of the organic matter;
3) leach compounds that may inhibit the activity of S-oxidizing bacteria;
4) reductively dissolve ferric oxides and prevent indirect sulfide oxidation;
5) reduce hydraulic conductivity and decrease seepage through compaction;
6) use as a substrate for vegetation; and
7) prevent erosion of tailings.

Organic carbon covers have also been found to be more economical than other remediation technologies and can be sourced in sufficient quantities for use in tailings storage facilities (MEND, 1994). In Ontario alone, it is estimated that 300,000 dry metric tonnes of municipal sewage biosolids are produced annually, of which 40% are landfilled and 20% are incinerated (CIELAP, 2009). Also, 3.7 million tonnes of food and yard waste were produced in 2015 alone, of which 60% was landfilled (Ontario MOECC, 2015). These values represent a large supply of potential cover material; however, cost depends on transportation from major urban centers where these materials are generated in larger quantities (MEND, 1994). The potential for using certain organic materials to treat AMD in the long-term, such as Municipal Solid Waste (MSW) compost or treated biosolids, requires further study.

Organic matter has been used in the past as a cover material on the surface of sulfide tailings, either as a standalone substrate or in combination with mineral material (Dudeney et al.,

2004; Hallberg et al., 2005; Hey & Simms, 2021). Though vegetation cannot remediate AMD on its own, it can be used to improve the aesthetics of tailings impoundments and reduce wind erosion by stabilizing the surface (Blowes et al., 1988; Pierce, 1995). Growth of vegetation on unremediated mine tailings is limited due to a lack of organic matter, which can be overcome by the addition of an organic substrate (Tisch, 2012) and can be used as part of a phytostabilization strategy by mine managers (Campbell et al., 2017). Thus, an organic cover has the potential to be vegetated, reduce erosion, and reduce metal mobility. For a summary of cover types used on tailings impoundments, see Table 1.1.

Table 1.1: Summary of select cover types. DST = desulfurized tailings, EWT = elevated water table, CCBE = covers with capillary barrier effects, GCL = geosynthetic clay liner.

Cover Class	Cover Type	Benefits	Drawbacks	References
O_2 Transport Barrier	Water	• Strongly limits O_2 diffusion • Minimal maintenance	• Most jurisdictions no longer allow for disposal in a natural water body • Engineered systems can be expensive and carry geotechnical risk	1) Blowes et al. (2014) 2) Dold, B (2014)
	Monolayer cover of DST with EWT	• Can be less expensive than other reclamation techniques • Potential for long-term efficiency	• Very sensitive to climatic condition • Specific design criteria required for pre-oxidized mining sites	1) Éthier et al. (2018) 2) Rey et al. (2020)
	CCBE	• Can maintain high water saturation (i.e. > 85%) • Material can be sourced onsite	• Long-term effects of freeze/thaw, desiccation, root penetration and erosion are unclear	1) Hotton et al. (2020) 2) Proteau et al. (2020)
	GCL	• Extremely low hydraulic conductivity (10^{-12} – 10^{-10} m s^{-1})	• Installation can be expensive for large tailings facilities	1) Makusa et al. (2014) 2) Shackelford et al. (2010)
O_2 Consuming Barrier	Wood-waste	• Inexpensive • Source material usually found close to the mine	• Reaction rate will decrease as the material matures	1) Germain et al. (2009) 2) Tassé, N. (2004)
	Peat	• Inexpensive • Source material can typically be found near mine	• Material may not sufficiently limit O_2 ingress in the long term	1) Rakotonimaro et al. (2021) 2) Smart et al. (2015)
	Biosolids	• High material availability • Avoids landfilling • Can be vegetated	• Reaction rate will decrease as the material matures	1) Jia et al. (2014) 2) Nason et al. (2016)
	Compost	• High material availability • Avoids landfilling • Can be vegetated	• Reaction rate will decrease as the cover matures	1) Arvizu-Valenzuela et al. (2020) 2) Asemaninejad et al. (2021)

1.1.2.1 *Microbial Communities*

Oxidative dissolution of sulfide minerals can be greatly enhanced by microbial processes. Therefore, the presence and abundance of certain bacteria can be used as a diagnostic tool to indicate cover performance. SO_4-reducing bacteria (SRB), for example, are strict anaerobes and therefore their presence indicates low $O_{2(g)}$ concentration (Beauchemin et al., 2018) and by implication, minimal AMD production. Conversely, Fe- and S-oxidizing microorganisms, such as *Acidithiobacillus ferrooxidans,* contribute to AMD formation through both the regeneration of aqueous Fe(III) and the oxidation of reduced inorganic S^0 compounds to sulfuric acid (Schippers et al., 2010). Microbial mitigation of AMD production can occur by SRB through bacterially-mediated SO_4 reduction (Lindsay et al., 2009; Benner et al., 2002; Shen and Buick, 2004) mediated by the heterotrophic microbial community which, in turn, is fueled by an organic-carbon substrate (Table 1.2). This phenomena reduces SO_4 concentrations and increases the pH, which could result in metal-sulfide precipitation and the immobilization of metals (Lewis, 2010).

Table 1.2: Microbially-induced reactions using organic carbon. Reactions will generally occur from the top down but will depend on the availability of the reactants (Morel & Herring, 1993). Note: Gibbs Free energy values are for standard temperature and pressure, pH = 7.

Reaction	**Balanced Equation**	**ΔG° (KJ mol^{-1})**
Respiration	$\frac{1}{4}CH_2O_{(s)} + \frac{1}{4}O_{2\,(g)} \rightarrow \frac{1}{4}CO_{2\,(g)} + \frac{1}{4}H_2O_{(l)}$	- 119
Denitrification	$\frac{1}{4}CH_2O_{(s)} + \frac{1}{5}NO_{3\,(aq)}^{-} + \frac{1}{5}H^{+}_{\,(aq)} \rightarrow \frac{1}{4}CO_{2\,(g)} + \frac{1}{10}N_{2\,(g)} + \frac{7}{20}H_2O_{(l)}$	- 113
MnO_2 Reduction	$\frac{1}{4}CH_2O_{(s)} + \frac{1}{2}MnO_{2\,(s)} + H^{+}_{(aq)} \rightarrow \frac{1}{4}CO_{2\,(g)} + \frac{1}{2}Mn^{2+}_{\,(aq)} + \frac{3}{4}H_2O_{(l)}$	- 96.9
Fe Oxide Reduction	$\frac{1}{4}CH_2O_{(s)} + Fe(OH)_{3\,(s)} + 2H^{+}_{(aq)} \rightarrow \frac{1}{4}CO_{2\,(g)} + Fe^{2+}_{(aq)} + \frac{11}{4}H_2O_{(l)}$	- 46.7
SO_4 Reduction	$\frac{1}{4}CH_2O_{(s)} + \frac{1}{8}SO_{4\,(aq)}^{2-} + \frac{1}{8}H^{+}_{\,(aq)} \rightarrow \frac{1}{4}CO_{2\,(g)} + \frac{1}{8}HS^{-}_{\,(aq)} + \frac{1}{4}H_2O_{(l)}$	- 20.5
Methanogenesis	$\frac{1}{4}CH_2O_{(s)} \rightarrow \frac{1}{8}CO_{2\,(g)} + \frac{1}{8}CH_{4\,(g)}$	- 17.7

1.1.2.2 *Leachable Products*

Organic materials, such as wood waste, have been noted to have the potential to leach organic acids, which subsequently move into the underlying tailings (Blowes et al., 2014). These natural organic compounds can subsequently influence the transport and infiltration of heavy metals beneath the cover (Bolan et al., 2014) and increase phosphorus availability through solubilization and decreased adsorption (Bolan et al., 1994). Extraction experiments completed by Ribet et al. (1995) on weathered tailings found that > 50% of total Fe, Ni, Co, Cr and K were within ferric bearing secondary minerals (i.e. the reducible fraction) and therefore susceptible to release via reductive dissolution by an $O_{2(g)}$ consuming organic layer. The redissolution of these secondary Fe (oxy)hydroxides, formed through reactions such as that described in Equation 1.5, could create further contamination by re-introducing metals into the pore water such as Fe^{3+}, which could further oxidize sulfide minerals, as was shown in Equation 1.3. Therefore, it is important to understand which products are being leached from the organic cover and the status of the tailings (i.e. weathered vs. unweathered). Nitrate leaching from the covers has been demonstrated to induce microbial oxidation of pyrite or pyrrhotite even under reducing conditions where nitrate serves as an electron acceptor for autotrophic Fe and S oxidizing bacteria (Cravotta III, 1998; Li et al., 2016), as shown in Equation 1.7. Despite these challenges, organic carbon covers have been installed at some Canadian mine sites because they are cost-effective and successful at controlling wind and water erosion, while also improving revegetation success. As indicated by Beauchemin et al. (2018), there is a need for more field investigations to study whether organic covers are a viable approach for the rehabilitation of acid-generating tailings in temperate climates.

(1.7) $$10FeS + 18NO_3^- + 16H_2O \rightarrow 9N_2 + 10Fe(OH)_3 + 10SO_4^{2-} + 2H^+$$

1.1.2.3 *Longevity*

To perform effectively, organic covers must maintain high moisture content and minimize hydraulic conductivity (Peppas et al. 2000). Saturated hydraulic conductivity (K_s) values and porosity can vary depending on the origin and maturity of the compost. In an experiment conducted by Pierce et al (1995), K_s values decreased from 10^{-4} cm s^{-1} in fresh compost to 10^{-6} cm s^{-1} in mature compost, while the volume shrunk by 10 to 20 %; indicating a decrease in porosity. As organic material matures, this decrease in porosity could lead to higher moisture content and a decrease in hydraulic conductivity within the organic cover, helping it to remain an effective $O_{2(g)}$ barrier over time.

The reactivity of organic material in the long term is a concern for its use as a long term $O_{2(g)}$-consuming layer. Tassé et al. (1994) studied a cover composed of wood waste and found that it would only be an effective $O_{2(g)}$ barrier for the short term, as the reactivity of this cover would decrease as it matured. According to Nason et al. (2016), total organic matter (TOM) decomposition rates are highest at the beginning of deposition. It has also been found that the integrity of the material will diminish over time as organic carbon is consumed, however the addition of decayed plants, grasses, and leaves from established vegetation present on the organic cover may add a fresh source of biodegradable material (Peppas et al., 2000).

Temperature is a major controlling parameter in the rate of biodegradation, and it will vary seasonally. Experiments conducted by Nason et al. (2016) found that the total organic matter (TOM) decreased by 14.8, 27.2, and 26.7 % at ambient, mesophilic, and thermophilic temperatures; illustrating that peak biodegradation occurred at mesophilic temperature ranges. Biodegradation was found to be much slower in the field, due to lower mean annual

temperatures. Thus, biodegradation rates will vary over time and be affected by varying climatic conditions.

A second controlling parameter in the rate of biodegradation is the amount of $O_{2(g)}$ available for the degradation of the organic matter. In a study by Forsberg and Ledin (2006), 50 % of the organic fraction of biosolids placed at the surface, under aerobic conditions, degraded after 5 years. In contrast, Ahlberg (2006) reported only a 5 to 10 % removal of the organic fraction of biosolids that were placed in a buried sub-surface layer after 16 years, with this loss being attributed specifically to anaerobic degradation processes. These findings show that the gradual loss of organic matter from the cover over time poses a challenge to their use as long-term solutions to AMD. For reference, Equation 1.8 and Equation 1.9 illustrate aerobic and anaerobic degradation, respectively (Tassé et al., 1994).

(1.8) $$(CH_2O)_{106}(NH_3)_{16}H_3PO_{4(s)} + 138O_{2(g)} \rightarrow 106CO_{2(g)} + 16HNO_{3(l)} + H_3PO_{4(l)} + 122H_2O_{(l)}$$

(1.9) $$(CH_2O)_{106}(NH_3)_{16}H_3PO_{4(s)} \rightarrow 53CO_{2(g)} + 53CH_{4(g)} + 16NH_{3(l)} + H_3PO_{4(l)}$$

1.2 Research Goal and Objectives

The primary goal of this research was to evaluate the performance of a cover system (composed of a 0.5 m thick organic layer underlain by a 2 m thick DST layer) as a remediation strategy for the treatment of acid mine drainage. The specific objectives were to:

- improve the understanding of the cover system operation;
- characterize the hydrology, aqueous geochemistry and solid-phase geochemistry of the cover system and the underlying tailings;
- aid in the assessment of the presence and structure of microbial communities;
- determine its effect on porewater quality and of $O_{2(g)}$ ingress into the subsurface;
- evaluate groundwater flow, pore-water geochemistry and pore-gas concentrations of oxygen and carbon dioxide; and
- determine the impact of the cover system on the water quality of the adjacent environment.

Following these objectives, the effectiveness of the cover system was determined based on two performance metrics: 1) the degree to which the cover system consumed/limited transport of $O_{2(g)}$; and 2) whether the cover system stabilized metals through metal-sulfide precipitation or through the formation of secondary-S phases. The goal of this research was to use these two metrics as criteria to evaluate the performance of this cover system at suppressing sulfide oxidation.

1.3 Thesis Organization

This thesis is presented as a research paper that is related to the objectives outlined in the previous section. The paper, presented as Chapter 2, describes the installation of monitoring equipment, along with sample collection, and laboratory analysis conducted to characterize the study site and evaluate the performance of the cover system over several seasons. Chapter 3 presents recommendations for future research and the overall contribution of this thesis research to the science of passive remediation systems in mine environments.

Chapter 2

Effectiveness of a Cover System with Organic Carbon Components over Tailings: A Field Study of a Long-Term Installation

2.1 Summary

The generation of acidic metal-laden water is a serious concern in the mining industry, with the effects occurring over decades to centuries and billions in associated remediation costs. The use of organic carbon components in cover systems has previously been implemented but the long-term effectiveness of these cover systems requires further investigation. The performance of a cover system consisting of a 0.5 m organic layer (composed of a biosolids fertilizer and municipal compost) underlain by a ~ 2 m layer of desulfurized tailings (DST) was studied. Five locations were instrumented; one location with a 1-layer cover of DST and four locations with a 2-layer cover system. The DST layer had been in place for up to 12 years and the organic cover components in place between 5 and 8 years. Volumetric water content (VWC) and subsequent saturation values were higher in the DST portion of the cover system. Total S contents of the tailings portion of the cover system were < 1.4 wt.% S with most samples showing > 30% of S as SO_4 and the most extensive oxidation observed in the upper portion of the DST. Pore-gas O_2 concentrations and $\delta^{13}C$-CO_2 results show that $O_{2(g)}$ is being consumed through aerobic degradation of organic carbon, however, $O_{2(g)}$ concentrations at the base of the organic cover remained > 10 v/v %. Pore gas O_2 was completely consumed in the DST layer and did not penetrate into the underlying higher S (> 10 wt.% S) tailings. Aqueous phase results showed that neutral pH (6.5 – 8.5) conditions dominated the locations with a 1-layer cover or 2-layer cover system at depths < 6 m, with large variations in alkalinity (from < 50 to > 1400 mg L^{-1} as $CaCO_3$), dissolved SO_4 concentrations < 5000 mg L^{-1} and maximum dissolved metal concentrations of 148.6 mg L^{-1} Ni, 18.9 mg L^{-1} Cu, 116.6 mg L^{-1} Fe, 12.6 mg L^{-1} Al, and 3.7 mg L^{-1} Zn. The chemical composition of pore water collected from these five locations was compared to pore water from a location without a cover, which showed low pH values (3.0 – 4.5)

and high concentrations of dissolved Ni (571.7 mg L^{-1}), Cu (288.8 mg L^{-1}), Fe (4705 mg L^{-1}) Al (1566.0 mg L^{-1}), and Zn (18.3 mg L^{-1}) were observed. Minimum concentrations of Ni, Cu, Fe, Al and Zn at or below detection limits (1 mg L^{-1}) were also noted at this location. Results from this study demonstrate that cover systems integrating organic layers with layers of DST can limit oxidation of underlying tailings and prevent the release of acidity. However, occasional replenishment of these organic carbon components will be required if the cover system is to maintain $O_{2(g)}$ consumption and/or limit $O_{2(g)}$ diffusion in the long-term.

2.2 Introduction

The generation of acid mine drainage (AMD) and release of dissolved metals is a significant concern in the mining industry. AMD is the result of bacterially mediated oxidation of sulfide minerals, such as pyrite (FeS_2) and pyrrhotite ($Fe_{(1-x)}S$), through exposure to $O_{2(g)}$ and water, as shown in Equation 2.1. This generation of ferrous iron (Fe^{2+}) can be further oxidized to ferric iron (Fe^{3+}) by Equation 2.2 to form ferrihydrite [$Fe(OH)_3$)] and other secondary minerals, such as goethite [αFeOOH] by Equation 2.3 or jarosite [$KFe_3(SO_4)_2(OH)_6$] by Equation 2.4.

(2.1) $$FeS_{2(s)} + \frac{7}{2}O_{2(g)} + H_2O_{(l)} + \rightarrow Fe^{2+}_{(aq)} + 2SO^{2-}_{4(aq)} + 2H^{+}_{(aq)}$$

(2.2) $$Fe^{3+} + 3H_2O \rightarrow Fe(OH)_3 + 3H^{+}$$

(2.3) $$Fe^{3+}_{(aq)} + 2H_2O_{(l)} \leftrightarrow \alpha FeOOH_{(s)} + 3H^{+}_{(aq)}$$

(2.4) $$K^{+}_{(aq)} + Fe^{3+}_{(aq)} + 2SO^{2-}_{4(aq)} + 6H_2O_{(l)} \leftrightarrow KFe_3(SO_4)_2(OH)_{6(s)} + 6H^{+}_{(aq)}$$

Pyrite, pyrrhotite and other sulfide minerals are the waste products after ore extraction, concentration and separation, when the economically valuable ore is separated from waste

material (i.e. tailings). Tailings are generally fine-grained, as the host rock is pulverized to extract the ore. Then, the tailings are transported with water, as a slurry, and retained within tailings impoundments or other storage facilities. After placement, the tailings either remain under water (subaqueous) or above water (subaerial). Oxidation of sulfide minerals typically results in the release of elevated concentrations of dissolved metals (Ni–Cu–Pb–Zn), SO_4, iron (Fe) and acidity within the shallow groundwater and surface water bodies that are adjacent to tailings storage facilities. This release of acidic, metal-laden water can continue for decades to centuries (Moncur et al., 2005), with the liability of acid mine drainage estimated to be between $2 and $5 billion in Canada alone (Mining Watch Canada, 2017).

In most tailings storage areas, the generation of acidic conditions and the release of metals into tailings pore water increases when active deposition ends, as the moisture content decreases in the shallow portion of the tailings, increasing the rate of $O_{2(g)}$ diffusion from the atmosphere into the impoundment (Woyshner & St. Arnaud, 1994). The diffusion of $O_{2(g)}$ decreases rapidly when saturation is over 70% and therefore the maintenance of water saturation can be important in tailings management (Collin, 1987).

Technologies to mitigate AMD formation in tailings storage areas have been extensively studied (Benner et al., 1999; Peppas, A., Komnitsas, K. & Halikia, I., 2000; Hulshof et al., 2003; Nason et al., 2013; Moncur et al., 2005) and have included the study of organic material. The use of organic material is based on microbial oxidation of organic matter, which reduces the amount of $O_{2(g)}$ available for AMD generation and is generally understood to be a first-order process (Qdais & Al-Widyan, 2016), occurring rapidly at the beginning but lessening as the readily degradable fraction is consumed and the more recalcitrant fraction remains. The addition of organic material has been documented to shift the bacterial and archaeal community (BAC)

structure in metal-rich tailings amended with organic materials up to 10 years after placement (Touceda-Gonzales et al., 2017; Pepper et al., 2012). The increase in relative $\delta^{34}S$ in mine water can be used as a tool to observe the activity of SO_4-reducing bacteria (SRB) in these environments (Seal, 2006). While several different types of organic covers have been studied in the field (Elliot et al., 1996; Tisch et al., 2012; Beauchemin et al, 2018), the availability of field plots several years after placement is rare and provides an opportunity to evaluate the impacts of the cover system on the hydrology and water quality within shallow tailings. It is critical that organic covers be effective for decades to centuries if they are to be used as long-term solutions to AMD.

Sudbury Integrated Nickel Operations is a Cu-Ni mining complex located in the Sudbury Region, ON, Canada, consisting of two mines (Fraser and Nickel Rim South), the Strathcona Mill and the Sudbury Smelter, owned by Glencore Inc. (Glencore, 2018). The Strathcona Mill is currently operational and is located adjacent to the community of Onaping (part of the City of Greater Sudbury). The primary focus of the Strathcona Mill is the production of Cu and Ni concentrates. One of the tailings containment areas located on this property is the Strathcona Waste Water Treatment System, (SWWTS; Figure 2.1) which received tailings from ore processing at the Strathcona Mill from 1970 to 2012 (Glencore, 2018). Deposition of the original tailings occurred for 25 years (1970 to 1995) and began with subaqueous disposal by infilling a portion of Moose Lake. After some time, however, the tailings were deposited above the water level of the lake and subsequent tailings storage became subaerial. To increase moisture content, limit $O_{2(g)}$ diffusion and increase neutralizing capacity, a desulfurized tailings (DST) cover of < 1.4 wt. % S was placed over the original tailings from 1996 until closure in 2012. This low-S tailings cover was produced as the cyclone overflow from the scavenger flotation units of the

Strathcona Mill and contained lime kiln dust or reject material from lime production. These tailings have the potential to be acid generating if the neutralization potential is consumed, though the mass of metals that can be leached from these tailings is generally low (EcoMetrix, 2014). Beginning in 2008 and continuing until recently, an organic carbon cover was placed on a portion of the site, as part of the Green Mines Green Energy (GMGE) initiative, a program focused on establishing biofuel crop growth and stabilizing the cover from erosion by wind and water (Lock et al. 2010).

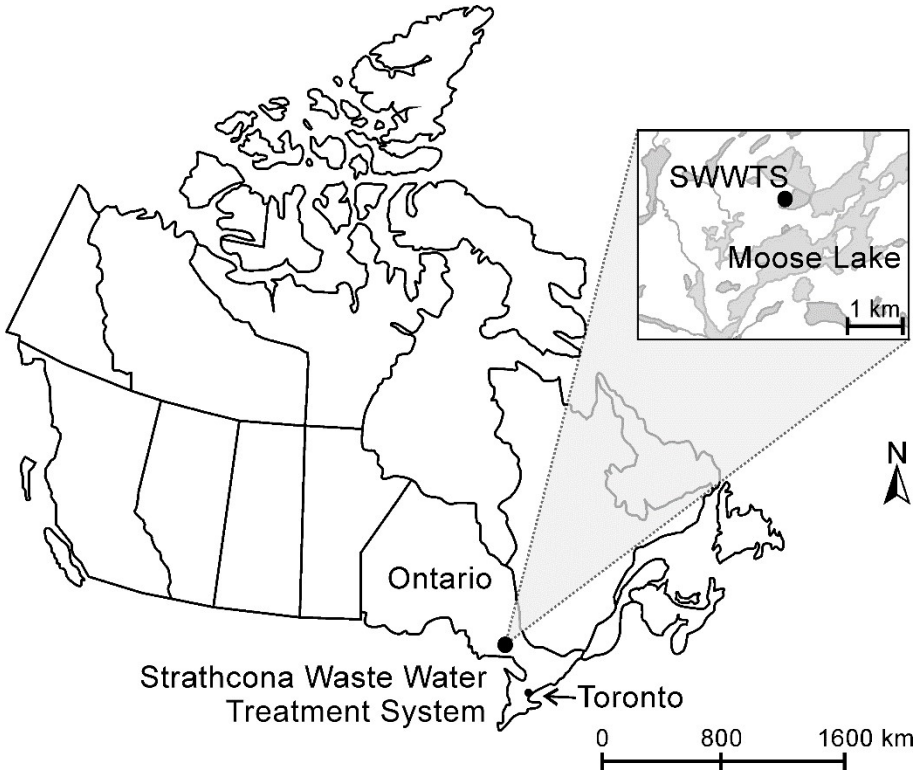

Figure 2.1: Location of the Strathcona Waste Water Treatment System.

Currently, the SWWTS is 60 ha in size and multi-layer cover systems have been installed over portions of the site (see Figure 2.2). The organic carbon covers are 0.50 m thick and predominantly vegetated with grasses and shrubs. This layer is composed of two materials: 1) a biosolids fertilizer (characterized by a pH of ≥ 12, organic carbon content of ≥ 12%, free CaO of

≥ 45% and a total neutralizing value of > 40% $CaCO_3$ equivalency); and 2) a mixed municipal compost (characterized by a pH around 6, organic carbon content of ≥ 30% and minimal neutralization capacity. The organic carbon cover overlies the ~ 2m thick layer of desulfurized mill tailings, which overlies the tailings deposited on or before 1995.

Six locations were studied; four locations (ML32, ML33, ML34 and ML35) with a 2-layer cover system of both the organic cover and the DST layer; and one location with a 1-layer cover of DST (ML5); the initial reactive tailings at the final location were not covered (ML25) (Figure 2.2). Deposition of the DST occurred from 1996 until 2006 and the organic layer was installed between 2011 and 2014 (Glencore, personal communication). Expansion of the organic cover over the remainder of the site was ongoing and biosolids fertilizer was stockpiled adjacent to ML5 beginning in the Fall of 2018, lasting for the duration of the study. Comparisons between locations were used to assess the impact of the organic cover on the consumption of $O_{2(g)}$, oxidation of sulfide minerals and water quality.

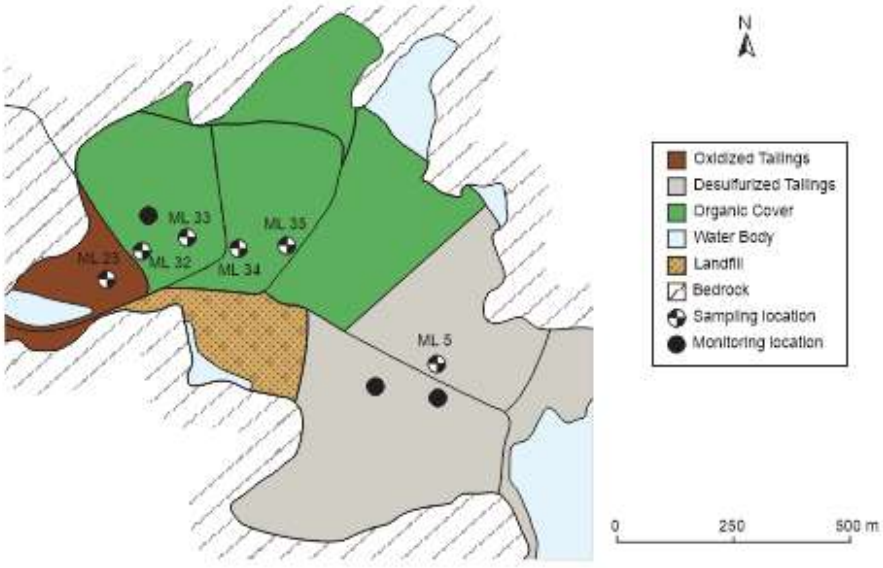

Figure 2.2: Plan view map of the sampled wells located at the SWWTS.

2.3 Methodology

2.3.1 Instrumentation Installation and Monitoring

A network of piezometer nests was installed in December 2016. Two types of piezometers were installed to depths of up to 6 m using a Pionjar 120 jackhammer; 0.32 cm (0.125 inch) steel drive point or 3.8 cm (1.5 inch) PVC pipe fitted with a screened drive-point. The steel drive point piezometers were installed by driving the steel rods directly into the ground while the wells constructed with PVC pipe were installed after core samples were taken following the continuous coring technique described by Starr and Ingleton (1992). Wells were surveyed and monitored using water level meters to calculate total head values, vadose zone thickness, and groundwater flow directions. Well nests were monitored to determine vertical hydraulic gradients, where possible. Single well response tests (SWRTs) were conducted at select locations within the SWWTS for the determination of hydraulic conductivity (K) and included both:

1) constant head tests for wells with a well volume > 2.5 L, which were performed by pumping water out of the well at a rate that maintained a constant water level in the well. The data were analyzed following Hvorslev (1951) with a well shape factor of uniform soil, and
2) rising head tests for wells with well volumes < 2.5 L, which were performed by pumping out a known volume of water and monitoring the rate of water level rise over time toward the static level. The data were analyzed using AquiferTest® and the Bouwer and Rice (1976) model.

At each of the four locations with a 2-layer cover system, soil moisture sensors (ECH_2O 5TE probes by the METER group of Pullman, WA) and standard tensiometers (Model 2710ARL connected to a Model 5301 Current Transducer by Soil Moisture of Santa Barbara, CA) were installed at four depths, including 0.20, 0.45, 0.75, and 1.05 meters below ground surface (mbgs)

(Figure 2.3). The first two depths were within the organic layer, and the remaining two were in the underlying DST. The soil moisture sensors were connected to EM50 dataloggers (METER group of Pullman, WA) and the tensiometers were connected to Data Dolphin Model 400 dataloggers (Optimum Instruments of Edmonton, AB) to study the changes in volumetric water content (VWC), electrical conductivity (E/C), temperature (T) and matric potential (Ψ_m) versus depth and over time. Medium-specific calibrations for VWC were completed using the organic cover materials and the DST following the methods described by Cobos and Chambers (2010). These calibrations have been noted to improve the accuracy to ± 0.02 m^3 m^{-3} (METER group, 2018). These soil moisture sensors logged data throughout the winter season, however, the tensiometers were not in operation through the winter season, due to freezing conditions. Matric potential was converted to total head to determine direction of pore water flow. Infiltration tests within the organic cover were performed with the single head method using a Guelph Permeameter (Model 2800, Soil Moisture, Santa Barbara, CA) and the results were used to determine K values with the *K calculator* (Soil Moisture, 2012).

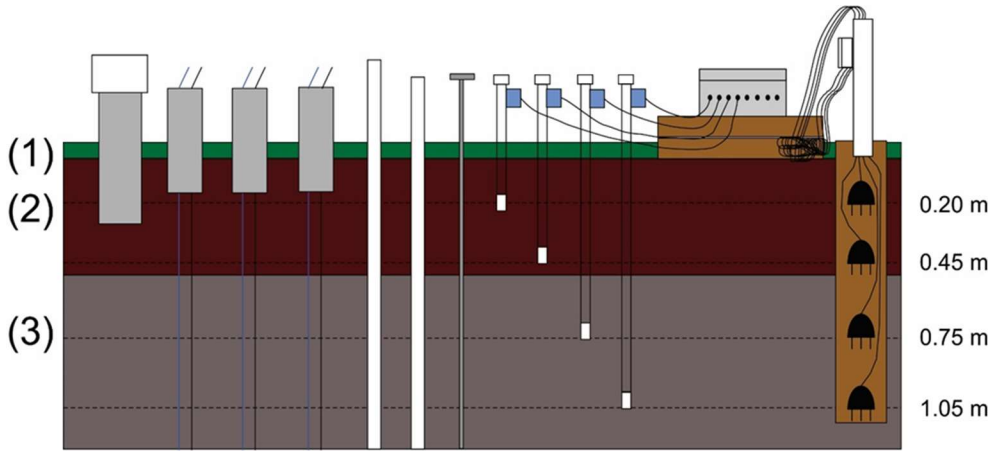

Figure 2.3: Schematic diagram of installations at the locations with a 2-layer cover system (ML32, ML33, ML34 and ML35). From left to right, there is one O_2 consumption chamber, three lysimeters, two piezometers, one steel gas rod, four tensiometers, and four ECH_2O sensors. Note: Numbers (1), (2) and (3) represent the vegetation, organic cover and desulfurized tailings layer, respectively.

2.3.2 Sample Collection and Analysis

Core samples of the underlying tailings at the location with a 1-layer cover and the locations with a 2-layer cover system were collected during two episodes, following the method described by Starr and Ingleton (1992). Core samples were taken in approximately 1.5 m (5 foot) sections up to ~ 4.5 m (15 ft) and using 5.08 or 7.12 cm (2 or 3 inch) diameter aluminum tubes. The core samples for physical and geochemical analyses were frozen on site and sent to the University of Waterloo for subsequent analysis.

2.3.2.1 *Pore water*

Piezometers and lysimeters were used to sample groundwater and porewater for the determination of water quality. Piezometers were purged until dry prior to sampling, as the yield was too low to purge a normal 3 to 5 well volumes. pH and E_H measurements were conducted in the field using Orion pH and E_H probes (Thermo Scientific, USA) coupled to Orion Star A321 pH Portable Meters (Thermo Scientific, USA). Alkalinity values were also determined in the field by titration with either 0.16N or 1.6N H_2SO_4 using a HACH digital titrator and colour indicator (HACH method 8203). Cation samples were filtered in the field using 0.45 µm syringe filters and preserved using HNO_3 to pH < 2. Concentrations were determined through inductively coupled plasma-optical emission spectrometry (ICP-OES, Thermo Scientific ICAP 6500) and inductively coupled plasma-mass spectrometry (ICP-MS, Thermo Scientific X Series II). Anion samples were also filtered in the field and were analyzed by ion chromatography (IC, Dionex DX 600). Detailed descriptions of water analysis methods can be found in Bao et al. (2020) or in Appendix A.

Porewater samples were analysed for dissolved organic carbon (DOC) following a wet oxidation method with heated sodium persulfate (Aurora 1030W TOC Analyser, O.I Analytical, College Station, TX) after inorganic carbon was removed from the sample with the addition of 5% phosphoric acid.

Analyses of $\delta^{18}O$ and $\delta^{2}H$ were performed using a Picarro cavity ringdown spectrometer (model L2130-i, Picarro Inc., Santa Clara, CA).

Isotope analysis of S in aqueous samples were first acidified with 10% HCl to precipitate S as barium sulphate ($BaSO_4$), then the pH was neutralized with deionized water rinses and dried in an oven before analysis through combustion conversion of sample material to gas through an 4010 Elemental Analyzer (Costech Instruments, IT) coupled to a Isochrom (Micromass UK) continuous flow isotope ratio mass spectrometer (CFIRMS).

Eleven samples were collected from within the four locations with the 2-layer cover system at depths ranging from 1.78 mbgs to 5.89 mbgs. These samples were diluted 10× and analyzed for artificial sweetener compounds Acesulfame-K, Cyclamate, Saccharin and Sucralose through ion chromatography (IC) coupled to tandem mass spectrometry. Four additional samples were collected from two of these locations between 4.81 mbgs and 5.89 mbgs. These samples were prepared by diluting 5× and then concentrating 500× through solid-phase extraction (i.e. final concentration factor of 100×). Samples were then analyzed by high-performance liquid chromatography (HPLC) followed by tandem mass spectrometry to determine concentrations of the pharmaceutical compounds carbamazepine, caffeine, ibuprofen, gemfibrozil, sulfamethoxazole, and naproxen. Additional details on these analyses can be found in Liu et al. (2014).

Samples for NH_3-N, S^{2-} and PO_4-P were analyzed using a Hach DR/2400 portable spectrophotometer (Hach Company, Loveland, CO) following U.S. EPA methods 10023 and 10031 for NH_3-N and U.S. EPA methods 8131 and 8048 for S^{2-} and PO_4-P, respectively. Samples for NH_3-N and S^{2-} were completed in the field, while samples for PO_4-P were completed in the laboratory.

Depth-discrete porewater samples were collected from the vadose zone following the porewater extraction method of Moncur et al. (2013). Eh, pH and alkalinity measurements were taken within minutes after porewater extraction, following the same methods described previously. Where there was sufficient volume, additional samples were collected for analysis of cations, anions, and DOC.

2.3.2.2 *Pore Gas*

A modified technique of Reardon and Poscente (1984) was used to sample the pore gas in the unsaturated zone, using 10 cm sampling intervals. The pore gas was extracted using a 60 mL polypropylene syringe and the O_2 and CO_2 concentrations were measured in the field using a Quantek 902P O_2/CO_2 Analyzer (Quantek Instruments, Grafton, MA). Measurements continued to the depth where $O_{2(g)}$ concentrations reached < 0.1% v/v or where saturated conditions prevented further sampling. Samples were also collected in glass vials (12 mL Exetainers®, Labco, High Wycombe, UK) and analyzed for both δ^{13}C-CO_2 and δ^{18}O-CO_2 at the University of Waterloo Environmental Isotope Laboratory using dual inlet isotope ratio mass spectrometry (DI-IRMS).

Tests were completed to determine the flux of $O_{2(g)}$ into the subsurface, following methods similar to those described in Elberling and Nicholson (1996). A steel cylinder (14.5 cm in diameter) was driven into the organic cover and then isolated from the atmosphere using a

PVC cap so that there was ~ 20 cm of headspace. An air pump, pumping at 2.6 L min^{-1}, was connected to one of the air intake ports of an AMI Model 65 O_2 analyzer (AMI Instruments, Huntington Beach, CA) to stimulate air flow through the $O_{2(g)}$ analyzer. Then, the electrical wiring was connected to a Data Dolphin Model 400 datalogger (Optimum Instruments, Edmonton, AB). The $O_{2(g)}$ analyzer was fitted to the PVC cap and the air pump was placed inside the chamber. A reading was taken at short time intervals (2 or 5 minutes) for a maximum of three hours and any datapoints deemed to be outliers (based on their proximity to the line of best fit) were removed to achieve an R^2 value of ≥ 0.90. Tests were completed in May, July, August, and October to test over a range of VWC and temperature conditions.

2.3.2.3 *Cover System Solids*

Core samples collected in the field were cut longitudinally, visually classified, and sub-sampled at various depths to include both the DST and the historical tailings. A total of 44 core samples were taken (at least seven per location) at depths beneath the organic cover to appropriately capture the oxidation zones and delineate the stratigraphy at each location. For reference, the methodology described below is outlined in greater detail in Appendix B.

Particle size analysis (PSA) was performed by placing a 1 g sample into a laser particle size analyzer (Fritsch Analysette 22, Idar-Oberstein, DE) and running it in duplicate. Dry bulk densities were calculated by measuring the volume of the material in the aluminum collection tubes and the weight after drying for 24 hours at 100^0C. Particle density was determined by placing a known mass of sample (± 0.001 g) into a Beckman air-comparison pycnometer (model 930, Beckman Coulter Inc, Porterville, CA) and determining its volume (± 0.01 cm^3) by running each sample in quadruplicate. Average porosity for each material was determined using Equation 2.5.

$$n = \left(1 - \frac{\rho_b}{\rho_s}\right) \quad (2.5)$$

where n is the porosity (unitless), ρ_b is the dry bulk density ($g \times cm^{-3}$), and ρ_s is the particle density ($g \times cm^{-3}$).

Chemical characterization of the cover system included total % C and total % S determination for each tailings sample using a CS 2000 Carbon Sulfur Analyzer (Eltra Elemental Analyzers of Newtown, PA) with an accuracy of ± 0.5% of the measured C and S content, respectively. A two-part extraction procedure, described in Dold (2003), for the determination of the relative proportions of solid-phase S including sulfide, soluble SO_4 and insoluble SO_4 was applied to each tailings sample. Bulk solid-phase chemistry to determine the abundance of the major elements (Si, Al, Fe, Ca, Mg, etc.) were completed on tailings samples with an accuracy of ± 10% using a PANalytical MiniPal4 X-ray fluorescence (XRF) spectrometer (Malvern Panalytical, Malvern, UK).

Bulk $\delta^{13}C$ of the organic cover and tailings were analysed for bulk $\delta^{13}C$ [with an accuracy of ± 0.2 ‰ Vienna Pee Dee Belemnite (VPDB)] by combustion conversion of sample material to gas through a 4010 Elemental Analyzer (Costech Instruments, IT) coupled to a Delta Plus XL (Thermo-Finnigan, DE) CFIRMS at the University of Waterloo Environmental Isotope Laboratory.

A total of four core profiles were taken for microbiological analyses which focused on microbial communities typical of mine environments as well as organic-rich environments. Three core profiles were taken from two of the locations with a 2-layer cover system (ML33, ML33 duplicate, and M34) and one was taken at the site with the 1-layer cover of DST (ML5).

These core samples were analyzed for culturable microorganisms using the Most Probable Number (MPN) technique (Cochran, 1950).

Six microbial groups studied were quantified to determine specific genera of microorganisms that metabolize S and/or Fe: 1) neutrophilic S oxidizing bacteria (nSOB); 2) acidophilic S oxidizing bacteria (aSOB); 3) neutrophilic SO_4 reducing bacteria (nSRB); 4) acidophilic Fe oxidizing bacteria (aIOB); 5) neutrophilic Fe reducing bacteria (nIRB); and 6) neutrophilic heterotrophs (nHET). Total 16S rRNA sequences were completed using the Next-Generation Sequencing (NGS) technique (Thomas et al, 2012) to determine specific genera of microorganisms that metabolize S and/or Fe. For further information about the analytical methods, see Appendix C.

2.3.3 Data Management and Modelling Methods

Based on the grain size distribution (GSD) from the PSA, K was calculated using two methods: 1) the Hazen equation (Hazen, 1892); and 2) a modified version of the Kozeny-Carmen equation (Aubertin et al., 1996). AquiferTest® was used to determine K from the rising head tests, based on Bouwer & Rice analysis (Bouwer and Rice, 1976). Head measurements for each of the monitoring episodes was used to determine hydraulic gradient. Groundwater velocity and flow direction were calculated using the hydraulic gradient and K values using the Excel-based program HydroGeoEstimatorXL (Devlin, 2017). K values from slug tests analyses were compared to K values from PSA and infiltration tests to help understand the uncertainty in hydraulic conductivity between the cover system components.

Data was collected from an onsite weather station, which recorded parameters such as temperature, relative humidity, wind speed, and solar radiation using a CR1000X datalogger

(Campbell Scientific Inc., Logan, UT). The readings were used to calculate reference crop evapotranspiration (ET_0) hourly using the Standardized Reference Evapotranspiration Equation (ASCE, 2005).

Results of groundwater chemistry analyses were input into the geochemical model PHREEQCi (Parkhurst and Appelo, 1999) for the determination of the saturation index (SI) of select minerals. The Wateq4f database (Ball and Nordstrom, 1991) was used, updated with thermodynamic data for cobalt, taken from the MINTEQA2 database (Allison et al., 1990). SI values were calculated using Equation 2.6, where IAP is the Ion Activity Product and Ksp is the solubility product. Three samples contained a charge balance error (CBE) of > 15% and were not included in further analysis and subsequent discussion.

$$SI = log\left(\frac{IAP}{Ksp}\right) \tag{2.6}$$

A modified version of the 1-D sulfide oxidation model *Pyrox* (Wunderley, 1996), was used to model the extent of sulfide oxidation in the DST. These models were compared to the vertical profiles of $O_{2(g)}$ sampled in August 2019 and October 2019.

Further details of the data management and modelling methods can be found in Appendix A.

2.4 Results

2.4.1 Cover System Hydrology

The thickness of the vadose zone was found to vary by several meters across the site and was generally the most extensive in the summer. At the location without a cover (ML25), the vadose zone was 1.5 to 2 mbgs, while the vadose zone at the location with a 1-layer cover (ML5) varied

from 2.58 mbgs in July 2018 to 0.45 mbgs in May 2019. At the locations with a 2-layer cover system, the thickness of the vadose zone varied between 0.8 and 4.4 mbgs. The vadose zone was generally thinner in locations that were closer to Moose Lake, in the southeast corner of the SWWTS (Figure 2.2). Groundwater flow direction was generally southeast.

Particle size analysis was performed using static laser light scattering (i.e. laser diffraction) and the calculated geometric mean K and standard deviation of the DST and the historical tailings were 3×10^{-8} m s^{-1} ± 9×10^{-7} m s^{-1} using the Hazen equation and 4×10^{-8} m s^{-1} ± 1×10^{-6} m s^{-1} using the modified Kozeny-Carmen equation. Previous studies have noted that K values of tailings materials are typically underestimated when calculated using grain-size analysis (Robertson, 1994) however, it has been industry practice to calculate K using the Hazen formula (Adajar et. al., 2014) and the modified Kozeny-Carmen equation has been validated to be accurate for estimating K of sandy silts with low plasticity (ML) according to the Unified Soil Classification System (USCS) (Aubertin et al., 1996). Results from infiltration tests show that field-saturation hydraulic conductivity (Kfs) of the organic cover had a geometric mean of 5×10^{-6} m s^{-1} with a standard deviation of 2×10^{-5} m s^{-1}. Results from SWRTs conducted at these locations determined horizontal K to be between 1×10^{-7} m s^{-1} and 8×10^{-7} m s^{-1}, with a geometric mean of 4×10^{-7} m s^{-1}. Vertical hydraulic gradients were generally found to be downward. Horizontal groundwater velocities were calculated using the geometric mean K value from the SWRTs and varied between 4 and 7 m yr^{-1} over the monitoring episodes.

Calculated total head values from the logged tensiometer data showed that the total head varied by up to 10 m at each location during the monitoring period, particularly in the organic cover. At ML32 and ML33, the total head in the organic layer showed high variability and was disconnected from the total head values in the DST layer. Total head values of the wells at ML33

were similar to those in the DST layer, whereas at the other three locations (ML32, ML34 and ML35) the total head values of the wells were generally higher, showing potential for an upward gradient at the water table. Based on the total head values at each depth, pore water flow was generally downward at ML32, ML34 and ML35 but upward fluxes were noted from July to August at ML32 and from July to October at ML33. Total head values generally decreased in the summer months, when evapotranspiration was greatest (Figure 2.4). At the deeper locations, the temperature was warmer in the spring and cooler in the summer and winter, due to the delay of cold infiltrating rainwater and snowmelt into the DST layer (Figure 2.4). None of the locations recorded freezing ($< 0^0$C) temperatures during the December 2018 – October 2019 monitoring period. VWC and water saturation were highest in the spring and decreased in the summer and correlated well with the increase in temperature and decrease in total head during the summer months. The E/C values were generally higher in the DST portion of the cover system and were higher at the older locations. E/C values varied little over the winter until the spring melt in April (Figure 2.4).

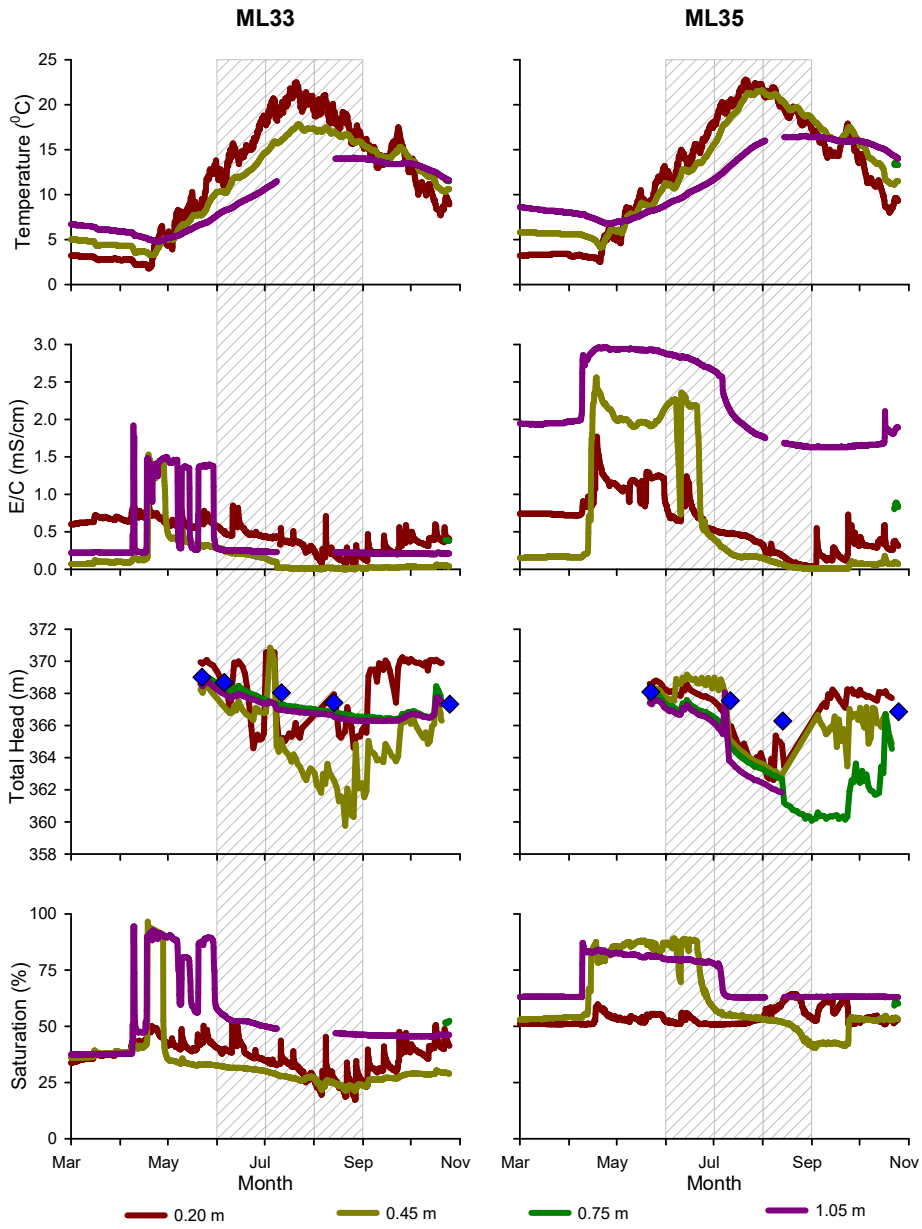

Figure 2.4: Total head, saturation, and temperature within and beneath the organic cover at ML33 and ML35 between March and October, 2019. Note: blue diamonds represent the manual water level monitoring episodes between May and October 2019, the water table levels ranged from 367.38 to 369.01 masl at ML33 and 366.29 to 368.09 masl at ML35. The grey hatched boxes represent months where the total evaporation (mm) was higher than the total precipitation (mm). Saturation was derived by dividing VWC by porosity.

2.4.2 Solid Phase Analysis

Based on the grain size distribution of all tailings samples, most of the samples were dominated by silt-sized particles which averaged 79.59 % ± 14.07 % of the sample and were predominantly

classified as non plastic silts (ML) using the USCS. For the DST, values of 60% passing (d_{60}), 10% passing (d_{10}) and the coefficient of uniformity (C_U) were 0.029 ± 0.026, 0.002 ± 0.001, and 14.785 ± 12.007 (mean ± S.D., n = 44) respectively. These results indicate that fine-grained material are the most prevalent within the tailings at the SWWTS.

Total solid-phase S content of the DST samples ranged from 0.42 % to 1.58 wt.% (0.81 wt.% ± 0.38 wt.%, mean ± s.d., n=23) while samples of the historical tailings ranged from 0.32 wt.% to 28.1 wt.% (5.83 wt.% ± 8.43 wt.%, mean ± s.d., n=21). The highest S values (between 5 and 28%) were found below the DST layer at ML5, where high S-content pyrrhotite tailings were present. The DST was generally found to contain < 1.4 wt.% S.

Total solid-phase C content of the DST samples ranged from 0.032 wt.% to 0.57 wt.% (0.21 wt.% ± 0.15 wt.%, mean ± s.d., n=23) while samples of the historical tailings ranged from 0.027 to 0.31 wt.% (0.10 wt.% ± 0.078 wt.%, mean ± s.d., n=21). Based on analyses conducted by third party laboratories, the composted municipal food and yard waste had average S and organic C contents of < 0.1% and 40%, respectively. The biosolids fertilizer had average S and organic C contents of 2.5% and 13%, respectively.

The proportion of unoxidized S in the tailings at each location had no discernable trend with depth but was the highest at ML35 (see Figure 2.5). In samples within the DST layer, most locations showed that > 30% of the total solid-phase S content was in the form of SO_4 (Figure 2.5). Soluble SO_4 and insoluble SO_4 were detected in every location at depths both within and below the DST layer but were lowest with depth at ML5.

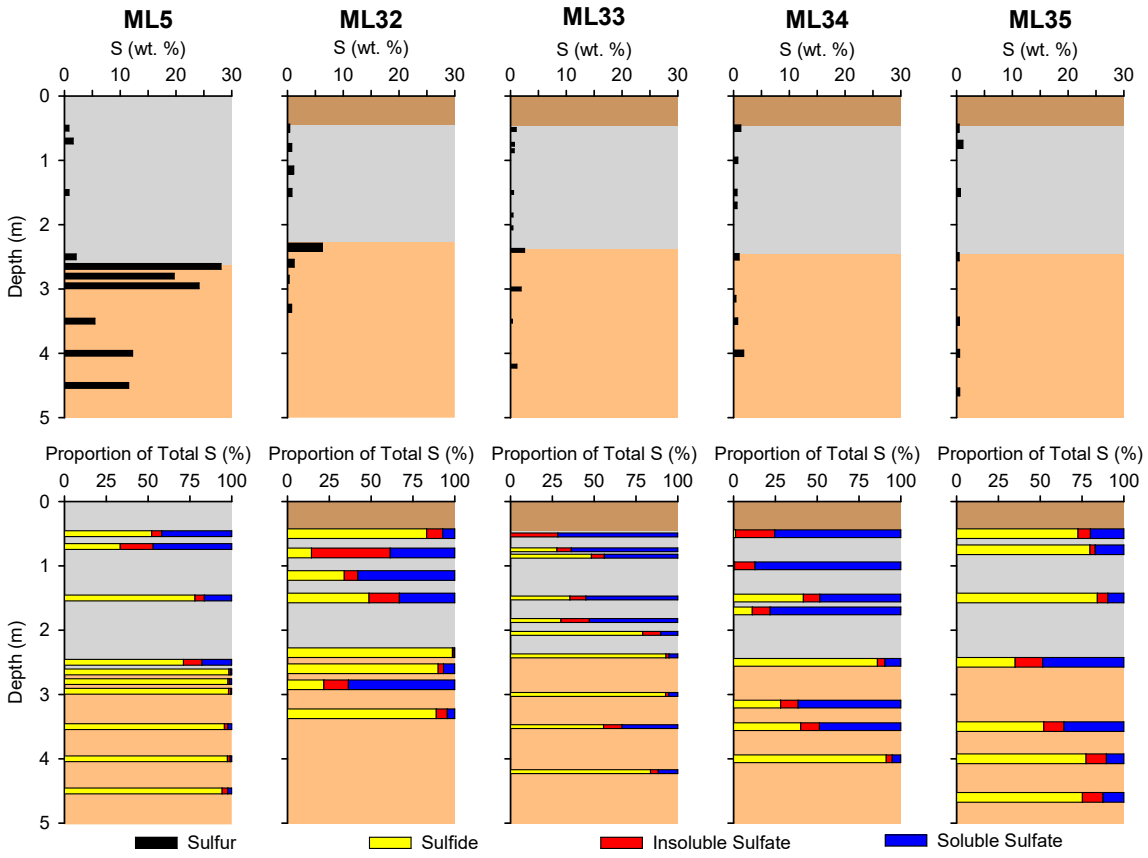

Figure 2.5: Total S (wt. %) of tailings and solid phase S speciation (% of total) for locations with a 1-layer cover (ML5) and 2-layer cover system (ML32, ML33, ML34, ML35). The brown, grey, and orange represent the organic carbon cover, desulfurized tailings layer, and historical tailings, respectively.

The major components in the tailings were aluminum (Al), calcium (Ca), iron (Fe), magnesium (Mg) and silica (Si), with smaller amounts of potassium (K) and sodium (Na). Based on the 22 unoxidized tailings samples retrieved at the locations with 1-layer and 2-layer cover systems, the mean weight % and standard deviation of Al, Ca, Fe, Mg, and Si were (6.39 ± 1.96), (4.06 ± 1.31), (15.67 ± 12.26), (2.93 ± 1.21), and (22.01 ± 6.77), respectively. As noted earlier, the high S-pyrrhotite tailings showed higher Fe content (> 35 wt.%) and lower Si content (< 12 wt.%) than the other tailings. Other than at ML5, the concentrations of these major constituents generally varied < 5 wt.% throughout the profiles and did not have large variations between the DST layer and the historical tailings.

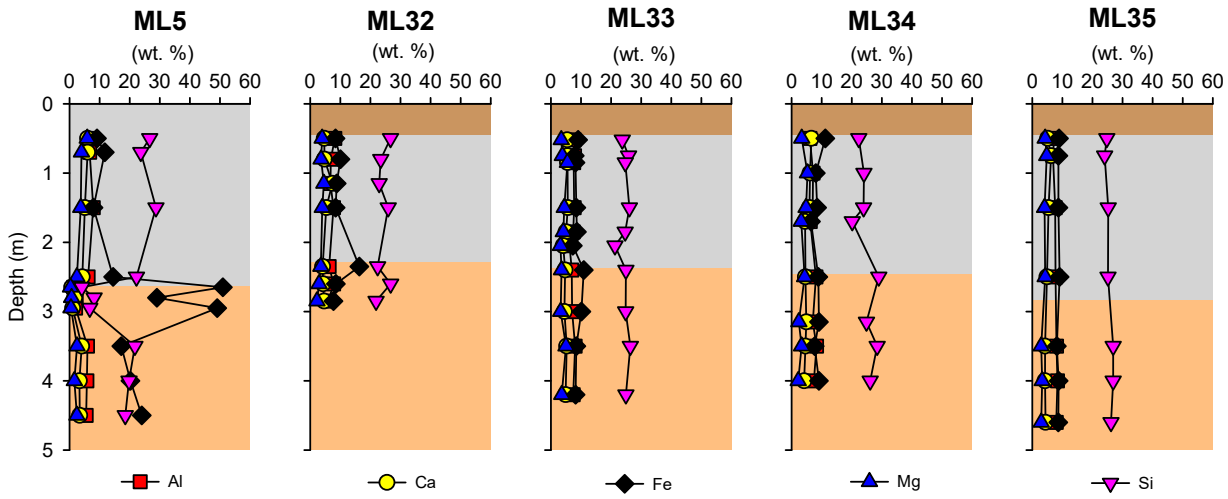

Figure 2.6: Concentrations (wt. %) of Al, Ca, Fe, Mg, and Si with depth. Concentrations (wt. %) of Al, Ca, Fe, Mg and Si for locations with the 1-layer cover (ML5) and 2-layer cover system (ML32, ML33, ML34, ML35). The brown, grey and orange represent the organic carbon layer, desulfurized tailings layer, and historical tailings, respectively.

The bulk $\delta^{13}C$ isotopes of the tailings and organic cover material were -26.40 ‰ ± 1.34 ‰ VPDB (mean ± S.D., n = 5) and -16.19‰ ± 3.12 ‰ VPDB (mean ± S.D., n = 9), respectively.

Viable cell counts, determined by colony forming units (CFU), between the two locations with a 2-layer cover system (ML33 and ML34) and that with a one-layer cover (ML5) were not significantly different (Appendix C). Neutrophilic groups of microorganisms dominated over acidophiles in all circum-neutral (pH 6.5 -8.5) tailings samples. High numbers of nSOM (between 10^4 and 10^9 CFU), with low numbers of aSOM (generally between 10^0 and 10^5, with one sample at 10^7) and nSRB (between 10^0 up to 10^3 CFU) were detected, with nSRB cell counts stable at depths beneath the organic carbon cover. Counts of IRM were high within the organic cover (10^5 MPN g^{-1} at ML33 and 10^9 MPN g^{-1} at ML34) but decreased sharply underneath the cover at a depth of 0.7 m (10^1 MPN g^{-1} at ML33 and 10^4 MPN g^{-1} at ML35). This trend was not found at the location with a 1-layer cover. At depths > 2.5 m, nHET were found to be between

10^4 and 10^8 at the locations with a 2-layer cover system (ML33 and ML34) and was 10^0 in the location with a 1-layer cover (ML5).

16S rRNA gene sequencing showed that Proteobacteria were the most abundant phylum in most samples (accounting on average for 48.9% of the total amplicons), followed by Actinobacteria (9.7%), Firmicutes (6.7%), Chloroflexi (6.0%), Bacteroidetes (4.4%), and Acidobacteria (4.1%). The two most abundant genus were the nSOB Thiobacillus (1.32% of total reads) and Sulfurifustis (0.81% of total reads) and nSOM were more numerous in the SWWTS samples than aSOM (4.4% vs. 1.3% of total reads). The mean abundance of obligate S-oxidizing genera was 4.75% of total reads in the samples. Microorganisms that oxidize both S and Fe (SOM/IOM) accounted for 0.5% of total reads, out of which 0.3% was Acidithiobacillus spp. Genera that oxidize iron (but not sulfur) were detected with the mean abundance of 0.5% (Appendix C). Thus, in total, 5.75% of the total reads were from genus that can metabolize Fe and/or S; the principle reactants in the generation of AMD.

2.4.3 Pore Gas Analysis

The $O_{2(g)}$ concentrations decreased with increasing depth at all locations. The profiles were similar for all locations except for ML33, where less $O_{2(g)}$ depletion occurred within the first meter compared to the other locations. $O_{2(g)}$ was depleted at ~1 mbgs at the location with a 1-layer cover (ML5), while $O_{2(g)}$ was depleted around 1.5 – 2 mbgs for the locations with a 2-layer cover system (ML32, ML33 ML34 and ML35) (Figure 2.7). The locations with a 2-layer cover system showed that the majority of $O_{2(g)}$ depletion occurred in the DST portion of the cover system, and that this depletion occurred at a greater depth in August than in October. August data showed that, at ML32, ML34, and ML35, $O_{2(g)}$ concentration decreased from 18.1 %, 16.1 % and 15.1 % v/v at the bottom of the organic cover to 2.1 %, 4.4 % and 0.6 % v/v at a depth of 1.0

mbgs (~0.5 m below the bottom of the organic cover). At location ML33, $O_{2(g)}$ concentrations decreased slightly from 19.5 % to 17.3 % v/v over this same depth interval, though $O_{2(g)}$ concentrations decrease from 17.3 % to 4.5 % in the 1.0 - 1.5 m depth interval. In all locations with a 2-layer cover system, $O_{2(g)}$ concentrations at the base of the organic cover were $\geq$ 10 % v/v.

The $CO_{2(g)}$ profiles at each of these locations showed an increase in $CO_{2(g)}$ concentrations with depth (Figure 2.7). At ML5, $CO_{2(g)}$ concentrations did not increase past a depth of 0.5 mbgs, reaching a maximum of 5.4 % v/v. At the locations with a 2-layer cover system, the CO_2 concentrations reached a maximum of 12 % v/v. The organic cover at each of these locations had $CO_{2(g)}$ ranging from 3 % v/v at ML32 to 8 % v/v at ML35. Locations ML32, ML34 and ML35 showed that $CO_{2(g)}$ concentrations increased the most from the surface to ~ 30 cm below the organic cover, while ML33 was more stable over this interval. All locations with the 2-layer cover system show higher $CO_{2(g)}$ concentrations in October (if only slightly), while the location with the 1-layer cover had higher $CO_{2(g)}$ concentrations in August.

$\delta^{13}C$-CO_2 results ranged from -8.052‰ to -20.72‰ VPDB showing an increase with depth (Figure 2.4). The profiles of the three locations are similar, even between the two locations with a 2-layer cover system and the one location with a 1-layer cover. $\delta^{18}O$-CO_2 results ranged between -1.483‰ and -6.824‰ Vienna Standard Mean Ocean Water (VSMOW). The profiles showed that the highest values of $\delta^{13}C$-CO_2 were near the surface and increased with depth.

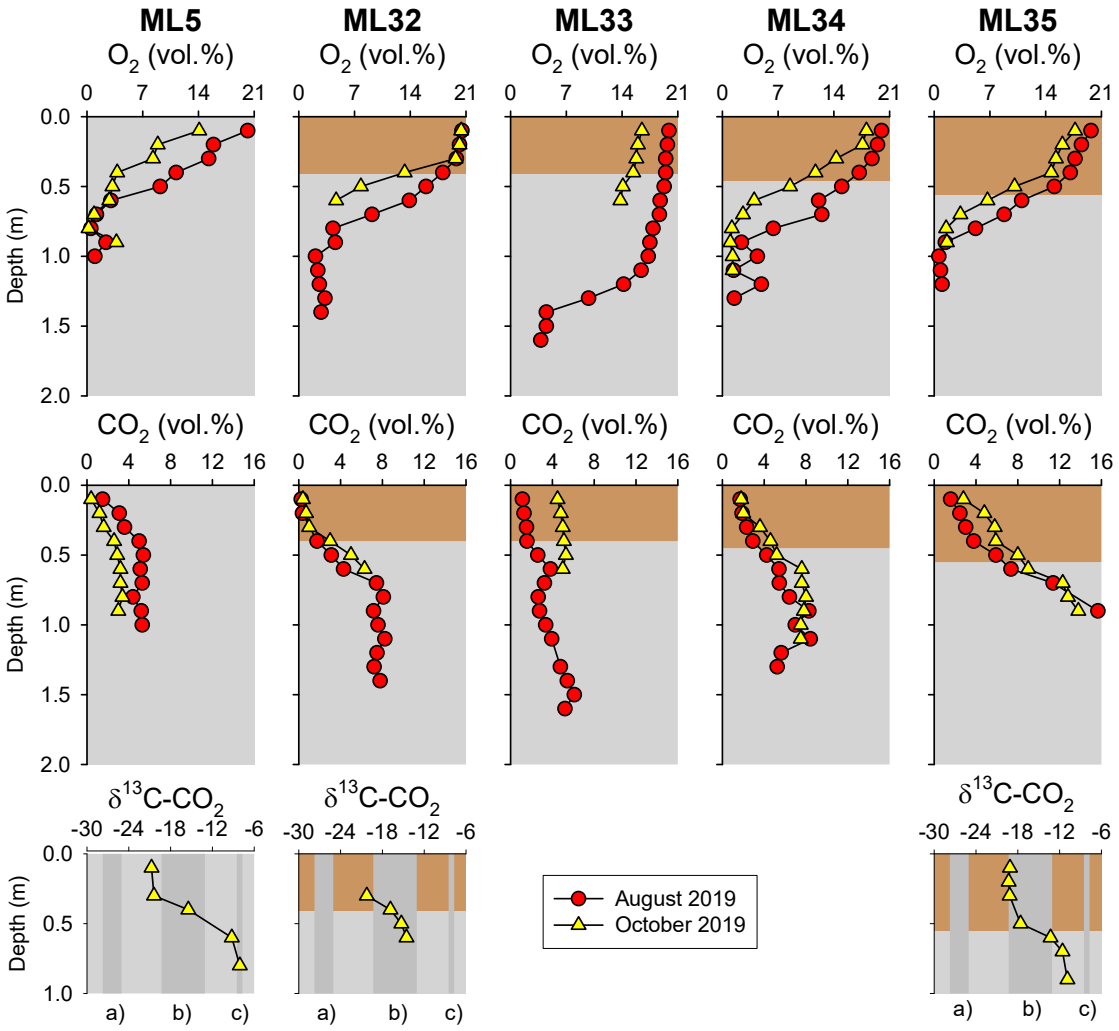

Figure.7: Pore-gas $O_{2(g)}$ and $CO_{2(g)}$ concentrations and select $\delta^{13}C$-CO_2 measurements vs. depth. The brown and grey represent the organic carbon layer and desulfurized tailings layer, respectively. Vertical grey bars a), b) and c) represent solid-phase $\delta^{13}C$ values for the organic carbon cover, desulfurized tailings, and atmosphere, respectively (average ± standard deviation). Note: The water table depths at the location with a 1-layer cover were 1.9 m and 0.8 m in August and October, respectively. The water table depth at the locations with a 2-layer cover system ranged from 2.9 m to 4.5 m in August and between 2.6 m and 3.7 m in October.

$O_{2(g)}$ flux measurements into the subsurface at ML33, ML34 and ML35 were the highest in July (between 149 and 270 mol $O_{2(g)}$ m^{-2} yr^{-1}) when the average temperature in the organic cover was around 20^0C. In comparison, $O_{2(g)}$ fluxes were lowest in October (between 32 and 118 mol $O_{2(g)}$ m^{-2} yr^{-1}) when the average temperature in the organic cover was around 10^0C. The general trend showed lower $O_{2(g)}$ fluxes in May and October when compared to July and August.

$O_{2(g)}$ flux decreased with increasing saturation. The flux into the subsurface at ML33, for example, decreased from 260 to 36 mol $O_{2(g)}$ m^{-2} yr^{-1} when the water saturation increased from 50 to 87 % at the deepest monitoring depth within the DST (1.05 mbgs). At ML5, the $O_{2(g)}$ flux approached 1 mol $O_{2(g)}$ m^{-2} yr^{-1} when the saturation exceeded 80%. At all locations with a two-layer cover system, the $O_{2(g)}$ flux into the cover system was limited by the DST layer and the amount of $O_{2(g)}$ diffusion was correlated to the degree of water saturation in this layer.

2.4.4 Water Quality

In the vadose zone of the location without a cover system (ML25), the pH was 3 – 4, E_H was between 240 and 710 mV and the alkalinity was depleted (< 10 mg L^{-1} as $CaCO_3$). The maximum concentrations of SO_4 (16,600 mg L^{-1}), Fe (1820 mg L^{-1}), Ni (572 mg L^{-1}), Al (1570 mg L^{-1}), Zn (18.3 mg L^{-1}), Cu (339 mg L^{-1}) and Co (60.21 mg L^{-1}) were observed, while minimum concentrations of 504.1 mg L^{-1} and < 0.05 mg L^{-1} were noted for SO_4 and the dissolved metals, respectively (see Figure 2.8). In the saturated zone, the pH increased to 6 - 7, E_H decreased to between 310 and 640 mV, and alkalinity increased to 10 - 260 mg L^{-1} as $CaCO_3$. Concentrations of SO_4, Fe, and Zn remained high, ranging from 3200 – 14,100 mg L^{-1}, 500 - 4700 mg L^{-1}, and < 0.5 - 16.4 mg L^{-1}, respectively. Throughout the profile, Cl^- concentrations increased with depth, from < 5 mg L^{-1} in the vadose zone to > 100 mg L^{-1} below the water table (see Figure 2.9).

In the vadose zone of the location with a 1-layer cover, pH ranged between 7 and 8, E_H was between 200 and 500 mV, and alkalinity varied between 158 - 298 mg L^{-1} as $CaCO_3$ (see Figure 2.8). In this zone, maximum concentrations of SO_4 (2980 mg L^{-1}), Fe (0.11 mg L^{-1}), Ni (1.41 mg L^{-1}), Al (0.07 mg L^{-1}), Zn (0.16 mg L^{-1}), Cu (0.09 mg L^{-1}) and Co (0.08 mg L^{-1}) were observed, while minimum concentrations of 1690 mg L^{-1} and < 0.05 mg L^{-1} were noted for SO_4

and the dissolved metals, respectively. In the saturated zone, the pH was 5 – 7; decreasing slightly compared to the vadose zone. E_H also decreased to as low as 150 mV, and alkalinity decreased to between 22 and 140 mg L^{-1} as $CaCO_3$. In this saturated zone, maximum concentrations of SO_4 (1850 mg L^{-1}), Fe (58.7 mg L^{-1}), Ni (1.32 mg L^{-1}), Al (1.49 mg L^{-1}), Zn (0.29 mg L^{-1}), Cu (0.36 mg L^{-1}) and Co (0.04 mg L^{-1}) were observed, while minimum concentrations of from 950 mg L^{-1} and < 0.05 mg L^{-1} were observed for SO_4 and dissolved metals, respectively. Cl^- concentrations generally increased with depth, from ~10 mg L^{-1} in the vadose zone to 184.9 mg L^{-1} below the water table. DOC concentrations were between 7.9 and 65.5 mg L^{-1} in the vadose zone and saturated zone and had no clear trend with depth (see Figure 2.9).

The locations with a 2-layer cover system showed water quality that was similar to the location with the 1-layer cover, though DOC and alkalinity were higher. In the vadose zone at these locations, the pH was generally between 6.5 and 8.5, except for a few shallow locations at ML32, ML33 and ML34 where pH as low as 4.48 was detected. The E_H at each location varied from as low as 93 mV to as high as 530 mV. Alkalinity had a range of 10 mg L^{-1} to 968 mg L^{-1} as $CaCO_3$ and was lower at the locations with acidic (< 6) pH values (see Figure 2.8). SO_4 concentrations were generally between 2000 and 3000 mg L^{-1} except at a depth of 0.5 mbgs at ML34, which was 4840 mg L^{-1}. Fe concentrations were generally < 5 mg L^{-1}, except at ML35 where the Fe concentration was as high as 24.3 mg L^{-1}. Ni concentrations were generally < 25 mg L^{-1}, except at depths of 1.85 mbgs at ML32, 0.75 mbgs at ML33 and 0.5 mbgs at ML34 where pH was < 5.5. Al, Zn, Cu and Co concentrations were highest at a depth of 1 mbgs at ML33 (12.65 mg L^{-1}, 3.69 mg L^{-1}, 18.9 mg L^{-1}, and 4.54 mg L^{-1}) though > 95 % of samples taken had concentrations < 1.0 mg L^{-1}. The depths within ML32 and ML34 where pH was < 5.5

became more neutral between December 2016 and November 2017. Within the vadose zone at ML34 between December 2016 and November 2017, alkalinity increased while SO_4 concentrations decreased at corresponding depths. Ni concentrations increased at ML32 and ML33. Zn increased at ML33 between December 2016 and November 2017 but decreased at the other locations over this same time.

In the saturated zone, the pH was between 6.5 and 8.5. E_H was generally < 300 mV, except for 2.7 mbgs and 2.9 mbgs at ML34 and ML35, with maximum values of 413 mV and 414 mV, respectively. There was a large range in alkalinity, with values as low as 50 mg L^{-1} as $CaCO_3$ a depth of 4.7 mbgs at ML32 in November 2017, though the value at this depth increased to 305 mg L^{-1} as $CaCO_3$ in July 2019. Values as high as 1540 mg L^{-1} as $CaCO_3$ were measured, though most values were < 800 mg L^{-1} as $CaCO_3$. Alkalinity values in the saturated zone increased over the course of the sampling program. SO_4 values were between 670 mg L^{-1} and 3600 mg L^{-1}, with most values around 2000 mg L^{-1}. Fe concentrations between 4.5 and 117 mg L^{-1}, and values > 60 mg L^{-1} were only observed at ML34 and ML35. Ni concentrations > 5 mg L^{-1}, were observed, though most samples were < 1.0 mg L^{-1}. Al concentrations were < 1.0 mg L^{-1}, with the exception of two samples; one at ML34 (1.68 mg L^{-1}) and one at ML35 (5.3 mg L^{-1}). Zn concentrations ranged from < 0.017 mg L^{-1} to a maximum of 0.45 mg L^{-1}. Cu and Co concentrations were < 1.0 mg L^{-1}. Chloride concentrations were the highest at these locations, with the highest concentrations reported at ML34, up to 8116 mg L^{-1}. The concentrations generally decreased over time in the vadose zone. Dissolved Cl^- concentrations at all four locations showed peaks between 1140 and 4852 mg L^{-1} at depths of 1 - 2 mbgs in November 2017.

Nitrate concentrations were generally < 10 mg L^{-1}, with the exception of select shallow depths within ML32 and ML33, which had maximum concentrations of 52.7 and 778.7 mg L^{-1}, respectively. All nitrate concentrations at ML34 and ML35 were below the detection limit (< 1.0 mg L^{-1}). Concentrations of ammonia were < 10 mg L^{-1} at most locations, with the exception of some locations within the saturated zone at ML34 and ML35, which had values as high as 67.6 and 224 mg L^{-1}, respectively. DOC concentrations in the vadose zone ranged from 28.1 to 475.3 mg L^{-1}, with the highest concentration at ML32. The DOC concentrations in the saturated zone were generally lower and varied by < 50 mg L^{-1} over the sampling episodes (see Figure 2.9). ML35 had the highest value at 418.9 mg L^{-1}. Nitrate concentrations reached as high as 1182 mg L^{-1} at ML32 and 779 mg L^{-1} at ML33, though most of the results were < 10 mg L^{-1}. Collection of NH_3-N, PO_4-P and S^{2-} samples was limited to locations with piezometers and lysimeters. Concentrations of NH_3-N were generally < 5 mg L^{-1}, with the exception of one elevated concentration of 224.2 mg L^{-1} at ML35 in December 2016. PO_4-P and S^{2-} concentrations were 2 – 120 µg L^{-1} and 3 – 77.7 µg L^{-1}, respectively.

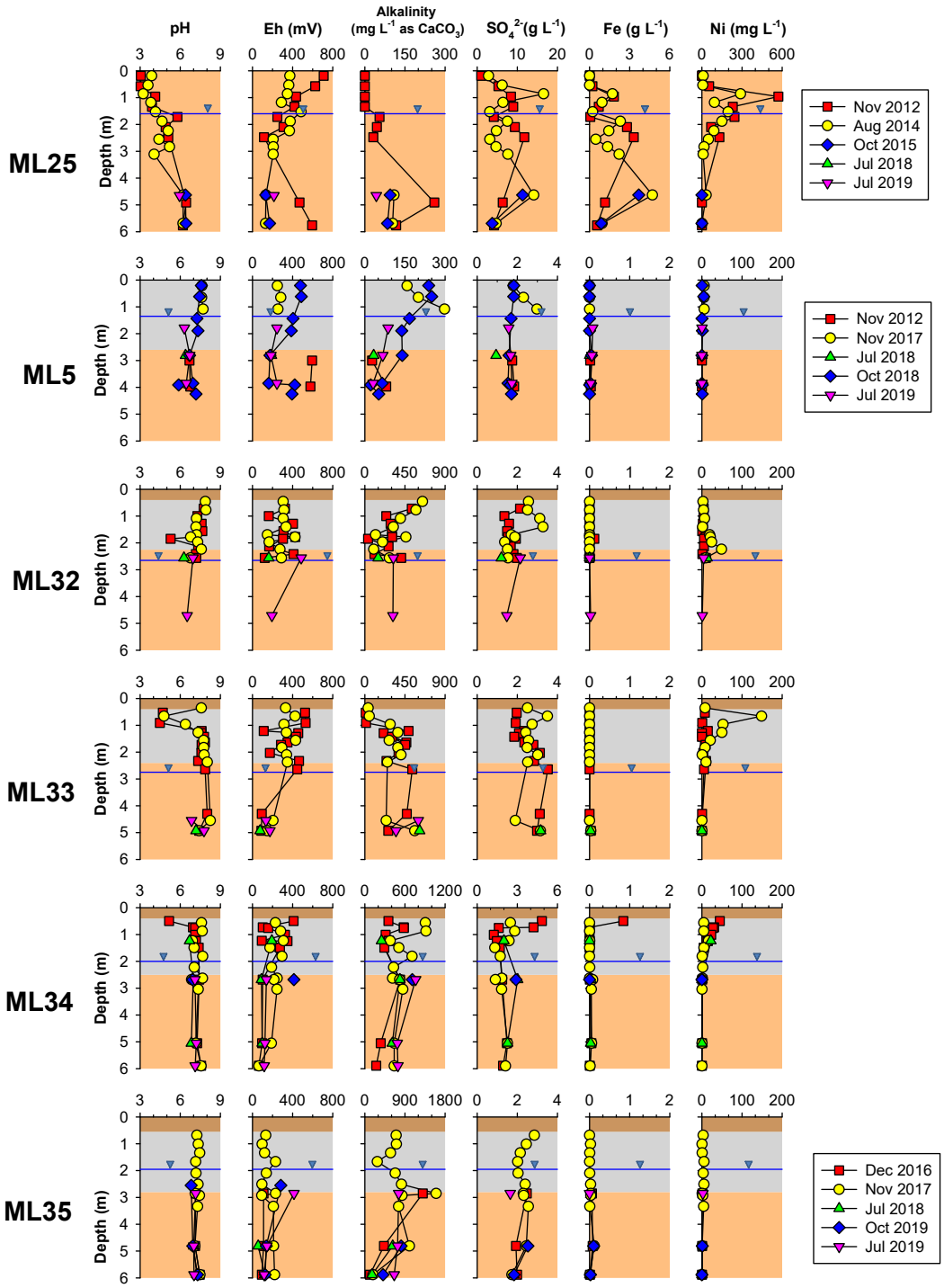

Figure 2.8: Water quality at sites without a cover (ML25), 1-layer cover (ML5), and 2-layer cover system (ML32, ML33, ML34 and ML35). The blue lines and the brown, grey, and orange zones represent the water table, organic carbon layer, desulfurized tailings layer, and historical tailings, respectively. The two inverted blue triangles represent the highest and lowest water levels observed during the 2018 and 2019 monitoring episodes while the highest and lowest water levels observed at ML25 were taken from Bain and Blowes (2013) and Parigi (2020). Note: the scales vary by location and by parameter.

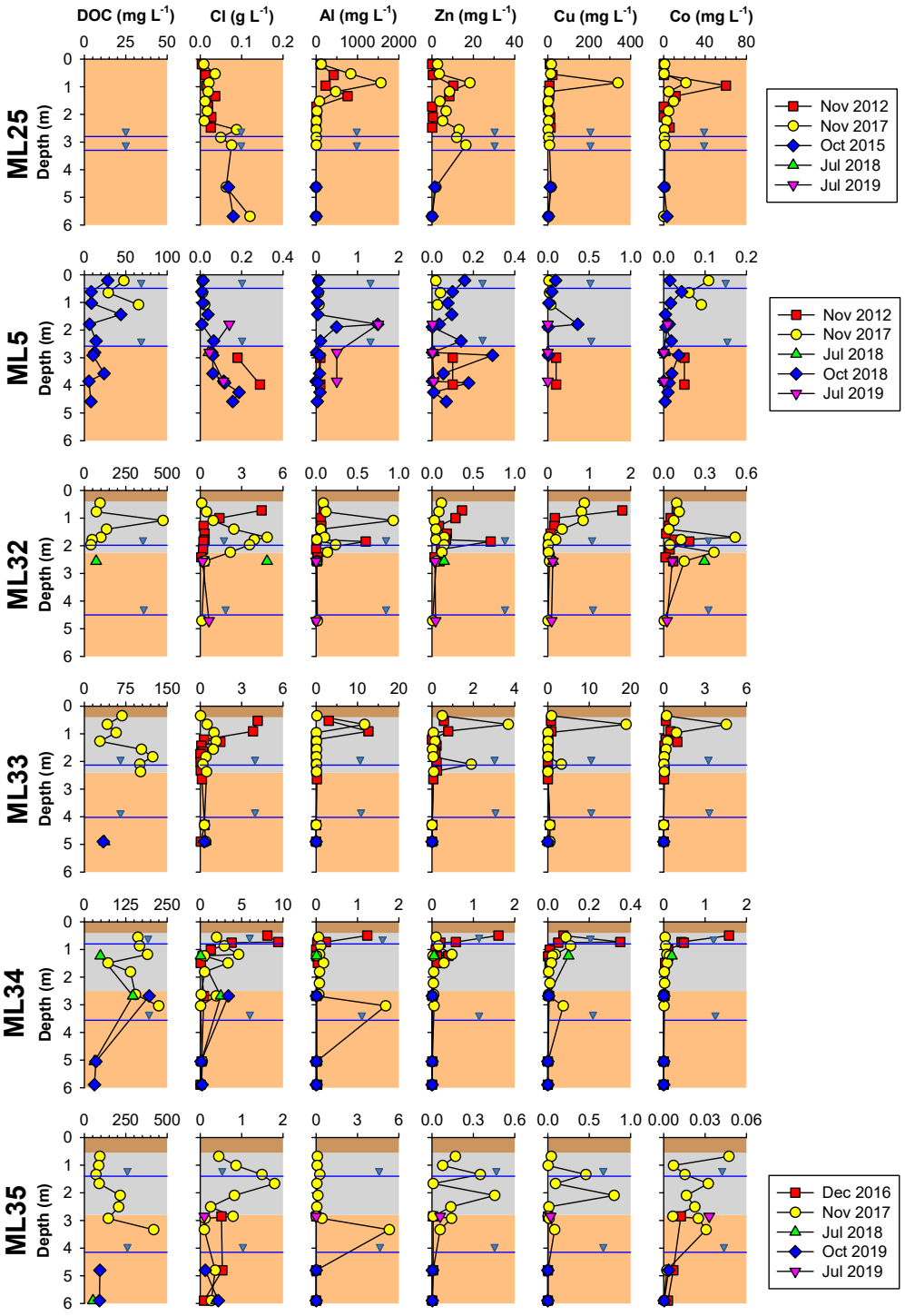

Figure 2.9: Water quality at sites without cover (ML25), 1-layer cover (ML5), and 2-layer cover system (ML32, ML33, ML34 and ML35). The blue lines and the brown, grey, and orange zones represent the water table, organic carbon layer, desulfurized tailings layer, and historical tailings, respectively. The two inverted blue triangles represent the highest and lowest water levels observed during the 2018 and 2019 monitoring episodes while the highest and lowest water levels observed at ML25 were taken from Bain and Blowes (2013) and Parigi (2020). Note: the scales vary by location and by parameter.

Acesulfame-K was detected at ML33, ML34 and ML35 between 1.6 and 5.4 µg L^{-1} and Sucralose was detected at ML32, ML34 and ML35 between 55 and 247 µg L^{-1}. Cyclamate and saccharin were not detected in any of these samples (Figure B.33). Carbamazepine (< 2.2 to 89.2 ng L^{-1}), caffeine (< 0.4 to 0.83 ng L^{-1}), ibuprofen (51.6 to 2610 ng L^{-1}), gemfibrozil (2.0 to 4.2 ng L^{-1}) and naproxen (< 0.6 to 10.4 ng L^{-1}) were also detected (Figure B.34) while sulfamethoxazole was not detected. All compounds that were detected were found between 2.56 and 5.89 mbgs.

The porewater and groundwater regression lines were defined as $5.55\delta^{18}O$ - 20.5 ‰ (R^2 = 0.925) and $6.35\delta^{18}O$ - 8.70‰ (R^2 = 0.899), respectively. $\delta^{18}O$ and $\delta^{2}H$ increased with depth (Figure B.29) in the pore water samples were statistically significant (n = 37, p values of < 0.003 and < 0.001 for $\delta^{18}O$-H_2O and $\delta^{2}H$-H_2O, respectively). The regression lines had a lower slope than that of the local meteoric water line (LMWL; 7.70), indicating evaporation.

The δS^{34}-SO_4 measurements of the process water used in the milling process were analyzed in December 2018 and were found to be 2.9 ± 0.06 ‰ Vienna Canyon Diablo Troilite (VCDT) (mean ± s.d., n = 6). These samples were compared to samples taken from locations with a 1-layer cover and a 2-layer cover system. Samples from the location with a 1-layer cover had more positive values (3.7 ± 0.45 ‰ VCDT, mean ± s.d., n = 3) than locations with a 2-layer cover system (2.1 ± 0.79 ‰ VCDT, mean ± s.d., n = 6). The furthest deviation from δS^{34}-SO_4 of the mill water was 1.3 ‰ VCDT. δS^{34}-SO_4 values were found to be insignificant with depth (p value of 0.50).

2.5 Discussion

2.5.1 Cover System Hydrology

An important factor in understanding the evolution of VWC and matric potential over time is to understand the differences in precipitation, recharge, and evapotranspiration over the year. The percent saturation (Sw) in the organic cover was < 70 % for much of the year, due to higher drainage and evapotranspiration. The vegetation on site includes shallow roots that do not penetrate into the DST (Glencore, personal communication) and the DST are more successful at maintaining their moisture throughout the year. The DST had Sw > 70 % in April, May and June, following the spring snowmelt, but the water saturation was generally between 50 and 60% for the rest of the year, particularly in July and August when evapotranspiration was highest. PSA has important implications for the maintenance of high-water saturation and the position of the water table which can significantly limit $O_{2(g)}$ diffusion if it is located within the DST layer. E/C was determined by the ionic potential of the pore water surrounding the sensors and therefore was highly correlated with the degree of water saturation, increasing in the spring and decreasing in July and August. E/C results also suggest that salts had leached from the organic cover and had reached > 1 mbgs. Based on the measured K values, the organic cover is two to four orders of magnitude more permeable than the DST. Due to the high permeability of the organic cover incoming rain or runoff will rapidly infiltrate this layer, but the infiltration rate through the DST layer is slower which maintains an elevated moisture content in the organic carbon layer.

2.5.2 Tailings Oxidation

An important factor in limiting AMD is to limit $O_{2(g)}$ diffusion into the subsurface where the S minerals are located. Results from the O_2 consumption tests revealed that the flux of $O_{2(g)}$

entering into the subsurface at these locations varied throughout the year and was influenced by the temperature and degree of saturation of the surficial material. Results showed that maintaining a higher degree of water saturation at the surface of the cover significantly limited $O_{2(g)}$ flux into the subsurface, with the DST limiting $O_{2(g)}$ flux more effectively than the organic cover.

Understanding of 1) S and 2) C content in tailings has important implications for its relative capacity for acid generation (through sulfide oxidation) and pH neutralization (through carbonate dissolution). Results from 1) S and 2) C analyses confirm that 1) the DST contain low concentrations of S and C (which have important implications regarding acid generation and subsequent neutralization) and 2) the organic materials had much larger carbon content and thus contribute significantly to pH neutralization within the cover system. Due to the subaerial nature of the tailings and Sw < 70% in the summer months, sulfide oxidation did occur in the DST prior to placement of the organic carbon cover. Currently, oxidation continues at locations with a 1-layer cover and a 2-layer cover system. The $O_{2(g)}$ concentrations show that $O_{2(g)}$ is generally consumed within a depth of 1 m of the DST layer. Bulk $\delta^{13}C$ of the organic cover and tailings were used as a tool to determine the isotopic differences of $^{13}C/^{12}C$ between the various components of the cover system and to link these results to the mechanism of $CO_{2(g)}$ generation (biotic vs. abiotic). The bulk $\delta^{13}C$ isotopes of the organic cover were found to be typical of organic material, while the bulk $\delta^{13}C$ isotopes of the tailings were closer to that of freshwater carbonates (Clark and Fritz, 1997). Profiles of $\delta^{13}C$-$CO_{2(g)}$ show that the $CO_{2(g)}$ present within the organic cover was generated through aerobic degradation, whereas $CO_{2(g)}$ present within the shallow portion of the DST was generated by carbonate-mineral dissolution. Speciation of solid-phase S show that the total S is composed of sulfide and sulfate forms (Figure 2.5), with the

exception of the high pyrrhotite tailings at ML5 which is composed of nearly all sulfide-S, due to it being stored subaqueously. In a few cases, such as within a depth of 2 m at ML33 and ML34, > 50% of the S in the DST is in the form of SO_4 minerals: likely gypsum and jarosite. This prevalence of secondary S phases indicates that sulfide oxidation has occurred at all of the sample locations, both in the DST and in the underlying historical tailings. However, the DST maintain higher levels of Sw than the organic cover (Figure 2.4), which will help limit $O_{2(g)}$ diffusion through this layer.

Modeling of the sulfide oxidation in the vadose zone of each location was completed using *Pyrox* (Wunderly, 1996); a 1-D numerical model that couples oxygen diffusion and sulfide oxidation (see Table B.8 for the dataset used in these simulations). $O_{2(g)}$ consumption in the organic cover was simulated by specifying the thickness of this layer in the model domain and selecting an oxygen consumption rate by adjusting sulfide concentrations to match with the measured $O_{2(g)}$ (Figure B.9). The extra sulfide oxidation products generated through this approach were not included in the subsequent calculations. The modelling results indicate that sulfide oxidation occurred rapidly after tailings cessation, prior to the placement of the organic cover. Simulations were generally run for a period of ~ 8.5 years because tailings cessation occurred around 2006 and sulfide oxidation was assumed to only occur when the average ambient air temperature was > 0^0C; which occurs for ~ 7 months per year. 1-D reactive transport was considered to be a valid assumption because mine tailings are generally spread laterally over hundreds or thousands of square meters, whereas the thickness over which oxidation occurs is commonly only a few meters (Wunderly, 1996). The depth of the unsaturated zone for these simulations ranged between 0.8 m and 3.3 m, depending on the location and the date of sampling. Based on the simulations, the oxidation front at each location ranged between 0.8 and

1.8 mbgs (Figure B.10). This corresponded to total volumes of reacted tailings between 0.8 and 1.8 m^3 at each of these locations, which is equivalent to a total mass between 1201 and 2790 kg. Estimated quantities of SO_4, Fe and Ni produced were 31 - 70 kg, 18 – 41 kg, and 6 – 21 kg, respectively (Figure B.11), and corresponds with reaction rates of 3.8 – 8.0 kg m^{-2} yr^{-1} for SO_4, 2.2 – 4.7 kg m^{-2} yr^{-1} for Fe, and 0.75 – 2.4 kg m^{-2} yr^{-1} for Ni. At the locations with a 2-layer cover system, the rate of sulfide oxidation slowed after cover placement, with the exception of ML33, which showed little change in the rate of sulfide oxidation product release. The model simulations for the October 2019 gas data showed slower release of sulfide oxidation products compared to the August 2019 simulations (Figure B.11), likely due to increased moisture content in these profiles. The location with a 1-layer cover had the smallest extent of sulfide oxidation, likely due to the higher moisture content associated with the shallow water table. These simulations showed that sulfide was depleted in the first 0.5 mbgs at the location with a 1-layer cover and in the first 0.5 below the organic cover at the locations with a 2-layer cover system. When comparing the actual sulfide remaining to that of the model simulations, the actual sulfide remaining does not always agree, showing that there are complicating factors, including the rate of microbially catalysed sulfide oxidation, intermittent placement of the tailings at these locations, variations in the sulfide content, temporal variations in the moisture content, and variations in the rate of oxygen consumption in the organic cover. The observational sulfide remaining at location ML5 showed a general increasing trend with depth and had the best overall agreement with the model; five of the seven observation data points agreed with the model and the other two were underestimated by < 30%. The four locations with an organic layer (ML32 – ML35) showed incidences where the remaining sulfide observed did not have a consistent increasing trend with depth. At these four locations, the model underestimated the remaining

sulfide at certain depths by as much as 80%, while overestimating the remaining sulfide by as much as 80% at other depths, though the model would generally agree with at least a few observation data points. The code *Pyrox* can also be used to estimate the time that it would take to deplete the sulfide present in the unsaturated portion of the desulfurized tailings. Using the moisture content profiles from the August 2019 and October 2019 pore-gas sampling events, the time that it would take for sulfide depletion varied at these five study locations between approximately 10 and 90 years, and was found to be mostly dependent on the moisture content profile and depth to the water table (i.e. thickness of the unsaturated zone).

XRF results show that high concentrations of Fe (> 30 wt.%) are present in the tailings, indicating that a large portion of Fe could be released by sulfide oxidation (if the mineral phase is pyrrhotite) or reductive dissolution (if the mineral phase is ferrihydrite or goethite) reactions occur. Concentrations of Ca, Mg and Al could also be present in minerals such as calcite [$CaCO_3$], dolomite [$(CaMg(CO_3)_2$], or gibbsite [$Al(OH)_3$], which are all compounds that contribute to acid neutralization.

The Chao's index (Chao et al., 2005) is used to represent microbial diversity and was determined for samples from locations with the 2-layer cover system and compared to the location with the 1-layer cover to determine if the organic cover affected microbial richness. A pairwise comparison revealed no significant differences ($p > 0.05$) between the two values. The Gini-Simpson's index (Simpson, 1949) is another metric that considers microbial richness and, similarly, no significant differences were found when a pairwise comparison of this metric was made between locations with the 2-layer cover system and a 1-layer cover (Appendix C). However, elevated numbers of neutrophilic heterotrophs (which can consume O_2 through aerobic degradation) were detected at depths > 1 m at locations with organic carbon layers (potentially

due to increased DOC concentrations). However, the depth of oxygen consumption is less than 1 m at all locations except ML 33.

Based on the $\delta^{34}S$ isotope values, there was no significant difference ($p > 0.05$) in the $\delta^{34}S$ values of the mill process water and the locations without a cover, a 1-layer cover, and a 2-layer cover systems, within the depths investigated. These results indicate that there is no evidence that nSRB are currently reducing aqueous SO_4 to sulfide. There was also no indication that the presence of the organic cover enhanced the occurrence and/or activity of nSRB based on work described in Appendix C. nIRM were found to be more prevalent in the tailings immediately beneath the organic cover but decreased with depth.

2.5.3 Water Quality

Comparison of the water quality between the locations revealed that the locations with a 1-layer cover or 2-layer cover system typically had pH values closer to neutral and had lower concentrations of SO_4 and dissolved metals. The location without a cover is characterized by low pH, low alkalinity (depleted in the vadose zone), and concentrations of dissolved metals and SO_4 as high as 1600 mg L^{-1} and 16,600 mg L^{-1}, respectively, along with low concentrations (< 150 mg L^{-1}) of Cl^-. The location with a 1-layer cover shows near-neutral pH conditions, with alkalinity < 400 mg L^{-1}. The exception is the July 2019 sampling episode, however, when alkalinity values were higher, though this was likely due to the influence of the stockpile of biosolids fertilizer placed adjacent to the site in the Fall of 2018. Low concentrations of dissolved metals (< 1.0 mg L^{-1}) and DOC (< 80 mg L^{-1}) prevail, which is consistent with the hypothesis that a water-retaining, low-S layer with an elevated water table would improve water quality. The locations with a 2-layer cover system contained high concentrations of DOC and Cl^-, illustrating infiltration through the organic cover. SO_4 concentrations were generally between

1000 and 4000 mg L^{-1}, with the exception of the December 2016 sampling episode at ML34 when the organic cover was new and oxidation products prior to cover placement remained in the shallow porewater. The leaching of DOC can be a concern, because certain metals can complex with organic carbon and become more mobile, due to their increased solubility (Stumm and Morgan, 1996). Despite this concern, a relationship between increased DOC concentrations and higher concentrations of dissolved metals was not observed.

At the location without a cover, SI values show undersaturation with respect to ferrihydrite [$5Fe_2O_3 \bullet 9H_2O$] in the unsaturated zone and supersaturation below the water table, whereas SI values indicate the porewaters are supersaturated with respect to goethite and jarosite through the entire profile. The pore water is undersaturated with respect to calcite, dolomite, and $Al(OH)_{3(a)}$ at all depths and is undersaturated with respect to gibbsite in the unsaturated zone, becoming slightly supersaturated with depth. The pore water is in equilibrium with gypsum below the shallowest pore-water sample (Figure 2.10).

At the location with a 1-layer cover, SI values indicate supersaturated conditions with respect to ferrihydrite and goethite, and near equilibrium conditions with respect to jarosite. Pore water in the vadose zone is near equilibrium with respect to calcite and dolomite and becomes undersaturated below the water table. The pore-water is slightly undersaturated with respect to $Al(OH)_{3(a)}$ and is generally in equilibrium or supersaturated with respect to gibbsite. The pore water is in equilibrium with gypsum throughout the depth profile.

At the sites with a 2-layer cover system, there is some variation with depth, over time and between sites. Most pore-water samples are supersaturated with respect to goethite. SI values vary between unsaturated and supersaturated with respect to jarosite and have a large range (as

low as -10 and as high as 7). Pore water throughout the profiles are near equilibrium with respect to calcite and dolomite, except for some shallow locations at ML32, ML33 and ML34, where undersaturated conditions prevail. The pore water is slightly undersaturated or in equilibrium with respect to $Al(OH)_{3(a)}$ and is in equilibrium or supersaturated with respect to gibbsite, particularly in later sampling episodes. The pore water is at equilibrium with respect to gypsum at all four locations.

Based on the SI values of water samples from the location without a cover, there is a high likelihood of the precipitation of goethite in the unsaturated zone, which could be contributing additional acid generation (Equation 2.3). The SI of gypsum [$CaSO_4 \bullet 2H_2O$] is around zero, indicating that porewater is in equilibrium with respect to this phase. Depletion of alkalinity in the shallow tailings, along with undersaturation with respect to calcite and dolomite and elevated concentrations of dissolved sulfide oxidation products in the tailings pore water are all indications that sulfide oxidation reactions have occurred (and continue to occur) at the location without a cover. Porewater became supersaturated with respect to ferrihydrite, goethite and jarosite with depth, indicating the potential for precipitation of all three of these minerals below the water table, thus limiting Fe and S mobility at these depths (according to Equations 2.3 and 2.4).

The SI values at the location with a 1-layer cover show a high likelihood of precipitation of ferrihydrite and goethite. Pore water in the unsaturated zone is near equilibrium with respect to jarosite, calcite and dolomite, but SI values show that these phases are likely dissolving/not forming below the water table. The pore water is in equilibrium with gypsum.

Pharmaceutical compounds and artificial sweetener compounds have been observed to enter the environment through discharges to surface water bodies from wastewater treatment plants (WWTPs) (Metcalfe et al., 2003; Liu et al., 2014). These compounds can also discharge to surface water bodies from groundwater contaminated by septic tanks (Carrara et al., 2008; Spoelstra et al., 2020), irrigation water from WWTPs (Kinney et al., 2006; Buerge et al., 2011), or by leaching from sewage sludge applied on land (Ternes et al., 2004; Dandan et al., 2021). In a study by Spoelstra et al. (2013), concentrations of artificial sweetener compounds acesulfame-K, sucralose, cyclamate and saccharin in the Grand River in Ontario, Canada were found to range from below the method detection limit (MDL) to maximums of 3,500 ng L^{-1}, 21,000 ng L^{-1}, 880 ng L^{-1}, and 7,200 ng L^{-1}, respectively, and were detected downstream at distances of up to 300 km. Results from this study show much lower concentrations of artificial sweeteners acesulfame-K (< MDL - 5.4 ng L^{-1}) and sucralose (55.0 – 247 ng L^{-1}) when compared to Spoelstra et al. (2013). Cyclamate and saccharin were not detected at any of the locations, which may indicate that they may have been biodegraded. In another study of the Grand River, Liu et al. (2014) found that the concentrations of caffeine, gemfibrozil, carbamazepine, naproxen, and ibuprofen in the river ranged from near the MDL to maximums of 3,400 ng L^{-1}, 30 ng L^{-1}, 150 ng L^{-1}, 500 ng L^{-1}, and 160 ng L^{-1} for caffeine, gemfibrozil, carbamazepine, naproxen, and ibuprofen, respectively, and were detected at distances of up to 30 km. Results from locations ML34 and ML35 in this study show that the concentrations of caffeine (< MDL – 0.83 ng L^{-1}), gemfibrozil (2.0 – 4.2 ng L^{-1}) and naproxen (<MDL – 10.4 ng L^{-1}) were much lower than those reported in the literature, however, concentrations of carbamazepine (< MDL – 89.2 ng L^{-1}) were similar to those reported in the literature and concentrations of ibuprofen observed (51.6 – 2610 ng L^{-1}) were greater than those observed in the Grand River. The high concentrations of

ibuprofen are in the range of those observed beneath the tile beds of septic systems (Carrara et al., 2008) and may indicate that this compound has not undergone significant biodegradation. The presence of these emerging contaminants beneath the 2-layer cover system indicates that these compounds, derived from the biosolids fertilizer, are transported by infiltrating recharge water into the vadose zone and the shallow groundwater zone. Based on the presence of acesulfame-K in the groundwater, infiltration rates in the cover system are estimated to average $\geq$1.25 m yr^{-1}. This is lower than the calculated estimate of infiltration (~2m yr^{-1}) but is within a factor of two. The estimate is based on 2019 data from the weather station located on site; accounting for precipitation, evapotranspiration, snowmelt (using a 10:1 ratio of snowpack depth to rainfall equivalency and assuming 50% contribution to infiltration, 50% contribution to runoff), and previously reported porosity values of the cover system material, suggesting that the infiltration calculations may have overestimated the rate of recharge.

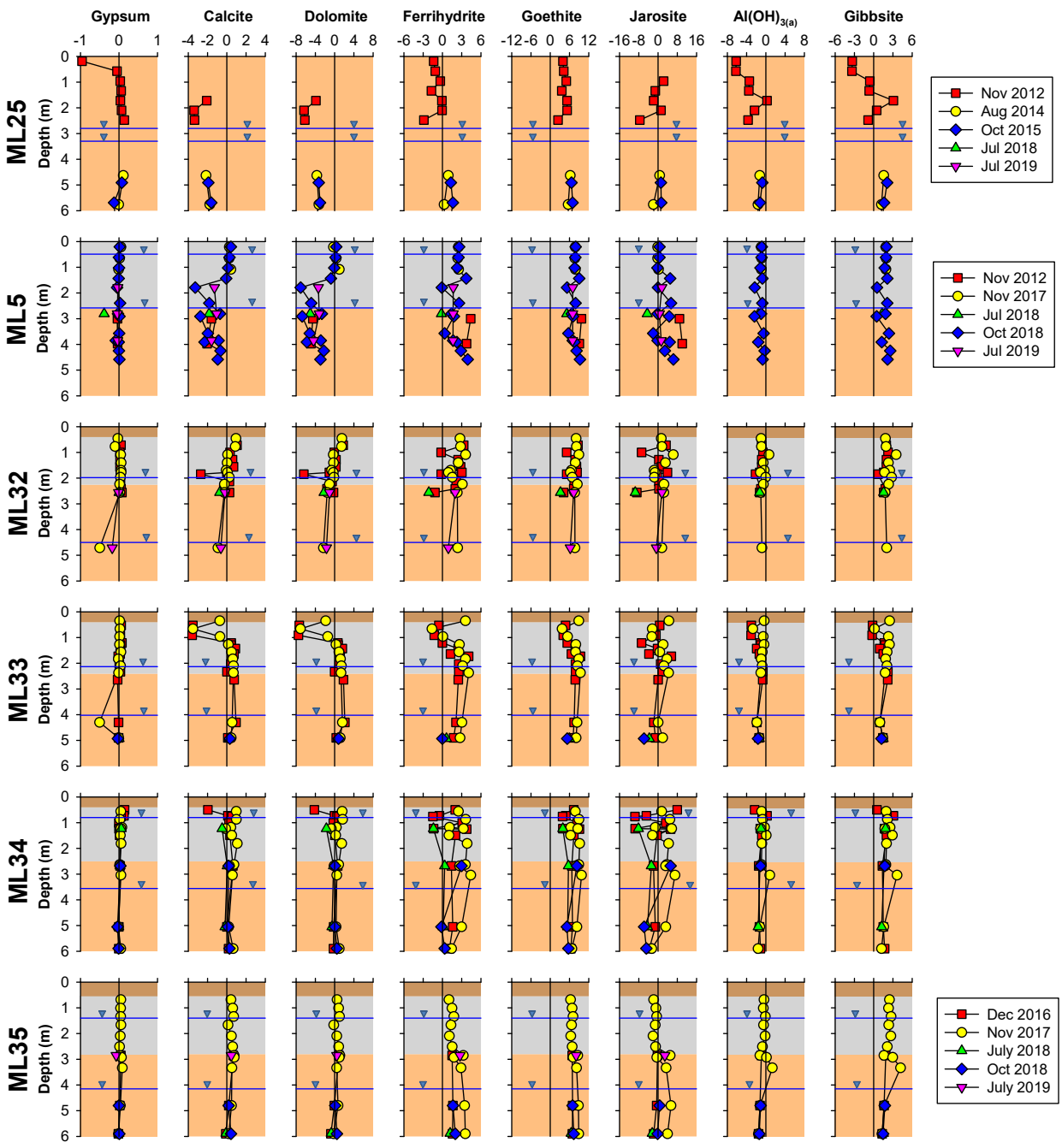

Figure 2.10: Saturation Indices between the sites without a cover, 1-layer cover, and 2-layer cover system. The blue lines and brown, grey, and orange zones represent the water table, organic carbon layer, desulfurized tailings layer, and historical tailings, respectively. The vertical solid lines represent the zero SI line. The two inverted blue triangles represent the highest and lowest water levels observed during the 2018 and 2019 monitoring episodes while the highest and lowest water levels observed at ML25 were taken from Bain and Blowes (2013) and Parigi (2020).

2.5.4 Cover System Longevity

An important consideration in tailings management is the longevity of the treatment, especially when considering passive systems that are intended to operate after mine closure. O_2 consumption tests showed that the integrated cover system (i.e. both the organic carbon layer and the DST layer) were reactive [i.e. had a reaction rate coefficient (Kr) > 0]. Simulations were completed to determine the O_2(g) flux at the base of the cover system using equations described by Mbonimpa et al. (2003), and estimating the VWC at 1.05 m depth as the average VWC for these simulations. From these simulations, the flux at the base of the cover system was found to be around 0 mol O_2 m^{-2} yr^{-1} for all locations. These results show that, under current conditions, the cover system significantly limits $O_{2(g)}$ from entering the higher-S tailings below. Simulations of $O_{2(g)}$ flux through the organic cover were determined using a K_r = 10 yr^{-1}; an estimate within the range of values described by Abu Qdais and Al-Widyan (2016) for agro-industrial wastes and Baptista (2009) for municipal solid waste, using August 2019 and October 2019 VWC measurements in the organic cover. Based on these assumptions, the rates of organic matter degradation were estimated to be 0.4 – 0.8 kg m^{-2} yr^{-1}. Extrapolation of this degradation rate to the entire area of the organic cover in Tailings Cell 1A (20 hectares), current degradation rates of organic matter in this cell are estimated between 8×10^4 – 1×10^5 kg yr^{-1}. Assuming that 30% of the organic matter in the biosolids fertilizer is available for degradation (Torrecillas et al., 2013), and 80% of the organic matter in the municipal compost is available for degradation (based on unpublished data acquired prior to this study), the estimated time required for consumption of the available organic matter in Tailings Cell 1A is on the order of 200 years. However, these calculations are complicated by the fact that rates of degradation will generally decrease exponentially over time and that the vegetation present could replenish some of the organic

matter over time. As the organic cover matures, it will also become thinner and more compact. This, in turn, will decrease the total travel time for $O_{2(g)}$ to reach the DST layer, below. The equation to calculate the total travel time of a gas to diffuse through a material is given by Equation 2.7.

(2.7) $$t = \frac{x^2}{2D_e}$$

Where t is time (days), x is distance (m), and D_e is the effective diffusion coefficient (m^2 day^{-1}). Using a thickness of 0.5 m (approximate thickness of the organic cover) and an estimated D_e of 0.08 m^2 d^{-1} [average calculated D_e from the Collin (1987) model for VWC observed within the organic cover in August 2019 and October 2019], the travel time of $O_{2(g)}$ through the organic cover is on the order of 1-2 days. Based on the observed $O_{2(g)}$ profiles, this timeframe is insufficient for the organic layer to consume the $O_{2(g)}$ that enters the subsurface. However, in terms of calculated transit times, the DST component is more effective at limiting $O_{2(g)}$ ingress into the waste deposit. Due to the greater thickness of this layer (2 m versus 0.5 m) and a lower estimated D_e of 0.025 m^2 d^{-1} (based on the average VWC observed at a depth of 1.05 m in August 2019 and October 2019), the travel time of $O_{2(g)}$ through the DST component of the cover system is estimated to be on the order of a few months. These calculations show the benefit of this component of the cover system, as it significantly limits $O_{2(g)}$ transport to the underlying reactive tailings.

It must be also be noted that oxygen is consumed in the DST through sulfide oxidation and the pore water could become acidic over time if the neutralization potential of the tailings is consumed. If this occurs, the previously precipitated secondary phases of S and Fe may dissolve,

increasing the metal loading below the cover system. In order to explore this case, acid base accounting (ABA) was calculated for the tailings samples based on total carbon content and sulfide content data collected during this study. Neutralization potential (NP) from carbonate (Carb-NP) was used, as it is generally considered to be the effective and available NP in mine materials (Ecometrix, 2014) while acid producing potential (AP) was calculated using sulfide content. Calculations of Carb-NP:AP ratios found that 21 of the 43 tailings samples had Carb-NP:AP ratios of less than one and 28 of the 43 tailings samples had ratios of less than two, which is considered a conservative approach (Ecometrix, 2014). These NP:AP ratios show the potential for the tailings to be acid-generating as the neutralization potential in the tailings is consumed. *Pyrox* simulations run using the sulfide content and moisture content observed during the pore-gas sampling episodes showed that all available sulfide within the unsaturated portion of the desulfurized tailings would be consumed within the span of decades, particularly at locations with lower moisture contents or shallower water tables. While the organic cover provides a source for replenishing alkalinity in the system, further study would need to be completed to evaluate the longevity of this source of NP to the DST.

2.6 Conclusions

The dissolution of calcite and dolomite in the organic cover and the DST has maintained neutral pH conditions at most depths within the pore water profiles. Geochemical modelling indicates a likelihood of precipitation of secondary iron phases, suggesting these phases constrain the concentrations of dissolved metals in the shallow portion of the tailings. Comparing the pore water data to applicable Federal (MDMER, 2002/2020) and Provincial (EEM, 1997/2017) regulations regarding effluent discharge from mine sites, concentrations of Ni exceeded the maximum monthly average concentration in > 50% of the samples. However, concentrations of

Cu, Zn, As, and Pb were at or below these regulatory limits in > 90% of these samples. Results from this study show that, although organic covers represent a potential for re-use of waste materials and have the potential to be cost-effective, their usefulness as a long-term passive-treatment technique depends on maintaining the moisture content, leaching alkalinity, and limiting aerobic degradation rates. These parameters, in turn, will be impacted by the moisture retention, application method, age of material, presence of vegetation and cover composition. The effectiveness of the DST layer depends on limiting $O_{2(g)}$ ingress, consuming $O_{2(g)}$ through sulfide oxidation, and maintaining neutral pH conditions in the shallow porewater. These parameters, in turn, will be impacted by the moisture content, water table depth, sulfide content, and buffering capacity of the DST. Further study would need to be completed to properly quantify how long the cover system could maintain neutral pH conditions, however, the use of an organic cover in conjunction with thickened, low wt.% S tailings along with maintaining the water table to near or above the surface of the historical tailings has improved the likelihood of short-term AMD mitigation at locations with this 2-layer cover system.

Chapter 3

Research Summary and Future Recommendations

This investigation of the two-layer cover system at the Strathcona Waste Water Treatment System focused on the characterization of the cover system and, in particular, it's effectiveness regarding the limitation of sulfide oxidation and the mobility and fate of metals in the shallow subsurface. In particular, the contributions of the organic-carbon cover were investigated relative to the cover system as a whole. This research was conducted to better understand the potential for using organic wastes for sustainable tailings management.

Field work was conducted to provide continuous measurements of VWC and matric potential during the 2018 and 2019 field seasons. Tensiometers and ECH$_2$O 5TE sensors were installed at four locations and at four different depths, along with sampling of the cover system material for the determination of porosity, particle size distribution, and hydraulic conductivity estimation. Slug tests and water level monitoring were also performed to estimate groundwater flow beneath the cover system. Based on this work, it was determined that the DST were more effective at maintaining a higher moisture content than the organic cover and variations in moisture content and porewater fluxes were observed throughout the 2019 field season.

Core sample collection of tailings solids were analyzed for bulk solid-phase chemistry to determine the major elements present, along with the quantification of total carbon, total S, and the species of solid-phase S present. The results indicated that Si is generally the most predominant element, followed by Fe, Al, Ca, and Mg. Total C and total S in the organic cover is around 12% and 2.5%, respectively, for the Sudbury n-rich and around 40% and 0.05%, respectively, for the Grobark compost and these materials have a $\delta^{13}C$ isotopic signature of organic material. Mean total C and total S in the tailings (excluding the high-S pyrrhotite concentrate) were 0.17% and 1.05%, respectively. S speciation on the tailings showed that the tailings had undergone varying amounts of sulfide oxidation due to the presence of secondary S

phases, particularly in the DST. ABA calculated using total carbon and total S^{2-} data showed that most samples had the potential to be acid-generating over time.

Pore gas was collected and analyzed in the field, at 10 cm intervals, for $O_{2(g)}$ and $CO_{2(g)}$ concentrations in August and October, 2019. O_2 consumption tests were also completed at each of the study locations throughout the 2019 field season. The results indicate that the organic cover is consuming $O_{2(g)}$ through aerobic degradation but is susceptible to ingress from the atmosphere, particularly in the summer months. The DST were observed to be more effective at limiting $O_{2(g)}$ diffusion due to the higher moisture content and greater $O_{2(g)}$ consumption rate through sulfide oxidation. The cover system achieved the overall goal of limiting $O_{2(g)}$ diffusion into the higher-S tailings below the cover system.

Pore water samples were collected through the combined methods of core squeezing and sampling of piezometers and lysimeters located at each of the study locations. Pore water analysis was completed in the laboratory and showed that the water quality was much improved at the locations that contained a layer of DST. The organic cover leaches DOC, alkalinity, and various emerging contaminants into the subsurface. Overall, metal loading to the subsurface was low at these locations, due to the precipitation of secondary phases under neutral pH conditions. Concentrations of artificial sweetener compounds and pharmaceutical compounds were detected at concentrations lower than those observed in surface waters receiving treated wastewater, with the exception of ibuprofen at ML35; which was detected at concentrations similar to those observed below tile beds of septic-systems. Based on ABA calculations, long term efficacy of this cover system requires further study, however, the benefit of the cover is improved due to the replenishment of alkalinity to the DST layer from the organic carbon cover.

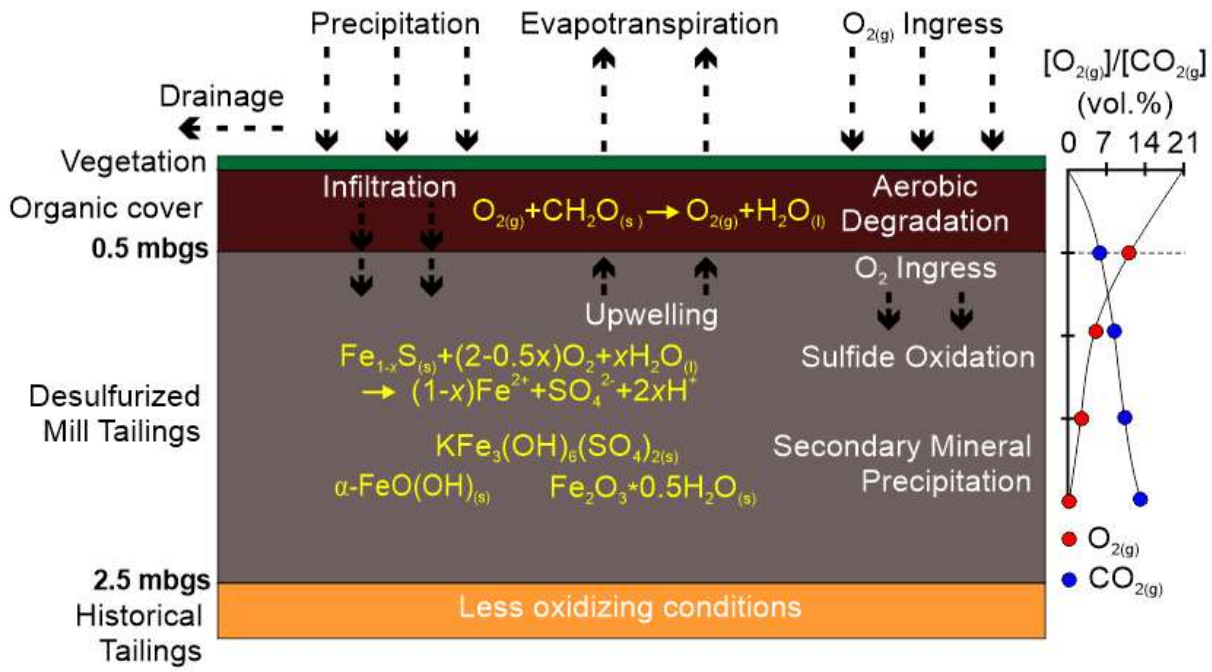

Figure 3.1: Summary of hydrological, geochemical, and microbiological processes occurring in the cover system.

Organic carbon covers are a promising approach for reducing acid generation at tailings storage facilities. However, results from this thesis show the importance of using organic material as a component of a multilayer cover system, because the organic carbon component, alone, may not provide sufficient inhibition to O_2 transport to prevent AMD generation over prolonged periods.

The effective oxygen consumption coefficient of the organic cover can be measured directly through the use of diffusion-consumption cells (Mbonimpa et al., 2003). This effective oxygen consumption coefficient could then be used within a numerical modeling tool designed for unsaturated zone hydrology, such as POLLUTEv7 (GAEA Technologies Ltd., 2004), SEEP/W (GEOSLOPE International Ltd., 2020), or MIN3P-HPC (Su et al., 2020) to back calculate K_r using the results of pore-gas sampling or the O_2 consumption tests. This work would improve the understanding of pore-gas transport through the cover system and would allow for quantitative estimates of organic cover performance in the future (Éthier et al., 2018). O_2

consumption tests should also be performed on the older tailings, which would help delineate the influence of the cover system on the $O_{2(g)}$ flux entering at the surface.

Samples of the tailings could be subjected to additional analyses; such as scanning electron microscopy with energy-dispersive spectroscopy (SEM-EDS) and synchrotron-based x-ray diffraction (XRD). These results could then be compared to pore water results to improve understanding of the mechanisms of release and attenuation of metals within the cover system.

Lastly, a field trial is recommended to understand the effectiveness of organic covers of varying thickness as part of an ongoing maintenance strategy for the organic component of the cover system. It is recommended that three field plots be constructed on the existing organic cover; one plot with a 0.1 m layer, another with a 0.25 m layer, and a third with a 0.5 m layer. The study would provide information on the effect these layers have on $O_{2(g)}$ ingress into the cover system and subsequent change in organic matter consumption rates. The impact of these cover thicknesses on the water table position/fluctuation would also be helpful to ensure that $O_{2(g)}$ diffusion in the DST remains low. This study would help to inform the tailings management team on how to maintain the benefits of the organic cover in the long term by determining 1) how much organic matter should be sourced; and 2) how frequently it should be sourced. This pilot study would help answer the questions “How often should we add organic material?” and “How much material should we add?” Based on current rates, the cost of the organic material, including transportation and installation, averages $23/tonne (Glencore, Personal Communication). At this rate, a 0.1 m increase in the thickness of the organic cover across the entire 20 hectare area of Tailings Cell 1A would cost approximately $350,000.

The results of this research can be used to inform industry and government agencies on the usefulness of using sources of organic carbon as a passive treatment technique for long term mitigation of AMD.

References

Adajar, M.A.Q., Zarco, M.A.H. (2014). An Empirical Model for Predicting Hydraulic Conductivity of Mine Tailings. *International Journal. of Geomate*, *7(2)*, 1054-1061.

Al, T. A., & Blowes, D. W. (1999). The hydrogeology of a tailings impoundment formed by central discharge of thickened tailings: implications for tailings management. *Journal of Contaminant Hydrology*, *38*, 489–505.

Allison, J.D., Brown, D.S., and Novo-Gradac, K.J., 1990, MINTEQA2/PRODEFA2--A geochemical assessment model for environmental systems--version 3.0 user's manual: Environmental Research Laboratory, Office of Research and Development, U.S. Environmental Protection Agency, Athens, Georgia, 106 p.

Arvizu-Valenzuela, L. v, Cruz-Ortega, R., Meza-Figueroa, D., Loredo-Portales, R., Chávez-Vergara, B. M., Mora, L. N., & Molina-Freaner, F. (2020). Barriers for plant establishment in the abandoned tailings of Nacozari, Sonora, Mexico: the influence of compost addition on seedling performance and tailing properties. *Environmental Science and Pollution Research*, *27*, 39635–39650.

The ASCE Standardized Reference Evapotranspiration Equation. Technical Committee on Standardization of Reference Evapotranspiration. American Society of Civil Engineers, 2005. [Online]. Retrieved from: https://ascelibrary.org/doi/book/10.1061/9780784408056

Asemaninejad, A., Langley, S., Mackinnon, T., Spiers, G., Beckett, P., Mykytczuk, N., & Basiliko, N. (2021). Blended municipal compost and biosolids materials for mine reclamation:

Long-term field studies to explore metal mobility, soil fertility and microbial communities. *Science of the Total Environment*, *760*, 143393.

Aubertin, M., Bussière, B., and Chapuis, R. (1996). Hydraulic Conductivity of Homogenized Tailings from Hard Rock Mines. *Canadian Geotechnical Journal*, *33*, 470-482.

Aubertin, M., Dionne, J., and Marcoux, L. (1997). Design, guidelines and stability criteria of engineering works for water covers. In: Proceedings of the Fourth International Conference on Acid Rock Drainage, *4*, May 31 – June 6, Vancouver, BC, pp. 1851-1866.

Aubertin, M., Ricard, J.F., Chapuis, R.P. (1998). A predictive model for the water retention curve: application to tailings from hard-rock mines. *Canadian Geotechnical Journal*, *35*, 55–69.

Ball, J.W. & Nordstrom, D.K., (1991). WATEQ4F—User's manual with revised thermodynamic data base and test cases for calculating speciation of major, trace and redox elements in natural waters: U.S. Geological Survey Open-File Report 90–129, 185 p.

Baptista, M. (2009). "Modelling of the kinetics of municipal solid waste composting in full-scale mechanical biological treatment plants." Ph.D. Dissertation, New University of Lisbon, Portugal.

Barbour, S.L., Wilson, G.W. & St-Arnaud, L.C. (1993). Evaluation of the saturated-unsaturated groundwater conditions of a thickened tailings deposit. *Canadian Geotechnical Journal*, *30(6)*, 935-946.

Beauchemin, S., Clemente, J. S., Thibault, Y., Langley, S., Gregorich, E. G., & Tisch, B. (2018). Geochemical stability of acid-generating pyrrhotite tailings 4 to 5 years after addition of oxygen-consuming organic covers. *Science of the Total Environment*, *645*, 1643–1655.

Benner, S.G., Blowes, D.W., Gould, W.D., Herbert, R.B., Ptacek, C.J. (1999). Geochemistry of a permeable reactive barrier for metals and acid mine drainage. *Environmental Science & Technology, 33(16)*, 2793-2799.

Benner, S.G., Blowes, D.W., Ptacek, C.J., Mayer, K.,U. (2002). Rates of sulfate reduction and metal sulfide precipitation in a permeable reactive barrier. *Applied Geochemistry*, *17*, 301-320.

Blowes, D.W., Ptacek, C.J., Jambor, J.L., Weisener, C.G., Paktunc, D., Gould, W.D. & Johnson, D.B. (2014). The Geochemistry of Acid Mine Drainage. In: Holland, H.D. & Turekian, K.K. (Eds.), Treatise on Geochemistry, 2nd edition, Elsevier Ltd, Oxford, UK, pp. 131-190.

Bolan, N. S., Mahimairaja, S., Baskaran, S., & Naidu, R. (1994). Influence of low-molecular-weight organic acids on the solubilization of phosphates. *Biology and Fertility of Soils*, *18*, 311–319.

Bolan, N., Kunhikrishnan, A., Thangarajan, R., Kumpiene, J., Park, J., Makino, T., Kirkham, M. B., & Scheckel, K. (2014). Remediation of heavy metal(loid)s contaminated soils-To mobilize or to immobilize? *Journal of Hazardous Materials*, *266*, 141–166.

Bouwer, H.M. & Rice, R.C. (1976). A Slug Test for Determining Hydraulic Conductivity of Unconfined Aquifers With Completely or Partially Penetrating Wells. *Water Resources Research*, *12(3)*, 423-428.

Buerge, I.J., Keller, M., Buser, H.R., Muller, M.D., Poiger, T. (2011). Saccharin and Other Artificial Sweeteners in Soils: Estimated Inputs from Agriculture and Households, Degradation, and Leaching to Groundwater. *Environmental Science & Technology*, *45*, 615–621.

Bussière, B. (2007). Colloquium 2004: Hydro-geotechnical properties of hard rock tailings from metal mines and emerging geo-environmental disposal approaches. *Canadian Geotechnical Journal, 44(9)*, 1019-1052.

Campbell, D., Stewart, K., Spiers, G., & Beckett, P. (2017). Growth and metal uptake of canola and sunflower along a thickness gradient of organic-rich covers over metal mine tailings. *Ecological Engineering*, *109*, 133–139.

Canadian Institute for Environmental Law and Policy. (2009). *CIELAP Brief on Biosolids Management in Ontario – June 2009*. Retrieved from: http://www.cielap.org/pdf/Brief_Biosolids.pdf

Carrara, C., Ptacek, C.J., Robertson, W.D., Blowes, D.W., Moncur, M.C., Sverko, E., Backus, S. (2008). Fate of Pharmaceutical and Trace Organic Compounds in Three Septic System Plumes, Ontario, Canada. *Environmental Science & Technology*, *42*, 2805–2811.

Catalan, L.J. (2000). Flooding of Pre-Oxidized Mine Tailings: Mattabi Case Study. (Noranda Technology Centre - MEND Project 2.15.1a). Canadian Centre for Mineral and Energy Technology (CANMET), Ottawa, Ontario. 231 pp. http://mend-nedem.org/wp-content/uploads/2151A.pdf

Chao, A., Chazdon, R.L, Colwell, R.K., Shen, T.J. (2005). A new statistical approach for assessing similarity of species composition with incidence and abundance data. *Ecology Letters 8*, 148-159.

Clark, I.D., & Fritz, P. (1997). Environmental Isotopes in Hydrogeology (1st ed.). CRC Press.

Cobos, D.R. & Chambers, C. (2010). Calibrating ECH2O Soil Moisture Sensors. Decagon Devices Application Note 15922-A. Retrieved from: https://res.cloudinary.com/iwh/image/upload/q_auto,g_center/assets/1/26/Calibrating_ECH2O_Soil_Moisture_Sensors.pdf

Collin, M. (1987). Mathematical Modeling of Water and Oxygen Transport in Layered Soil Covers for Deposits of Pyritic Mine Tailings. Licenciate Treatise, Royal Institute of Technology, Stockholm, Sweden.

Cravotta, C. A. (1998). Effect of Sewage Sludge on Formation of Acidic Ground Water at a Reclaimed Coal Mine. *Groundwater*, *36*(1), 9–19.

Demers, I., Bussière, B., Benzaazoua, M., Mbonimpa, M., & Blier, A. (2008). Column test investigation on the performance of monolayer covers made of desulphurized tailings to prevent acid mine drainage q. *Minerals Engineering*, *21*, 317–329.

Demers, I., Bussiè, B., Mbonimpa, M., & Benzaazoua, M. (2009). Oxygen diffusion and consumption in low-sulphide tailings covers. *Canadian Geotechnical Journal*, *46*, 454–469.

Dold, B. (2003). Speciation of the most soluble phases in a sequential extraction procedure adapted for geochemical studies of copper sulfide mine waste. *Journal of Geochemical Exploration*, *80(1)*, 55-68.

Dold, B. (2014). Submarine Tailings Disposal (STD)—A Review. *Minerals*, *4*(3), 642–666.

Dudeney, A. W. L., Tarasova, I. I., & Tyrologou, P. (2004). Co-utilisation of mineral and biological wastes in mine site restoration. *Minerals Engineering*, *17*, 131–139.

Effluent Monitoring and Effluent Limits – Metal Mining Sector. (1997). O. Reg. 590/94. Retrieved from: https://www.ontario.ca/laws/regulation/940560#BK29

Elberling, B. & Nichholson, R.V. (1996). Field determination of sulphide oxidation rates in mine tailings. *Water Resources Research*, *32(6)*, 1773-1784.

Elliott, L.C., Liu, L., Stogran, W.S. (1996). Organic cover materials for tailings: Do they meet the requirements of an effective long term cover? The Technical and Research Committee on Reclamation. In: Proceedings of the 20th Annual British Columbia Mine Reclamation Symposium in Kamloops, British Columbia, 1996.

Ethier, M. P., Bussière, B., Aubertin, M., Maqsoud, A., Demers, I., & Broda, S. (2018). In situ evaluation of performance of reclamation measures implemented on abandoned reactive tailings disposal site. *Canadian Geotechnical Journal*, *55*(12), 1742–1755.

Feasby, D.G., Tremblay, G.A. and Weatherell, C.J. (1997). A decade of technology improvement to the challenge of acid drainage – A Canadian Perspective. In: Proceedings of the Fourth International Conference on Acid Rock Drainage, *1*, May 31 – June 6, Vancouver, BC, pp. 435-447.

Forsberg, L.S. & Ledin, S. (2006). Effects of sewage sludge on pH and plant availability of metals in oxidising sulphide mine tailings. *Science of the Total Environment*, *358*, 21–35.

GAEA Technologies Ltd., Rowe, R.K., Booker, J.R. (2004). Pollutev7 – Version 7 Reference Guide. Whitby, Ontario, Canada.

GEOSLOPE International Ltd. (2020). Heat and mass transfer modeling with Geostudio 2020 (First Edition). Calgary, Alberta, Canada.

Germain, D., Tassé, N., Bergeron, M. (1992). INRS – Géoressources. Effectiveness of Wood Chips as Contaminant Cover for Mine Tailings. In: Report to Government of Québec, Centre de Recherches Minerales (translated from French).

Germain, D., Tassé, N., Cyr, J. (2009). The East-Sullivan mine site: merging prevention and treatment of acid mine drainage. In: Proceedings of the 14th British Columbia MEND Metal Leaching/Acid Rock Drainage Workshop. Vancouver, BC, Canada.

Grinenko, V.A. & Ivanov, M.V. (1983). Principal reactions of the global biogeochemical cycle of sulphur. In: Ivanov, M.V. & Freney, J.R. (Eds.), The Global Biogeochemical Sulphur Cycle, John Wiley & Sons, Chichester, pp. 1-23.

Gunsinger, M. R., Ptacek, C. J., Blowes, D. W., Jambor, J. L., Moncur, M. C. (2006). Mechanisms controlling acid neutralization and metal mobility within a ni-rich tailings impoundment. *Applied Geochemistry, 21(8)*, 1301-1321.

Hazen, A. (1892). Some physical properties of sands and gravels. *Massachusetts State Board of Health, Annual Report*, pp. 539-556.

Hey, C. & Simms, P. (2021). Preliminary assessment of biosolids in covers with capillary barrier effects. *Engineering Geology*, *280*, 105973.

Hotton, G., Bussière, B., Pabst, T., Bresson, É., & Roy, P. (2020). Influence of climate change on the ability of a cover with capillary barrier effects to control acid generation. *Hydrogeology Journal*, *28*(2), 763–779.

Hulshof, A.H.M., Blowes, D.W. & Gould, W,D (2006). Evaluation of in situ layers for treatment of acid mine drainage: A field comparison. *Water Research*, *40*, 1816-1826.

Hvorslev, M.J. (1951). Time lag and soil permeability in ground-water observations. *U.S. Army Corps of Engineers Waterways Experiment Station Bulletin,* no. 36, pp. 57. Retrieved from https://luk.staff.ugm.ac.id/jurnal/freepdf/Hvorslev1951-USACEBulletin36.pdf

IAEA/WMO (2020). Global Network of Isotopes in Precipitation. The GNIP Database. Retrieved from: https://nucleus.iaea.org/wiser

The Interstate Technology & Regulatory Council Mining Waste Team (2008). Mine Waste Issues in the United States: A White Paper. pp. 64. Retrieved from https://dnr.wi.gov/topic/Mines/documents/overvu.pdf

Jambor, J.L. & Blowes, D.W. (1994). Acid-neutralization mechanisms in inactive mine tailings. In Blowes, D.W. & Jambor, J.L. (Eds.), The Environmental Geochemistry of Sulfide Mine-Wastes, vol. 22, Mineralogical Association of Canada, Nepean, ON, pp. 271-292.

Jambor, J.L. & Blowes, D.W., (1998). Theory and applications of mineralogy in environmental studies of sulfide-bearing mine tailings. In: Cabri, L.J., Vaughan, D.J. (Eds.), Modern Approaches to Ore and Environmental Mineralogy. Mineralogical Association of Canada, Ottawa, pp. 376–401.

Jambor, J. L., & Dutrizac, J. E. (1998). Occurrence and constitution of natural and synthetic ferrihydrite, a widespread iron oxyhydroxide. *Chemical Reviews*, *98*, 2549–2585.

Jia, Y., Nason, P., Alakangas, L., Maurice, C., & Öhlander, B. (2014). Degradation of digested sewage sludge residue under anaerobic conditions for mine tailings remediation. *Environmental Earth Science*, *72*, 3643–3654.

Kinney, C.A., Furlong, E.T., Werner, S.L., Cahill, J.D. (2006). Presence and Distribution of Wastewater-Derived Pharmaceuticals. *Environmental Toxicology and Chemistry*, *25(2)*, 317–326.

Komnitsas, K., Peppas, A. & Halikia, I. (2000). Prediction of the life expectancy of organic covers. *Minerals Engineering*, *13(14)*, 1589-1601.

Lakefield Research Limited Environmental Services (1996). Subaqueous deposition of tailings in the Strathcona Tailings Treatment System. (MEND Project PCA-1). Falconbridge Limited Sudbury Operations, Falconbridge, Ontario. pp. 145. Retrieved from http://mend-nedem.org/wp-content/uploads/PCA-1.pdf

Lakefield Research Limited Environmental Services. (1997). Evaluation of the use of covers for reducing acid generation from Strathcona Tailings. (MEND Project 2.25.3). Falconbridge Limited Sudbury Operations, Falconbridge, Ontario. pp. 262. Retrieved from http://mend-nedem.org/wp-content/uploads/2253.pdf

Lewis, A. E. (2010). Review of metal sulphide precipitation. *Hydrometallurgy*, *104*(2), 222–234.

Li, D., O'Brien, J.W., Tscharke, B.J., Okoffo, E.D., Mueller, J.F., Sun, H., Thomas, K.V. (2021). Artificial sweeteners in end-use biosolids in Australia. *Water Research*. *200*, 117237.

Li, R., Morrison, L., Collins, G., Li, A., & Zhan, X. (2016). Simultaneous nitrate and phosphate removal from wastewater lacking organic matter through microbial oxidation of pyrrhotite coupled to nitrate reduction. *Water Research*, *96*, 32–41.

Lindsay, M.B., Blowes, D.W., Condon, P.D., Ptacek, C.J. (2009). Managing pore-water quality in mine tailings by inducing microbial sulfate reduction. *Environmental Science & Technology*. *43*, 7086-7091.

Lindsay, M.B., Moncur, M.C., Bain, J.G., Jambor, J.L., Ptacek, C.J., Blowes, D.W. (2015). Geochemical and mineralogical aspects of sulfide mine tailings. *Applied Geochemistry*. *57*, 157-177.

Liu, Y.Y., Blowes, D.W., Groza, L., Sabourin, M.J., Ptacek, C.J. (2014). Acesulfame-K and pharmaceuticals as co-tracers of municipal wastewater in a receiving river. *Environ. Sci.: Processes Impacts*, **16**(12):2789-2795.

Makusa, G. P., Bradshaw, S. L., Berns, E., Benson, C. H., & Knutsson, S. (2014). Freeze-thaw cycling concurrent with cation exchange and the hydraulic conductivity of geosynthetic clay liners. *Canadian Geotechnical Journal*, *51*, 591–598.

Mbonimpa et al. (2003). Diffusion and consumption of oxygen in unsaturated cover materials. *Canadian Geotechnical Journal*, *40*, 916-932.

Metal and Diamond Mining Effluent Regulations. (2020). SOR/2002-222. Retrieved from: https://laws-lois.justice.gc.ca/eng/Regulations/SOR-2002-222/FullText.html

Metcalfe, C.D., Miao, X.S., Koenig, B.G., Struger, J. (2003). Distribution of Acidic and Neutral Drugs in Surface Waters Near Sewage Treatment Plants in the Lower Great Lakes, Canada. *Environmental Toxicology and Chemistry*. *22(12)*, 2881–2889.

METER group (2018). 5TE Manual. Pullman, Washington, U.S.A.

O'Kane Consultants Inc. (2017). Global Cover System Design Technical Guidance Document, Final Report. International Network for Acid Prevention (INAP). (Eds.), pp. 216. https://www.inap.com.au/wp-content/uploads/global-cover-system-design.pdf

SENES Consultants Limited (1994). Evaluation of alternate dry covers for the inhibition of acid mine drainage from tailings. (MEND Project 2.20.1). Canadian Centre for Mineral and Energy Technology (CANMET), Ottawa, Ontario. pp. 155. Retrieved from http://mend-nedem.org/wp-content/uploads/2013/01/2.20.1.pdf

Mining Watch Canada (2017, August 14). *Canadian Energy & Mines Ministers Conference: "No Clean Growth without Clean Mining*." Retrieved from: https://miningwatch.ca/news/2017/8/14/canadian-energy-mines-ministers-conference-no-clean-growth-without-clean-mining

Moncur, M.C., Blowes, D.W. & Ptacek, C.J. (2013). Pore-water extraction from the unsaturated and saturated zones. *Canadian Journal of Earth Sciences*, *50*, 1051-1058.

Moncur, M. C., Ptacek, C. J., Blowes, D. W., & Jambor, J. L. (2005). Release, transport and attenuation of metals from an old tailings impoundment. *Applied Geochemistry*, *20*, 639–659.

Morel, F., & Hering, J. G. (1993). Principles and applications of aquatic chemistry. John Wiley & Sons, Inc., New York. 588 p.

Nason, P., Jia, Y., Maurice, C., Alakangas, L., & Öhlander, B. (2016). Biodegradation of Biosolids Under Aerobic Conditions: Implications for Cover Materials for Sulfide Mine Tailings Remediation. *Mine Water and the Environment*, *35*, 273–282.

Nason, P., Alakangas, L. & Ohlander, B. (2013). Using sewage sludge as a sealing layer to remediate sulphidic mine tailings: a pilot-scale experiment, northern Sweden. *Environmental Earth Science*, *70*, 3093-3105.

Neal, A. L., Techkarnjanaruk, S., Dohnalkova, A., McCready, D., Peyton, B. M., and Geesey, G. G. (2001). Iron sulfides and sulfur species produced at hematite surfaces in the presence of sulfate-reducing bacteria. *Geochimica et Cosmochimica Acta,* 65, 223–235.

Nicholson, R.V., Gillham, R.W., Cherry, J.A. & Reardon E.J. (1989). Reduction of acid generation in mine tailings through use of moisture-retaining cover layers as oxygen barriers. *Canadian Geotechnical Journal*, *26*, 1-8.

O'Kane Consultants Inc. (2004). Design, construction, and performance monitoring of cover systems for waste rock and tailings. (MEND Project 2.21.4a), Canadian Centre for Mineral and Energy Technology (CANMET), Ottawa, Ontario. 82 p.p http://www.okc-sk.com/nz/wp-content/uploads/2012/10/MEND-2.21.4a.pdf

Ontario Ministry of the Environment and Climate Change. (2015). *Organic Waste Management in Ontario*. Retrieved from Government of Ontario report: https://files.ontario.ca/food_and_organic_waste_framework.pdf

Pakostova, E., Schmall, A. J., Holland, S. P., White, H., Ptacek, C. J., & Blowes, D. W. (2020). Performance of a geosynthetic-clay-liner cover system at a Cu/Zn mine tailings impoundment. *Applied and Environmental Microbiology*, *86*(8).

Parigi R. 2020. "Nickel isotope geochemistry in mine waste systems". Ph.D. Dissertation, University of Waterloo, ON, Canada.

Parkhurst, D.L., Appello, C.A.J (1999). Users Guide to PHREEQC (Version 2) – A Computer Program for Speciation, Batch-Reaction, One-Dimensional Transport, and Inverse Geochemical Calculations. Water-Resources Investigations Report 99-4259, 326 p.

Pedersen, T. F., Mueller, B., Mcnee, J. J., & Pelletier, C. A. (1993). The early diagenesis of submerged sulphide-rich mine tailings in Anderson Lake, Manitoba. *Canadian Journal of Earth Sciences*, *30*, 1099–1109.

Peppas, A., Komnitsas, K. & Halikia, I. (2000). Use of organic covers for acid mine drainage Control. *Minerals Engineering*, *13(5)*, 563-574.

Pierce, W.G. (1992). Reclamation of sulphide tailings using municipal solid waste compost: literature review and recommendations. (MEND Project 2.25.1a), Centre in Mining and Mineral Exploration Research, Laurentian University, Sudbury, Ontario. 193 pp. http://mend-nedem.org/wp-content/uploads/2251a.pdf

Pierce, W.G., Belzile, N. & Winterhalder, K. (1995). Reclamation of sulphide tailings using municipal solid waste compost: laboratory studies. (MEND Project 2.25.1b), Centre in Mining and Mineral Exploration Research, Laurentian University, Sudbury, Ontario. 127 pp. http://mend-nedem.org/wp-content/uploads/2251B.pdf

Pierce, W.G., Belzile, N., Wiseman, M.E. & Winterhalder, K. (1995). Composted organic wastes as anaeorbic reducing covers for long term abandonment of acid-generating tailings. In: Proceedings from the International Land Reclamation and Mine Drainage Conference and Third International Conference on the Abatement of Acidic Drainage, Pittsburgh, PA, April 24-29, 1994. pp. 148-157.

Proteau, A., Guittonny, M., Bussière, B., & Maqsoud, A. (2020). Aboveground and Belowground Colonization of Vegetation on a 17-Year-old Cover with Capillary Barrier Effect Built on a Boreal Mine Tailings Storage Facility. *Minerals*, *10*, 704–723.

Qdais, H.A. & Al-Widyan, L. (2016). Evaluating composting and co-composting kinetics of various agro-industrial wastes. *International Journal of Recycling of Organic Waste in Agriculture*. *5*, 273–280.

Rakotonimaro, T. v, Guittony, M., & Neculita, C. M. (2021). Compaction of peat cover over desulfurized gold mine tailings changes: Arsenic speciation and mobility. *Applied Geochemistry*, *128*, 104923.

Reardon, E.J. & Moddle, P.M. (1985). Suitability of peat as an oxygen interceptor material for the close-out of pyritic uranium tailings: column studies. *Uranium*, *2*, 83-110.

Reardon, E.J & Poscente, P.J. (1984). A study of gas compositions in sawmill waste deposits: evaluation of the use of wood waste in close-out of pyritic tailings. *Reclamation and Revegetation Research, 3*, 109-128.

Renken, K., Mchaina, D. M., and Yanful, E. K. (2005). Geosynthetics research and applications in the mining and mineral processing environment. In: *Proceedings from the North American Geosynthetics Society/Geosynthetic Institute Conference*, Las Vegas, NV, December 14–16.

Rey, N. J., Demers, I., Bussière, B., & Mbonimpa, M. (2020). Laboratory study of low-sulfide tailings covers with elevated water table to prevent acid mine drainage. *Canadian Geotechnical Journal*, *57*, 1998–2009.

Ribet, I., Ptacek, C. J., Blowes, D. W., & Jambor, J. L. (1995). Contaminant Hydrology The potential for metal release by reductive dissolution of weathered mine tailings. *Journal of Contaminant Hydrology*, *17*, 273.

Robertson, W.D. (1994). The physical hydrogeology of mill-tailings impoundments. In: Blowes DW and Jambor JL (eds.). The Environmental Geochemistry of Sulfide Mine-Wastes, *22*, pp. 1–17. Mineralogical Association of Canada.

Robinsky, E.I. (1975). Thickened discharge – a new approach to tailings disposal. Bulletin of the Canadian Institute of Mining and Metallurgy. *68(764)*, 47–53.

Scharer, J.M., Byerley, J.J., Kwong, E., Nicholson, R.V. (1993). Role of biologically assisted pyrrhotite oxidation in acid mine drainage. United States: Minerals, Metals and Materials Society. In: Proceedings of an International Biohydrometallurgy Symposium, Jackson Hole, WY, August 22-25, 1993. pp. 255-265.

Schippers, A., Breuker, A., Blazejak, A., Bosecker, K., Kock, D., & Wright, T. L. (2010). The biogeochemistry and microbiology of sulfidic mine waste and bioleaching dumps and heaps, and novel Fe(II)-oxidizing bacteria. *Hydrometallurgy*, *104*, 342–350.

Seal, R.R. (2006). Sulfur isotope geochemistry of sulfide minerals. *Reviews in Mineralogy and Geochemistry*, *61(1)*:633–677.

Shackelford, C. D., Sevick, G. W., & Eykholt, G. R. (2009). Hydraulic conductivity of geosynthetic clay liners to tailings impoundment solutions. *Geotextiles and Geomembranes*, *28*, 149–162.

Shen, Y., & Buick, R. (2004). The antiquity of microbial sulfate reduction. *Earth-Science Reviews*, *64*, 243–272.

Simpson, E. H. (1949). Measurement of diversity. *Nature*. *163(4148)*, 688.

Smart, D., Callery, S., & Courtney, R. (2016). The potential for waste-derived materials to form soil covers for the restoration of mine tailings in Ireland. *Land Degradation & Development*, *27*, 542–549.

Soil Moisture Equipment Corp. (2012). Guelph Permeameter 2800 Operating Instructions. Santa Barbara, California, U.S.A.

Spoelstra J, Schiff SL, Brown SJ (2013) Artificial Sweeteners in a Large Canadian River Reflect Human Consumption in the Watershed. *PLOS ONE, 8(12)*, 82706.

Spoelstra, J., Schiff, S., Brown, S.J. (2020). Septic systems contribute artificial sweeteners to streams through groundwater. *Journal of Hydrology X*., *7*, 100050.

Starr, R. C., & Ingleton, R. A. (1992). A new method for collecting core samples without a drill rig. *Groundwater Monitoring & Remediation*, *12*(1), 91–95.

Stogran, S.W. & Wiseman, M.E. (1995). A comparison of organic and inorganic covers for long term prevention or amelioration of acid mine drainage. In: Proceedings of the Sudbury ’95: Mining and Environment Conference, Sudbury, Ontario, May 28 - June 1, 1995, pp.555-563.

Stumm, W. & Morgan, J.J. (1996). Aquatic Chemistry, Third edition, John Wiley & Sons Inc., New York, 1022 p.

Su, D., Mayer, K.U. & MacQuarrie, K.T.B. (2021). MIN3P-HPC: A High-Performance Unstructured Grid Code for Subsurface Flow and Reactive Transport Simulation. *Mathematical Geosciences*, *53*, 517–550.

Tassé, N., Germain, M.D., Bergeron, M. (1994). Composition of Interstitial Gases in Wood Chips Deposited on Reactive Mine Tailings – Consequences for Their Use as an Oxygen Barrier. In: Alpers CN and Blowes, DW (eds.). Environmental Geochemistry of Sulfide Oxidation, vol. 550, pp. 631–644. American Chemical Society.

Tassé, N., Germain, M.D. (2004). The East Sullivan site: from abandonment to restoration. In: Proceedings from the 5th Joint CGS/IAH-CNC Conference, Québec (Québec), October 2004.

Ternes, T.A., Joss, A., Siegrist, H. (2004). Scrutinizing pharmaceuticals and personal care products in wastewater treatment. *Environmental Science and Technology*, *38(20)*, 392A-399A.

Tisch, B., Hargreaves, J., Beckett, P., Lock. A. & Spiers, G. (2012). Post-mining agriculture for biofuels on mine tailings: An overview of results from green mines green energy (GMGE) initiative. In: Hogan, C., Price, W.A., Tremblay, G. (Eds.), Proceedings of the 9th International Conference on Acid Rock Drainage (ICARD), Ottawa, ON May 20-26, 2012.

Waychunas, G. A., Kim, C. S., & Banfield, J. F. (2005). Nanoparticulate iron oxide minerals in soils and sediments: unique properties and contaminant scavenging mechanisms. *Journal of Nanoparticle Research*, *7*, 409–433.

Woyshner, M. & St. Arnaud, L. (1994). Hydrogeological evaluation and water balance of a thickened tailings deposit near Timmins, Ontario. In: American Society of Mining and Reclamation (Eds.), Proceedings from the International Land Reclamation and Mine Drainage

Conference and Third International Conference on the Abatement of Acidic Drainage, Pittsburgh, PA, April 24-29, 1994. pp. 198-207.

Wunderley, M.D., Blowes, D.W., Frind, E.O., Ptacek, C.J. (1996). Sulfide mineral oxidation and subsequent reactive transport of oxidation products in mine tailings impoundments: A numerical model. *Water Resources Research*, *32(10)*: 3173-3187.

Appendix A:

Further Description of Methods

Groundwater Flow

The groundwater flow system was characterized using available piezometers that were on site. Wells were surveyed and GPS-located by a contractor during the summer of 2018. Routine water level monitoring occurred every groundwater sampling episode by measuring the depth-to-water using model 101 or model 102 Solinst® water level meters. This depth-to-water was converted to total head using the following equation:

$$H = z + \psi$$

Where H, z and ψ are the total head, elevation head and pressure head, respectively.

Elevation head was determined by subtracting the surveyed elevation at the top of the well by the depth of the well. Pressure head was determined by measuring the length between the bottom of the well and the water level. Horizontal hydraulic gradients were determined by the difference in total head between two wells of similar depth, while the vertical hydraulic gradients were determined by the difference in total head between two wells within the same well nest.

Single Well Response Tests

Hydraulic conductivity in the saturated portion of the tailings was determined by both constant head tests and rising head tests, conducted at select locations within the SWWTS. Constant head tests were completed by pumping water out of the well at a constant rate; measuring the change in water level that occurred until the water level was constant (i.e. discharge = recharge), using a water level tape. The horizontal hydraulic conductivity could then be calculated through the following rearranged form of Hvorslev's equation (1951).

$$K_H = \frac{ln\left\{\frac{mL}{2r_w}\right\}}{2\pi L} \times \frac{Q}{\Delta H}$$

Where m is the anisotropy ratio (assumed to be 1), L is the length of the water column in the well (m), r_w is the radius of the well screen (m), Q is the pumping rate ($m^3\ s^{-1}$), and ΔH is the change in water level (m). These tests were completed on wells where rising head test were deemed impractical, due to the high pumping rates that would have been required.

Rising head tests involved pumping the water level in the well down to a specified point (usually the bottom of the well) and observing the recovery of the water level using a Levelogger®. The data from the levelogger was input into the analytical software AquiferTest® (Waterloo Hydrogeologic, 2020) using the Bouwer and Rice analysis. For further information on these tests, please refer to Butler (1997).

Once I had all of the head measurements for each of the five water level monitoring episodes as well as the geometric-mean K of the tailings from both the constant and rising head tests, I was able to input these values into the excel-based program HydroGeoEstimatorXL (Devlin, 2017) which calculated the hydraulic gradient, groundwater flow direction and groundwater velocity.

Installation of Soil Moisture Probes

Sixteen ECH$_2$O 5TE soil moisture probes (METER group, Pullman, WA, USA) were installed at four different locations by first excavating a borehole using a hand auger and then installing the probes vertically by removing the plastic coating and installing the prongs firmly into the material. All probes were originally installed within the same borehole, with excavated material being backfilled between each probe. All were connected to EM50 dataloggers (METER group, Pullman, WA, USA). Medium-specific calibrations were completed for the organic cover

material and the desulfurized tailings following methods described in Cobos and Chambers (2010).

Installation of Tensiometers

Sixteen Model 2710ARL standard tensiometers (Soil Moisture, Santa Barbara, CA, USA) were also installed by excavating a borehole using a hand auger and then installing the tensiometer, after ensuring that the porous ceramic tip was wetted and placed into the bottom of the borehole, ensuring that silica flour was placed around the anulus of the ceramic tip. Then, the excavated material was backfilled into the borehole. Each tensiometers was connected to a Model 5310 current transducer which were in turn connected to one DataDolphin Model 400 datalogger per location (Optimum Instruments of Edmonton, AB).

Core Sample Collection

Solid-phase samples of the organic layer were collected by hand, using a shovel and a 19 L utility pail. Samples of the underlying tailings were collected in 1.5 m (5 foot) aluminum tubes of 5.08 or 7.12 cm (2 or 3 inch) diameter. A scaffold was set up and a vibrating hammer was used to drive the piston and core barrel into the subsurface for core collection. This was completed to depths up to 4.5 m. After core collection, the core samples were retrieved, cut in order to remove headspace, capped on either end and frozen, where required. Further description of this method can be found in Starr and Ingleton (1992).

The compression of the tailings was then calculated using the following expression.

$$Compression\ factor = \frac{Theoretical\ length}{Actual\ length}$$

Where the theoretical length is based on the difference in the depth between the top and bottom of the core and the actual length is how long the core sample is once retrieved. The compression factor was calculated for each core sample and used to determine the actual depth. Core samples were then cut length-wise and changes in colour, lithology and the presence of potential oxidation were noted. They were then sub-sampled for further analyses.

Total Carbon-Sulfur Analysis

Total % carbon and total % sulfur of the tailings were determined by an ELTRA CS 2000 Carbon Sulfur Determinator attached to an induction furnace (Eltra Elemental Analyzers, Newtown, PA). The sample is heated up in the analyzer and the amount of gas-phase sulfur and carbon that is driven off is determined. The process involved the following steps:

1) Obtain a ceramic crucible and tare it on a scale
2) Place 1.4 g of Fe pellets into the crucible and tare
3) Place 2.2 g of Mn pellets into the crucible and tare
4) Place sample into crucible and place into analyzer

The amount of sample used depended on the concentration of C and S in the sample. Calibration curves for all four sensors (High/Low, C/S) were built for my samples, using Eltra standards and the proprietary software *Elements*. Each sample was run a minimum of five times and the values were averaged. Any values that were not within a relative percent difference (RPD) of 10% were not included in the average.

Sulfur Speciation

The speciation of S in solid-phase samples was completed using a modification of the extraction procedure described in Dold (2003).

Part 1

1) 0.8 g of dried tailings sample and 40 mL of Milli-Q® water were placed in a 50 mL falcon tube and mixed end-over-end for 1 hour at room temperature
2) Ran the samples on an ion chromatograph ()
3) Converted the SO_4 concentrations (in mg L^{-1}) to a mass of dissolved SO_4 by multiplying by the volume of each aqueous sample (i.e. 40 mL).

Part 2

4) Ammonium oxalate [$(NH_4)_2C_2O_4$] solution was made using Milli-Q® water and ammonium oxalate crystals. 2 N Hydrochloric acid (HCl) was added until the pH was 3.0
5) A fresh 0.5 g sample of dried tailings and 50 mL of ammonium oxalate solution were placed into a 50 mL falcon tube.
6) A 2 L glass beaker was filled and the falcon tubes (seven or eight at a time) were placed into it. This beaker was then placed on a hot plate for 1 hour at a temperature between 80 and 100^0C.
7) Converted the SO_4 concentrations (in mg L^{-1}) to a mass of dissolved SO_4 by multiplying by the volume of each aqueous sample (i.e. 50 mL).

Subtract the total weight of S by the total weight of the two forms of SO_4 in each sample. From this you can calculate the mass of sulfide. Divide each of these masses by the total mass of the sample to calculate the weight % of each proportion.

X-Ray Fluorescence

Pellets were made for x-ray fluorescence (XRF) analysis by mixing 7.5 g of sample with 1.5 g of cellulose binder (SamplePrep, Metuchen, NJ, USA) and pressed using a twenty tonne press (GENEQ inc., Montreal, QC, CA). A calibration curve was built for the tailings at the SWWTS by selecting one sample of pyrrhotite tailings (ML5-2.8m), one of visually-oxidized desulfurized tailings (ML34-3.15m) and one of visually-unoxidized desulfurized tailings (ML34-4.0m). All three of these samples were sent to 3 accredited commercial laboratories (ALS, BVM, and SGS) for analysis. After this, total elemental content in the tailings samples were determined using a PANalytical MiniPal4 X-ray fluorescence (XRF) spectrometer (Malvern Panalytical, Malvern, UK). Results were reported as oxide but were converted to elemental form by using the molar mass of each compound.

Pore Gas Sampling

A stainless steel rod system, consisting of an inner rod with a flat top and an outer rod (0.80 cm in diameter), were used for pore-gas sampling along with a portable O_2 and CO_2 analyzer (Quantek Instruments, Grafton, MA, USA). These were the steps:

1) Rod system was driven 10 cm into the subsurface
2) The inner rod was removed and a septum was placed over top of the outer gas rod
3) Used a 60 mL syringe with a thin (≥ 18 gauge) needle to purge ~120 mL from the gas rod
4) Sample was taken and inserted into the portable gas analyzer and the lowest number was taken. Typically 120 mL was used for sampling
5) Place sample in exetainer® (Labco Ltd., Lampeter, UK) for $\delta^{13}C$-CO_2

Pore Water

EH, pH and alkalinity measurements were taken immediately after pore-water extraction to avoid stagnant water in the syringe. All aqueous samples were stored at 4°C prior to chemical analyses and were filtered with either 0.2-µm polyether sulfone membrane or 0.45-µm sterile Durapore® PVDF membrane.

The following are parameters that were determined in the field, with an explanation of methods:

1) pH and Eh → Orion pH and EH probes (Thermo Scientific, USA) coupled to Orion Star A321 pH Portable Meters (Thermo Scientific, USA). EH and pH measurements were taken every one or two minutes for at least ten minutes per sample, with the lowest EH value considered the most representative.
2) Alkalinity → determined by titration with either 0.16N or 1.6N H_2SO4 using a HACH digital titrator and colour indicator, following HACH method 8203.
3) S^{2-} → used a HACH DR/2400 portable spectrophotometer (Hach Company, Loveland, CO) and followed HACH method 8131
4) NH_3-N → used a HACH DR/2400 portable spectrophotometer (Hach Company, Loveland, CO) and followed HACH method 10023 for low range (0-2.5 mg L^{-1} NH_3-N) and 10031 for high range (0-50 mg L^{-1} NH_3-N)
5) PO_4-P → used a HACH DR/2400 portable spectrophotometer (Hach Company, Loveland, CO) and followed HACH method 8048
6) Isotopes of H and O → determined using a cavity ringdown spectrophotometer (Picarro L2130-i, Santa Clara, CA, USA).
7) δS^{34}-SO_4 and δO^{18}-SO_4 → determined at the University of Calgary and University of Waterloo using an elemental analyzer high temperature conversion isotope ratio mass

spectroscopy (EA/HTC-IRMS). $\delta^{34}S$ was referenced using Vienna canyon diablo troilite (VCDT) and $\delta^{18}O$ was referenced using Vienna standard mean ocean water (SMOW) of precipitated $BaSO_4$

8) Cation samples → preserved in the field using HNO_3 to pH < 2. Concentrations determined through inductively coupled plasma-optical emission spectrometry (ICP-OES, Thermo Scientific ICAP 6500) and inductively coupled plasma-mass spectrometry (ICP-MS, Thermo Scientific X Series II).
9) Anions samples → analyzed by ion chromatography (IC, Dionex DX 600)
10) DOC samples → preserved using H_2SO_4 to pH < 2. Concentrations determined using an Aurora 1030W TOC Analyzer (O.I Analytical, College Station, TX, USA), using wet oxidation with heated sodium persulfate. Inorganic carbon was removed from the sample by the addition of 5% H_3PO_4 prior to analysis.
11) Pharmaceutical compounds carbamazepine, caffeine, sulfamethoxazole, ibuprofen, gemfibrozil, naproxen → analyzed using a solid-phase extraction process described by Liu et al. (2014).
12) Artificial sweetener compounds Acesulfame-K, Cyclamate, Saccharin, Sucralose → determined by IC-MS/MS (Dionex, Sunnyvale, CA, USA) which consisted of the ICS 5000 ion chromatography system coupled to a Agilent 6460 MS Quadrupole (Agilent, Mississauga, ON).

Appendix B:

Supplementary Materials

Table B.1: Results from grain size analysis at ML5. Note: Coefficient of Uniformity calculated based on measured d60/d10 values.

Sample ID	Grain Size Description	Effective Grain Diameters (mm)					Coefficient of Uniformity	Hydraulic Conductivity - Hazen (m/s)	Hydraulic Conductivity - Modified Kozeny-Carmen (m/s)
		d10	d17	d20	d50	d60			
ML5-0.5m	Poorly sorted clay with fines	0.001	0.003	0.003	0.013	0.017	12.28	1.91E-08	2.56E-08
ML5-0.5m (dup)	Poorly sorted clay with fines	0.001	0.002	0.003	0.012	0.015	12.47	1.54E-08	2.07E-08
ML5-0.7m	Poorly sorted silt with fines	0.002	0.004	0.005	0.018	0.022	11.74	3.52E-08	4.64E-08
ML5-0.7m (dup)	Poorly sorted silt with fines	0.002	0.003	0.004	0.017	0.021	11.92	3.25E-08	4.31E-08
ML5-1.5m	Poorly sorted sandy silt with fines	0.005	0.012	0.015	0.042	0.051	11.16	2.10E-07	2.72E-07
ML5-1.5m (dup)	Poorly sorted sandy silt with fines	0.004	0.012	0.014	0.040	0.050	11.23	1.98E-07	2.57E-07
ML5-2.5m	Poorly sorted silt with fines	0.003	0.007	0.010	0.026	0.032	10.85	8.74E-08	1.12E-07
ML5-2.5m (dup)	Poorly sorted silt with fines	0.003	0.007	0.009	0.025	0.031	11.00	7.97E-08	1.03E-07
ML5-2.65m	Poorly sorted clay with fines	0.001	0.002	0.003	0.013	0.016	12.57	1.72E-08	2.32E-08
ML5-2.65m (dup)	Poorly sorted clay with fines	0.001	0.002	0.003	0.013	0.017	12.77	1.73E-08	2.34E-08
ML5-2.8m	Poorly sorted silt with fines	0.002	0.004	0.005	0.019	0.023	12.10	3.63E-08	4.83E-08
ML5-2.8m (dup)	Poorly sorted silt with fines	0.002	0.003	0.005	0.018	0.022	12.41	3.09E-08	4.15E-08
ML5-2.95m	Poorly sorted silt with fines	0.002	0.003	0.004	0.017	0.021	12.86	2.78E-08	3.78E-08
ML5-2.95m (dup)	Poorly sorted silt with fines	0.002	0.003	0.004	0.016	0.020	12.77	2.54E-08	3.44E-08
ML5-3.5m	Poorly sorted sandy silt with fines	0.003	0.007	0.009	0.033	0.065	22.18	8.47E-06	1.38E-05
ML5-3.5m (dup)	Poorly sorted sandy silt with fines	0.003	0.006	0.008	0.029	0.057	20.90	7.48E-08	1.19E-07
ML5-4.0m	Poorly sorted silt with fines	0.002	0.004	0.005	0.020	0.025	12.66	3.77E-08	5.10E-08
ML5-4.0m (dup)	Poorly sorted silt with fines	0.002	0.003	0.004	0.018	0.023	12.99	3.04E-08	4.14E-08
ML5-4.5m	Poorly sorted clay with fines	0.001	0.002	0.003	0.010	0.014	10.65	1.68E-08	2.14E-08
ML5-4.5m (dup)	Poorly sorted clay with fines	0.001	0.002	0.003	0.011	0.014	10.91	1.64E-08	2.11E-08

Table B.2: Results from grain size analysis at ML32. Note: Coefficient of Uniformity calculated based on measured d60/d10 values.

Sample ID	Grain Size Description	Effective Grain Diameters (mm)					Coefficient of Uniformity	Hydraulic Conductivity - Hazen (m/s)	Hydraulic Conductivity - Kozeny-Carmen (m/s)
		d10	d17	d20	d50	d60			
ML32-0.5m	Poorly sorted clay with fines	0.001	0.003	0.003	0.012	0.016	11.57	1.91E-08	2.51E-08
ML32-0.5m (dup)	Poorly sorted clay with fines	0.001	0.002	0.003	0.011	0.015	11.36	1.74E-08	2.27E-08
ML32-0.8m	Poorly sorted silt with fines	0.003	0.005	0.007	0.019	0.023	8.90	6.70E-08	8.06E-08
ML32-0.8m (dup)	Poorly sorted silt with fines	0.002	0.005	0.006	0.018	0.022	9.26	5.61E-08	6.84E-08
ML32-1.15m	Poorly sorted silt with fines	0.002	0.004	0.005	0.018	0.022	10.26	4.72E-08	595E-08
ML32-1.15m (dup)	Poorly sorted silt with fines	0.002	0.004	0.005	0.017	0.021	10.51	4.14E-08	5.26E-08
ML32-1.5m	Poorly sorted clay with fines	0.002	0.003	0.004	0.015	0.019	12.13	2.53E-08	3.37E-08
ML32-1.5m (dup)	Poorly sorted clay with fines	0.002	0.003	0.004	0.016	0.020	12.42	2.62E-08	3.52E-08
ML32-2.35m	Poorly sorted sand with fines	0.002	0.004	0.005	0.085	0.149	78.94	3.57E-08	8.83E-08
ML32-2.35m (dup)	Poorly sorted sandy silt with fines	0.002	0.004	0.005	0.061	0.107	63.26	2.88E-08	6.62E-08
ML32-2.6m	Poorly sorted silt with fines	0.002	0.004	0.005	0.020	0.024	11.73	4.06E-08	5.35E-08
ML32-2.6m (dup)	Poorly sorted silt with fines	0.002	0.004	0.005	0.018	0.022	11.83	3.56E-08	4.70E-08
ML32-2.85m	Poorly sorted sand with fines	0.002	0.005	0.007	0.063	0.078	38.41	4.11E-08	8.01E-08
ML32-2.85m (dup)	Poorly sorted sandy silt with fines	0.002	0.004	0.006	0.062	0.076	39.43	3.73E-08	7.33E-08

Table B.3: Results from grain size analysis at ML33. Note: Coefficient of Uniformity calculated based on measured d60/d10 values.

Sample ID	Grain Size Description	Effective Grain Diameters (mm)					Coefficient of Uniformity	Hydraulic Conductivity - Hazen (m/s)	Hydraulic Conductivity - Modified Kozeny-Carmen (m/s)
		d10	d17	d20	d50	d60			
ML33-0.15m	Poorly sorted sandy silt with fines	0.004	0.009	0.011	0.030	0.047	10.96	1.86E-07	2.40E-07
ML33-0.15m (dup)	Poorly sorted sandy silt with fines	0.004	0.009	0.011	0.029	0.041	9.57	1.86E-07	2.29E-07
ML33-0.52m	Poorly sorted clay with fines	0.002	0.004	0.005	0.014	0.017	8.82	3.90E-08	4.68E-08
ML33-0.52m (dup)	Poorly sorted clay with fines	0.002	0.003	0.004	0.013	0.016	8.94	3.22E-08	3.88E-08
ML33-0.75m	Poorly sorted clay with fines	0.001	0.002	0.003	0.010	0.014	12.29	1.33E-08	1.78E-08
ML33-0.75m (dup)	Poorly sorted clay with fines	0.001	0.002	0.003	0.011	0.014	12.34	1.35E-08	1.81E-08
ML33-0.85m	Poorly sorted clay with fines	0.001	0.003	0.003	0.014	0.018	12.98	1.90E-08	2.59E-08
ML33-0.85m (dup)	Poorly sorted clay with fines	0.001	0.002	0.003	0.013	0.017	12.97	1.80E-08	2.45E-08
ML33-1.5m	Poorly sorted clay with fines	0.001	0.003	0.003	0.013	0.017	12.12	2.03E-08	2.70E-08
ML33-1.5m (dup)	Poorly sorted clay with fines	0.001	0.003	0.003	0.014	0.018	12.32	2.07E-08	2.77E-08
ML33-1.85m	Poorly sorted clay with fines	0.002	0.003	0.003	0.014	0.018	12.01	2.27E-08	3.02E-08
ML33-1.85m (dup)	Poorly sorted clay with fines	0.001	0.003	0.003	0.014	0.018	12.09	2.22E-08	2.96E-08
ML33-2.05m	Poorly sorted silt with fines	0.002	0.003	0.004	0.017	0.021	12.40	2.87E-08	3.85E-08
ML33-2.05m (dup)	Poorly sorted silt with fines	0.002	0.003	0.004	0.016	0.020	12.37	2.71E-08	3.63E-08
ML33-2.4m	Poorly sorted sand with fines	0.003	0.008	0.011	0.066	0.083	25.93	1.02E-07	1.75E-07
ML33-2.4m (dup)	Poorly sorted sandy silt with fines	0.003	0.008	0.011	0.061	0.077	25.43	9.08E-08	1.54E-07
ML33-3.0m	Poorly sorted sandy silt with fines	0.002	0.004	0.005	0.022	0.059	33.74	3.05E-08	5.70E-08
ML33-3.0m (dup)	Poorly sorted sandy silt with fines	0.002	0.004	0.005	0.023	0.057	31.74	3.20E-08	5.86E-08
ML33-3.5m	Poorly sorted clay with fines	0.001	0.002	0.003	0.010	0.013	11.08	1.35E-08	1.75E-8
ML33-3.5m (dup)	Poorly sorted clay with fines	0.001	0.002	0.003	0.010	0.014	11.36	1.44E-08	1.88E-08
ML33-4.2m	Poorly sorted clay with fines	0.001	0.002	0.003	0.012	0.015	11.75	1.68E-08	2.22E-08
ML33-4.2m (dup)	Poorly sorted clay with fines	0.001	0.002	0.003	0.011	0.015	11.77	1.55E-08	2.05E-08

Table B.4: Results from grain size analysis at ML34. Note: Coefficient of Uniformity calculated based on measured d60/d10 values.

Sample ID	Grain Size Description	Effective Grain Diameters (mm)					Coefficient of Uniformity	Hydraulic Conductivity - Hazen (m/s)	Hydraulic Conductivity - Modified Kozeny-Carmen (m/s)
		d10	d17	d20	d50	d60			
ML34-0.5m	Poorly sorted sandy silt with fines	0.004	0.008	0.010	0.032	0.049	13.68	1.28E-07	1.77E-07
ML34-0.5m (dup)	Poorly sorted sandy silt with fines	0.003	0.007	0.009	0.028	0.043	13.11	1.06E-07	1.45E-07
ML34-1.0m	Poorly sorted clay with fines	0.001	0.003	0.003	0.012	0.017	11.61	2.02E-08	2.65E-08
ML34-1.0m (dup)	Poorly sorted clay with fines	0.001	0.003	0.003	0.013	0.017	12.01	1.96E-08	2.60E-08
ML34-1.5m	Poorly sorted clay with fines	0.001	0.002	0.003	0.012	0.016	11.94	1.85E-08	2.45E-08
ML34-1.5m (dup)	Poorly sorted clay with fines	0.001	0.002	0.003	0.013	0.017	12.26	1.83E-08	2.45E-08
ML34-1.7m	Poorly sorted clay with fines	0.002	0.003	0.004	0.015	0.019	12.33	2.49E-08	3.34E-08
ML34-1.7m (dup)	Poorly sorted clay with fines	0.001	0.003	0.003	0.014	0.018	12.30	2.15E-08	2.88E-08
ML34-2.5m	Poorly sorted silt with fines	0.002	0.003	0.004	0.016	0.020	12.79	2.56E-08	3.47E-08
ML34-2.5m (dup)	Poorly sorted clay with fines	0.002	0.003	0.004	0.016	0.020	12.79	2.39E-08	3.24E-08
ML34-3.15m	Poorly sorted silt with fines	0.002	0.004	0.005	0.021	0.026	13.40	3.91E-08	5.38E-08
ML34-3.15m (dup)	Poorly sorted silt with fines	0.002	0.004	0.005	0.021	0.026	13.73	3.60E-08	5.00E-08
ML34-3.5m	Poorly sorted clay with fines	0.002	0.003	0.003	0.015	0.019	12.55	2.29E-08	3.09E-08
ML34-3.5m (dup)	Poorly sorted clay with fines	0.001	0.003	0.003	0.014	0.018	12.38	2.04E-08	2.74E-08
ML34-4.0m	Poorly sorted sandy silt with fines	0.002	0.005	0.007	0.027	0.038	16.54	5.25E-08	7.75E-08
ML34-4.0m (dup)	Poorly sorted silt with fines	0.002	0.005	0.006	0.025	0.036	16.70	4.64E-08	6.87E-08

Table B.5: Results from grain size analysis at ML35. Note: Coefficient of Uniformity calculated based on measured d60/d10 values.

Sample ID	Grain Size Description	Effective Grain Diameters (mm)					Coefficient of Uniformity	Hydraulic Conductivity - Hazen (m/s)	Hydraulic Conductivity - Modified Kozeny-Carmen (m/s)
		d10	d17	d20	d50	d60			
ML35-0.5m	Poorly sorted silt with fines	0.002	0.005	0.006	0.021	0.026	10.63	5.84E-08	7.45E-08
ML35-0.5m (dup)	Poorly sorted silt with fines	0.002	0.004	0.005	0.020	0.025	11.35	4.70E-08	6.13E-08
ML35-0.75m	Poorly sorted sandy silt with fines	0.003	0.007	0.009	0.033	0.057	16.98	1.14E-07	1.70E-07
ML35-0.75m (dup)	Poorly sorted sandy silt with fines	0.003	0.006	0.008	0.029	0.052	16.65	9.96E-08	1.47E-07
ML35-1.5m	Poorly sorted clay with fines	0.001	0.002	0.003	0.012	0.016	12.32	1.77E-08	2.37E-08
ML35-1.5m (dup)	Poorly sorted clay with fines	0.001	0.002	0.003	0.012	0.017	12.66	1.73E-08	2.34E-08
ML35-2.5m	Poorly sorted clay with fines	0.001	0.002	0.002	0.007	0.010	9.85	1.00E-08	1.24E-08
ML35-2.5m (dup)	Poorly sorted clay with fines	0.001	0.002	0.002	0.007	0.010	9.73	9.58E-09	1.19E-08
ML35-3.5m	Poorly sorted clay with fines	0.001	0.002	0.003	0.011	0.015	11.78	1.56E-08	2.06E-08
ML35-3.5m (dup)	Poorly sorted clay with fines	0.001	0.002	0.003	0.011	0.015	11.97	1.53E-08	2.03E-08
ML35-4.0m	Poorly sorted clay with fines	0.001	0.002	0.002	0.007	0.010	10.25	9.85E-09	1.24E-08
ML35-4.0m (dup)	Poorly sorted clay with fines	0.001	0.002	0.002	0.007	0.010	10.22	9.63E-09	1.21E-08
ML35-4.6m	Poorly sorted clay with fines	0.001	0.002	0.002	0.008	0.010	9.95	1.08E-08	1.35E-08
ML35-4.6m (dup)	Poorly sorted clay with fines	0.001	0.002	0.002	0.007	0.010	10.03	1.05E-08	1.31E-08

Table B.6: Results from x-ray fluorescence and carbon-sulfur analysis at ML5, ML32 and ML33. Note: % and ppm units are used.

Sample ID	Depth (m)	Al (%)	Ca (%)	Fe (%)	K (%)	Mg (%)	Mn (%)	Na (%)	S (%)	Si (%)	Ti (%)	C (ppm)	Cu (ppm)	Ni (ppm)	Zn (ppm)
ML5-0.5m	0.50	7.53	6.00	9.15	1.04	5.91	0.12	2.18	0.82	26.67	0.37	2156.6	343.8	1616.9	87.6
ML5-0.7m	0.70	6.68	6.03	11.73	0.89	3.98	0.10	2.16	1.59	23.71	0.37	890.5	428.3	948.3	88.4
ML5-1.5m	1.50	7.91	5.11	7.98	0.86	3.73	0.10	3.06	0.84	28.73	0.35	321.6	360.9	658.4	82.2
ML5-2.5m	2.50	6.07	4.23	15.86	0.81	2.49	0.09	0.56	2.12	22.14	0.36	738.4	2484.9	3233.6	115.4
ML5-2.65m	2.65	1.63	0.59	37.00	0.11	0.06	0.02	0.64	28.11	2.69	0.14	522.8	459.8	5353.9	85.1
ML5-2.8m	2.80	3.13	1.99	36.87	0.36	1.15	0.06	0.91	19.71	10.92	0.21	338.1	1278.3	6666.1	119.1
ML5-2.95m	2.95	2.21	1.05	48.50	0.22	0.58	0.08	0.97	24.16	6.74	0.22	535.9	1146.9	7540.5	121.9
ML5-3.5m	3.50	5.76	4.03	18.20	0.75	2.44	0.12	1.85	5.49	21.88	0.36	463.8	618.9	1646.2	100.8
ML5-4.0m	4.00	5.55	3.30	20.94	0.75	1.69	0.10	2.52	12.25	20.07	0.27	513.5	363.2	2682.4	89.2
ML5-4.5m	4.50	5.06	3.40	24.92	0.74	2.37	0.11	1.82	11.56	18.20	0.28	639.0	449.6	3576.8	101.0
ML32-0.5m	0.50	8.18	4.69	8.44	1.14	4.00	0.11	2.42	0.43	26.71	0.36	1850.0	325.6	1509.2	83.0
ML32-0.8m	0.80	6.86	4.75	10.05	1.20	3.62	0.10	2.09	0.79	23.47	0.33	1250.0	218.2	619.3	78.3
ML32-1.15m	1.15	6.75	7.39	8.81	1.09	4.53	0.10	1.18	1.14	22.96	0.37	4013.3	514.6	1922.5	99.9
ML32-1.5m	1.50	7.73	5.34	8.47	1.14	4.00	0.11	2.21	0.84	25.95	0.35	1533.0	329.5	1487.3	87.9
ML32-2.35m	2.35	6.29	4.15	16.34	0.71	3.55	0.13	1.50	6.29	22.44	0.41	268.5	1194.8	2004.6	104.8
ML32-2.6m	2.60	7.79	4.30	8.55	1.04	2.92	0.10	2.45	1.23	26.76	0.32	580.5	500.2	1646.3	91.3
ML32-2.85m	2.85	6.02	4.61	7.75	0.81	2.25	0.08	1.56	0.33	21.90	0.30	297.8	267.9	300.1	71.6
ML33-0.15m	0.15	5.64	7.10	9.47	0.83	4.22	0.11	0.94	1.33	20.05	0.30	1092.7	828.9	1728.0	90.7
ML33-0.52m	0.52	7.69	5.44	9.06	1.05	3.47	0.11	2.03	1.06	23.76	0.36	714.8	290.6	2257.9	84.0
ML33-0.75m	0.75	7.87	5.53	7.93	1.10	3.81	0.12	2.27	0.73	25.84	0.34	1863.2	493.8	2056.5	88.3
ML33-0.85m	0.85	7.57	5.54	8.19	0.98	5.51	0.12	2.00	0.70	24.76	0.32	2303.4	335.2	1447.9	80.4
ML33-1.5m	1.50	7.73	5.64	8.47	1.16	4.47	0.11	2.06	0.57	26.09	0.35	3270.3	328.1	1490.0	85.8
ML33-1.85m	1.85	7.42	5.07	8.65	1.07	4.14	0.11	1.83	0.48	24.70	0.36	1433.2	346.4	1188.6	86.1
ML33-2.05m	2.05	6.22	4.11	7.28	1.05	3.18	0.09	1.09	0.45	21.29	0.31	631.9	195.8	1151.9	77.3
ML33-2.4m	2.40	6.95	4.76	10.95	0.81	3.52	0.11	1.96	2.55	24.96	0.34	568.6	764.5	1195.0	92.7
ML33-3.0m	3.00	7.06	4.48	10.14	0.85	3.27	0.11	2.03	1.94	24.86	0.30	1595.9	874.8	1089.1	87.0
ML33-3.5m	3.50	8.06	5.27	8.48	1.10	5.02	0.13	1.86	0.37	26.44	0.34	3090.7	519.0	1395.1	89.5
ML33-4.2m	4.20	7.42	4.91	8.23	0.97	3.63	0.11	1.81	1.18	24.95	0.32	2528.9	2234.1	1444.0	88.1

Table B.7: Results from x-ray fluorescence and carbon-sulfur analysis at ML34 and ML35. Note: % and ppm units are used.

Sample ID	Depth (m)	Al (%)	Ca (%)	Fe (%)	K (%)	Mg (%)	Mn (%)	Na (%)	S (%)	Si (%)	Ti (%)	C (ppm)	Cu (ppm)	Ni (ppm)	Zn (ppm)
ML34-0.5m	0.50	6.11	6.56	11.20	0.88	3.36	0.11	1.93	1.32	22.32	0.35	1264.5	583.5	599.8	85.4
ML34-1.0m	1.00	7.16	6.16	8.07	1.13	5.30	0.12	1.73	0.79	24.07	0.36	1561.2	375.1	1795.3	85.7
ML34-1.5m	1.50	7.01	5.93	8.49	1.08	4.83	0.13	1.46	0.65	23.95	0.38	3468.2	269.7	1594.7	89.2
ML34-1.7m	1.70	6.23	4.50	6.46	1.07	3.24	0.08	1.08	0.65	20.19	0.29	1083.5	235.9	1257.6	72.6
ML34-2.5m	2.50	8.11	4.63	8.89	1.04	4.34	0.12	2.91	1.03	28.97	0.33	514.4	449.7	1418.8	86.4
ML34-3.15m	3.15	7.07	4.91	9.11	0.87	2.40	0.10	2.32	0.46	24.92	0.35	1846.5	288.6	614.1	78.1
ML34-3.5m	3.50	8.30	4.60	7.69	1.11	3.35	0.11	3.12	0.77	28.46	0.33	1103.0	319.8	1188.3	78.7
ML34-4.0m	4.00	7.43	4.19	9.11	1.04	2.23	0.10	2.48	1.85	26.14	0.29	860.0	1675.2	1279.4	87.6
ML35-0.5m	0.50	7.26	5.12	8.91	1.05	4.29	0.11	1.88	0.50	24.76	0.32	5673.3	287.0	1027.6	82.0
ML35-0.75m	0.75	6.91	6.24	8.68	0.78	4.81	0.10	1.82	1.18	24.05	0.26	4277.4	559.5	899.1	83.4
ML35-1.5m	1.50	7.60	5.43	8.71	1.08	4.09	0.11	1.92	0.71	25.27	0.36	4731.7	313.4	1361.1	89.6
ML35-2.5m	2.50	7.75	4.89	9.10	1.00	4.30	0.14	1.97	0.48	25.16	0.36	1343.0	298.3	2165.0	85.2
ML35-3.5m	3.50	8.04	4.27	8.18	1.09	2.98	0.12	2.56	0.52	26.91	0.35	687.5	432.9	1897.7	83.1
ML35-4.0m	4.00	8.37	4.26	8.78	1.25	3.30	0.14	2.43	0.58	26.91	0.36	1526.6	753.7	2633.2	88.6
ML35-4.6m	4.60	7.96	4.43	8.66	1.20	2.99	0.13	2.24	0.59	26.17	0.36	1896.3	403.0	2409.4	88.6

Table B.8: Parameters used in the Pyrox model for August 2019 and October 2019 modelling simulations. Note: data that differ between August and October are separated by a forward slash.

Location	ML5	ML32	ML33	ML34	ML35	Units	Source
Parameters							
D^2 of oxidized coating	1×10^{-14}	1×10^{-14}	1×10^{-14}	1×10^{-14}	1×10^{-14}	$m^2 \cdot s^{-1}$	Estimated
Initial Normalized O_2	1.00	1.00	1.00	1.00	1.00	N/A	Measured
Number of nodes – Aug / Oct 2019	39/17	71/71	67/67	61/61	65/65	N/A	N/A
Chemical properties							
Fraction of S	Variable	Variable	Variable	Variable	Variable	$kg \cdot kg^{-1}$	Measured
Fraction of Ni	0.008	0.008	0.008	0.008	0.008	$kg \cdot kg^{-1}$	Estimated
Temperature, T	Variable	Variable	Variable	Variable	Variable	^0C	Estimated
Physical properties							
Grain radius	0.016	0.010	0.008	0.010	0.012	mm	Measured
Bulk density	1.55	1.55	1.55	1.55	1.55	$kg \cdot m^{-3}$	Calculated Average
Porosity	0.45	0.45	0.45	0.45	0.45	$m^3 \cdot m^{-3}$	Calculated Average
Moisture Content	Variable	Variable	Variable	Variable	Variable	$m^3 \cdot m^{-3}$	Measured
Depth of vadose zone – August 2019/Oct 2019	1.9/0.8	3.5/3.5	3.3/3.3	3.0/3.0	3.2/3.2	m	Measured

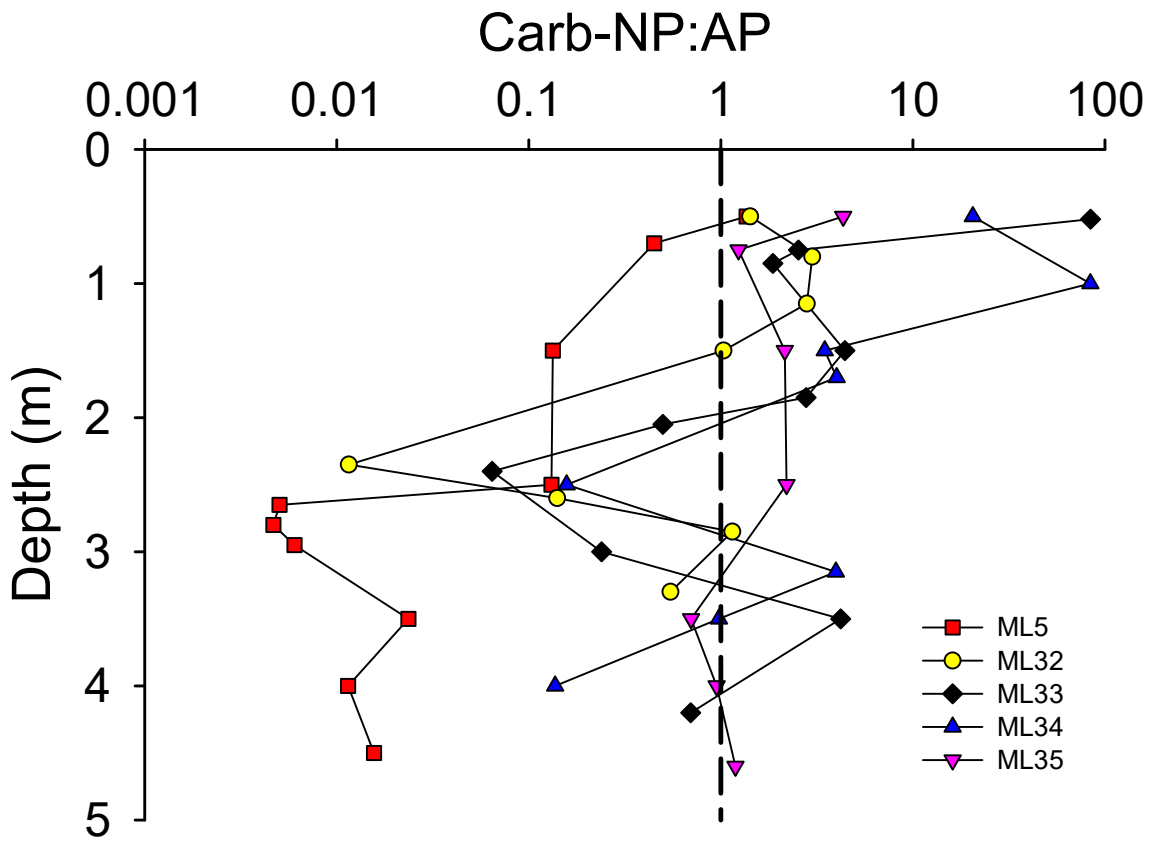

Figure B.1: Depth profiles of the ratio between the carbonate-neutralization potential and the acid generating potential of the tailings. The vertical dashed line represents Carb-NP:AP = 1.

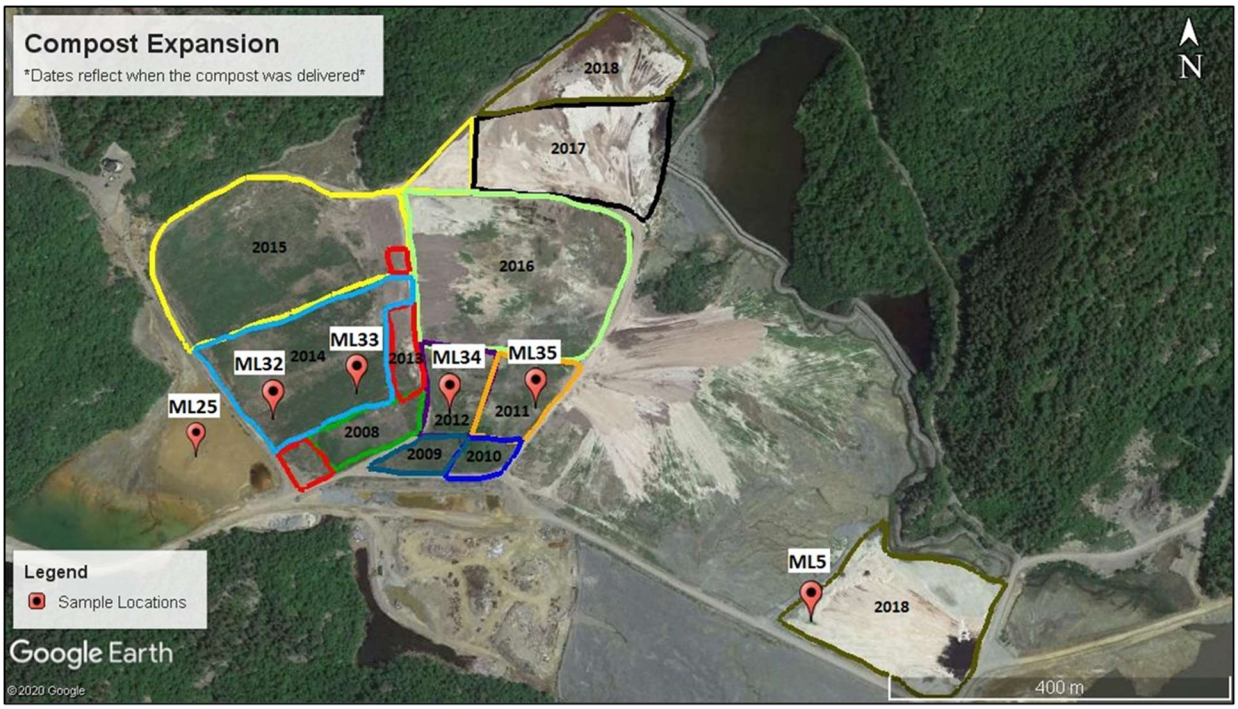

Figure B.2: Expansion of organic material at the SWWTS over time.

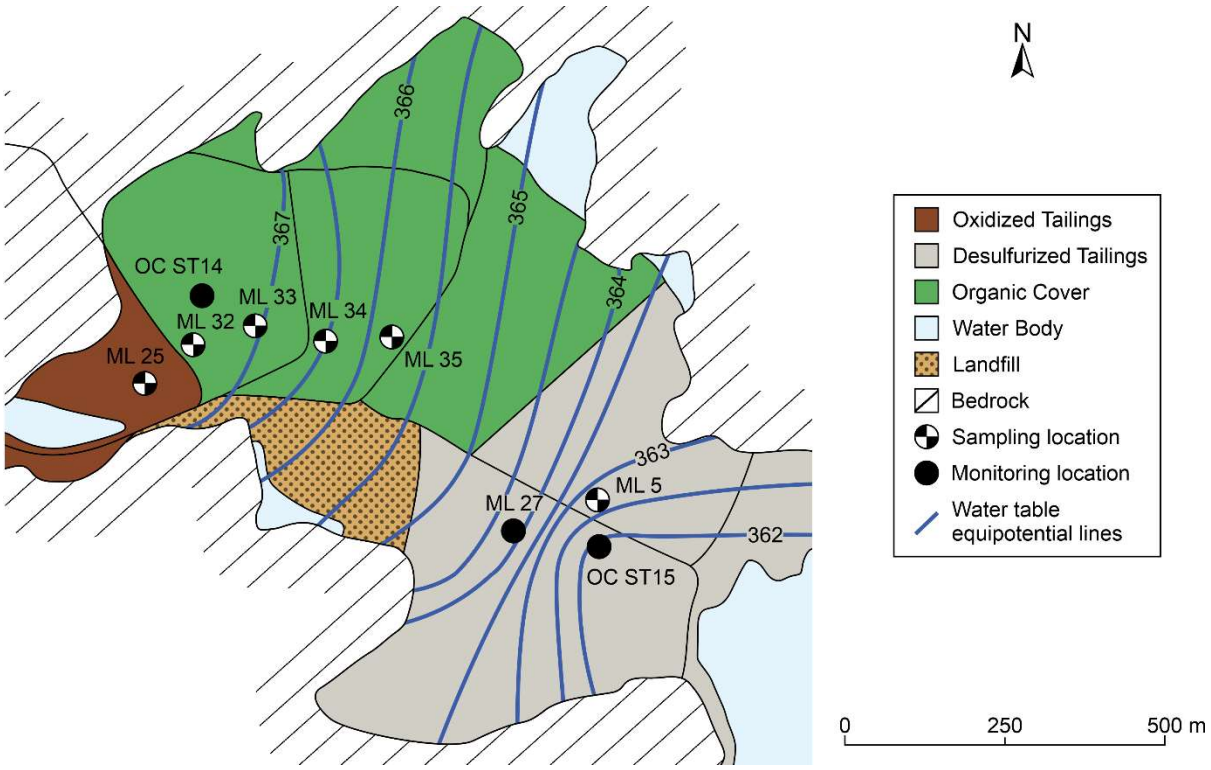

Figure B.3: Water table map of the SWWTS in July 2018.

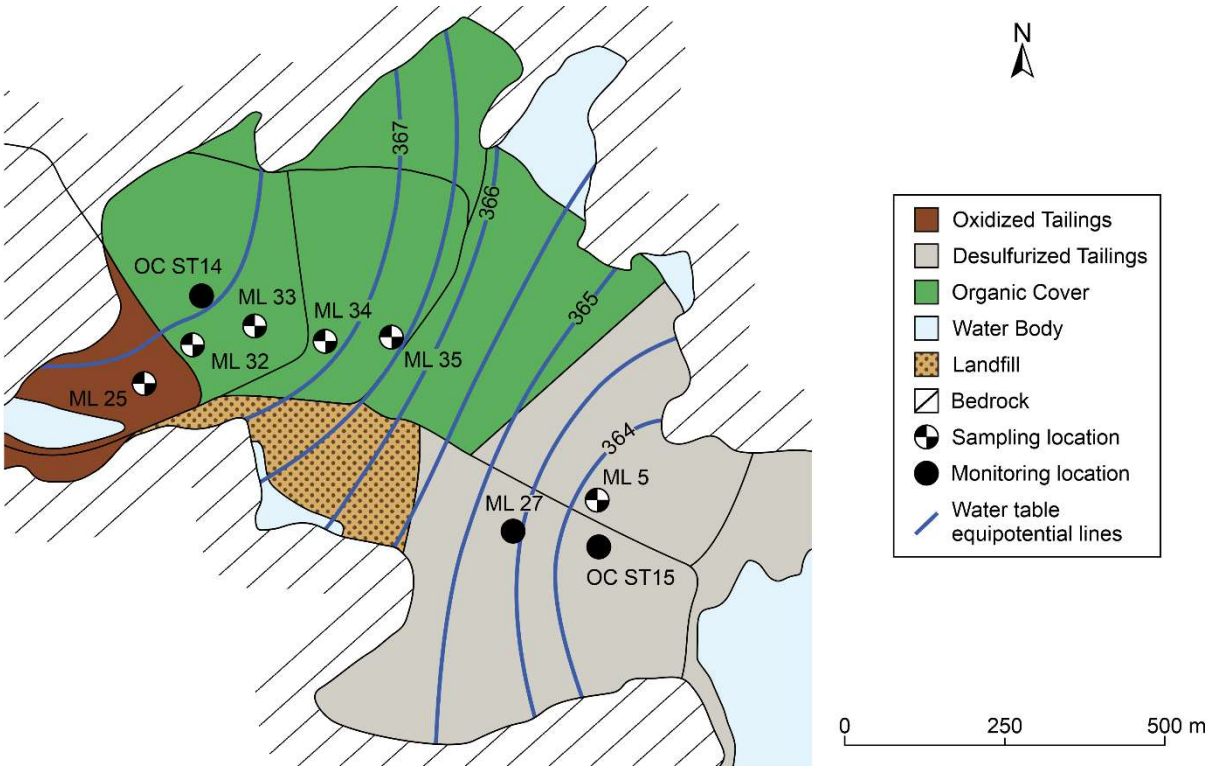

Figure B.4: Water table map of the SWWTS in December 2018.

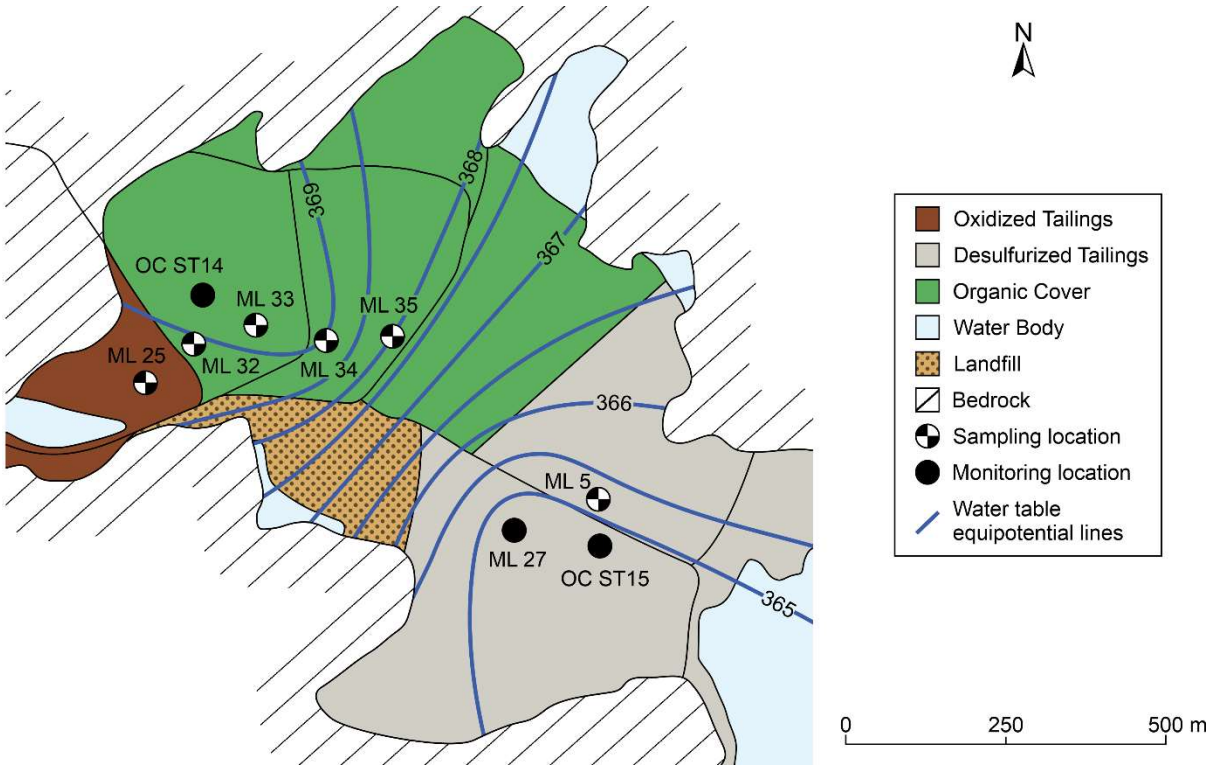

Figure B.5: Water table map of the SWWTS in May 2019.

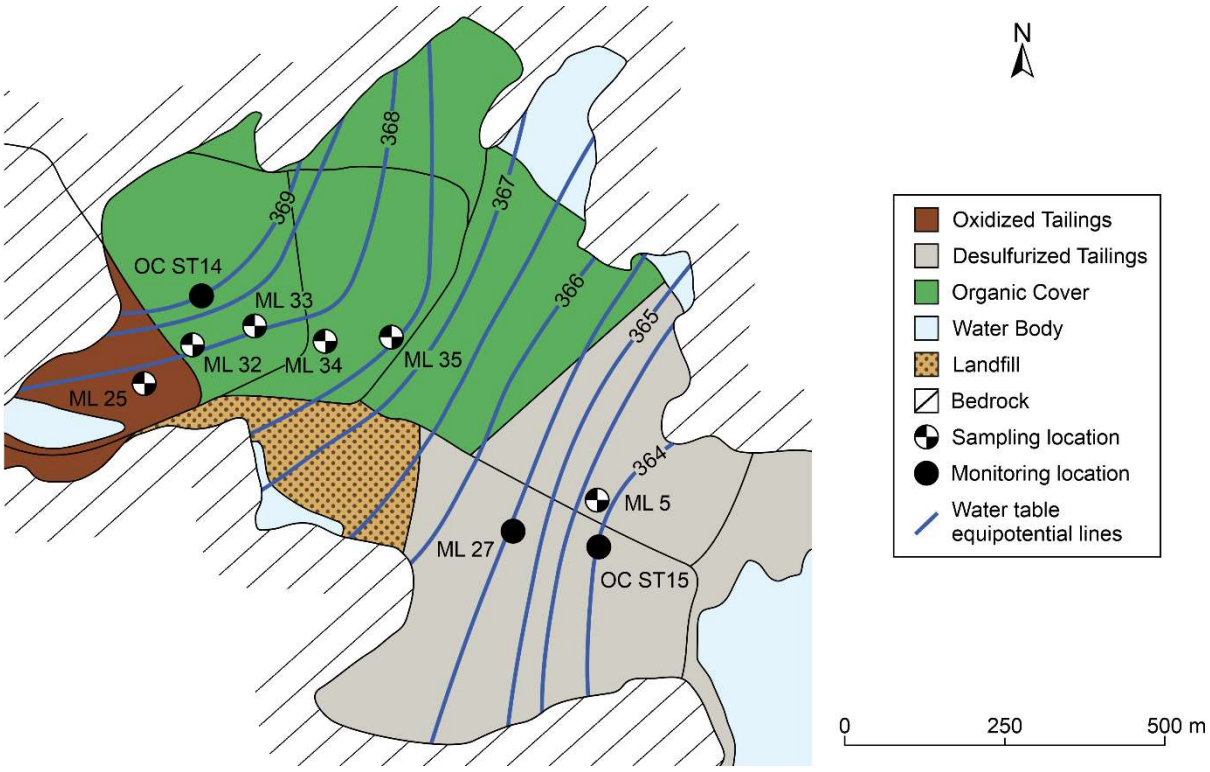

Figure B.6: Water table map of the SWWTS in July 2019.

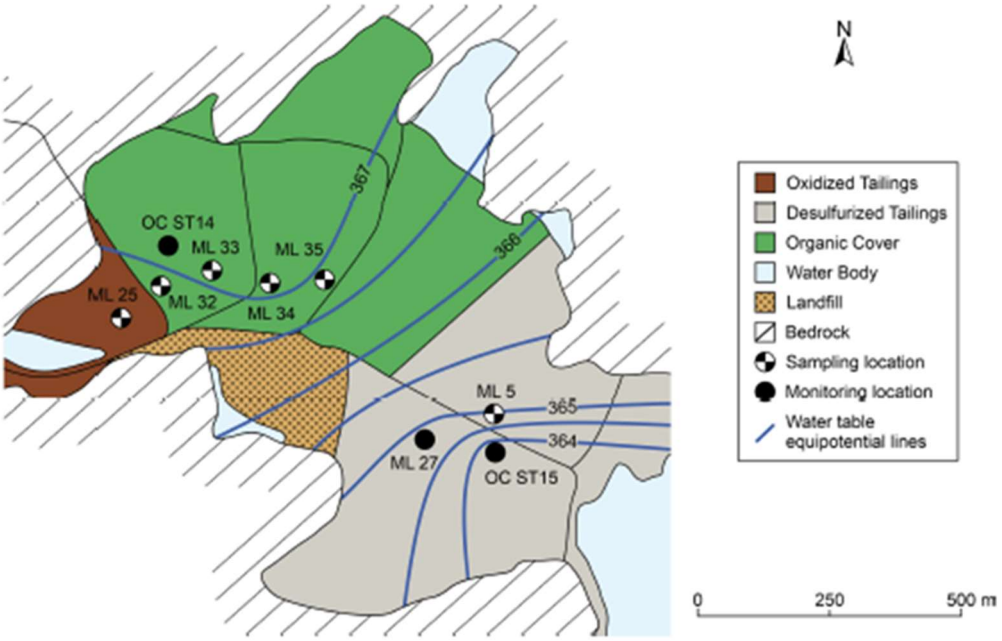

Figure B.7: Water table map of the SWWTS in October 2019.

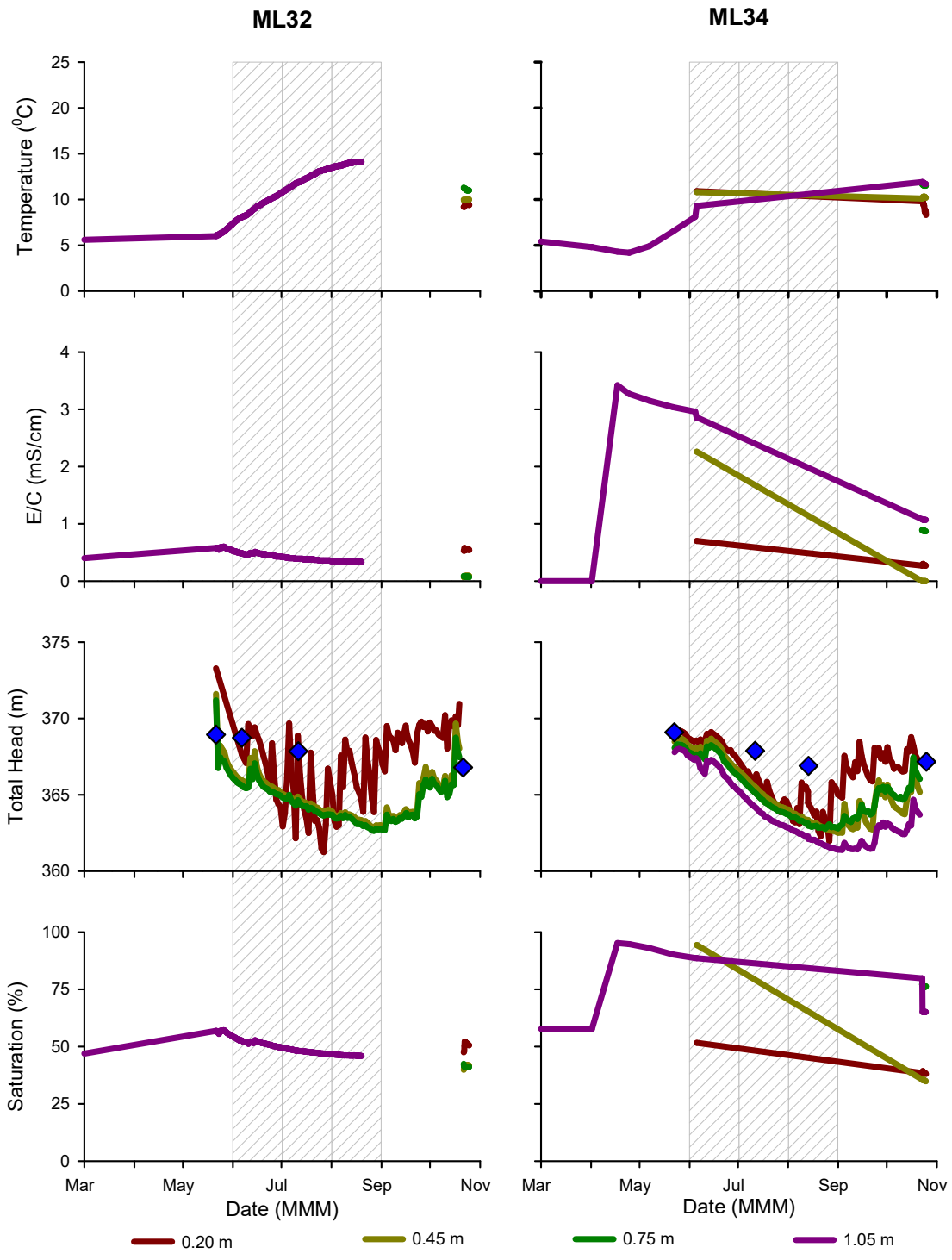

Figure B.8: Total head, saturation, and temperature within and beneath the organic cover at ML32 and ML34 during the 2019 field season. Note: blue diamonds represent the manual water level monitoring episodes between May and October 2019, the water table levels ranged from 366.79 to 368.94 masl at ML32 and 366.89 to 369.09 masl at ML34. The grey hatched boxes represent months where the total evaporation (mm) was higher than the total precipitation (mm). Saturation was derived by dividing VWC by porosity.

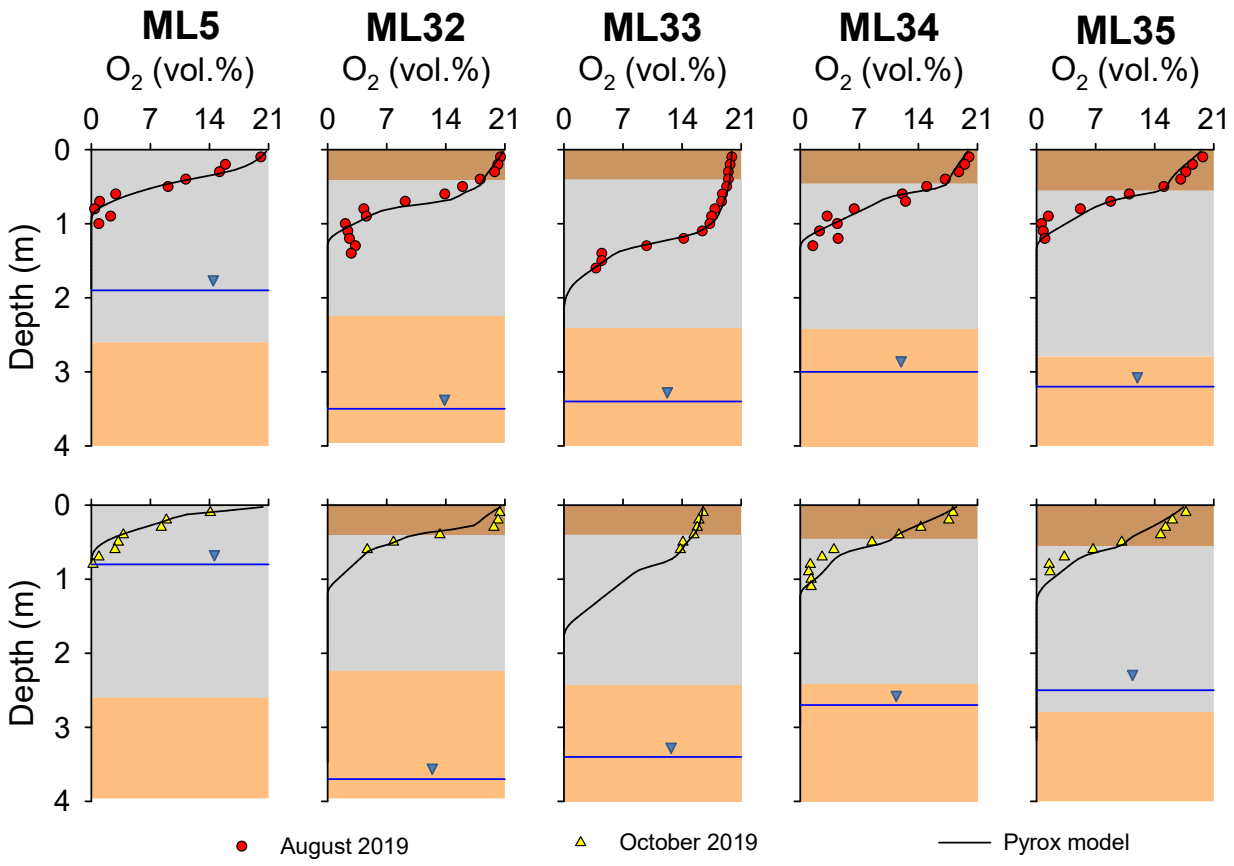

Figure B.9: Pyrox simulations based on August 2019 and October 2019 $O_{2(g)}$ profiles. Note: the blue lines, medium dashed lines, and long dashed lines represent the water table, base of organic cover and base of desulfurized tailings, respectively.

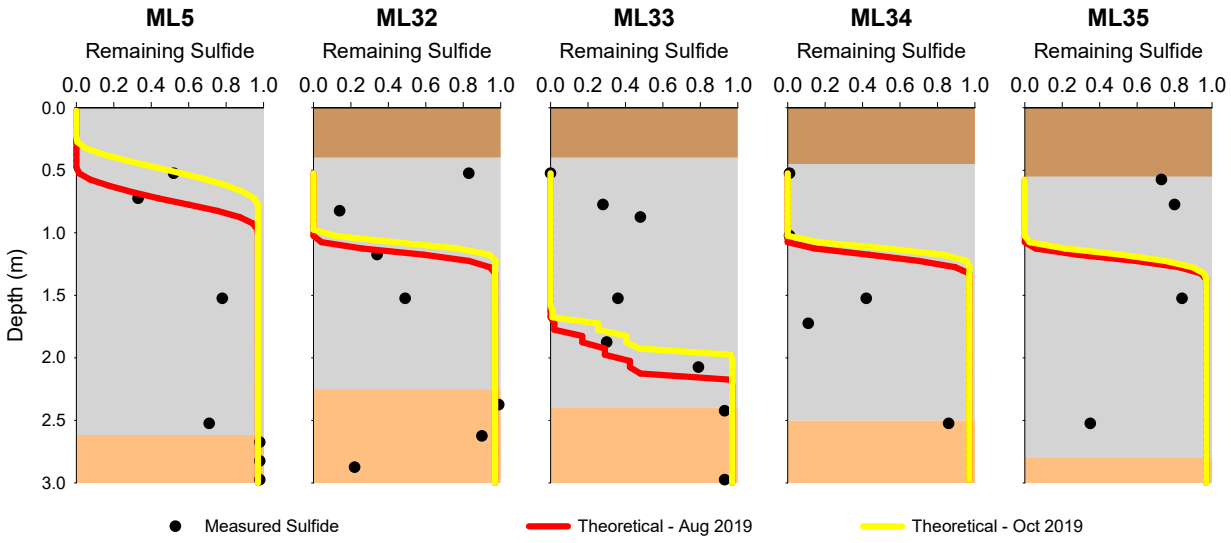

Figure B.10: Profiles of measured proportions of sulfide remaining in the tailings compared to calculated proportions of sulfide remaining for the August 2019 and October 2019 modelling simulations. Note: the medium dashed lines, and long dashed lines represent the base of organic cover and base of desulfurized tailings, respectively.

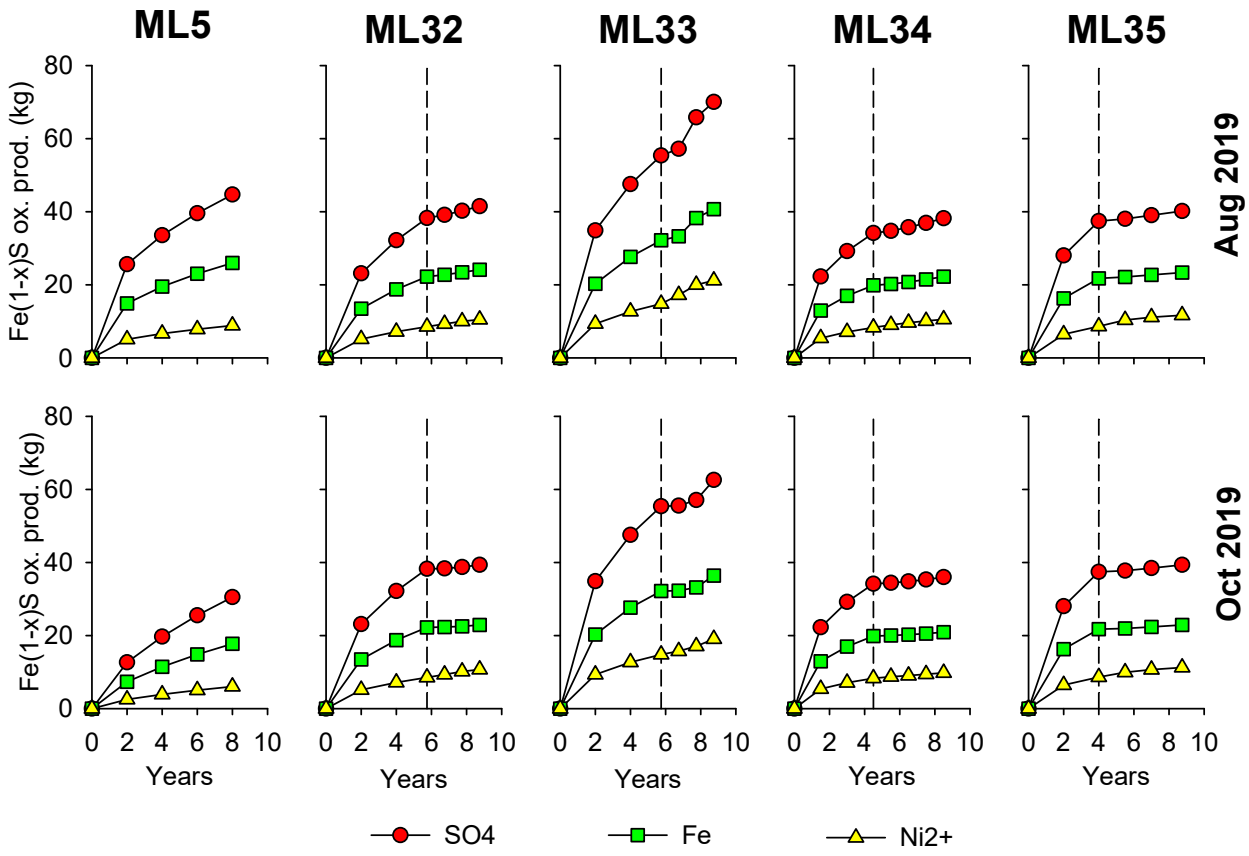

Figure B.11: Oxidation products released over time during the August 2019 and October 2019 modelling simulations. Note: the vertical dashed line represents the placement of the organic cover.

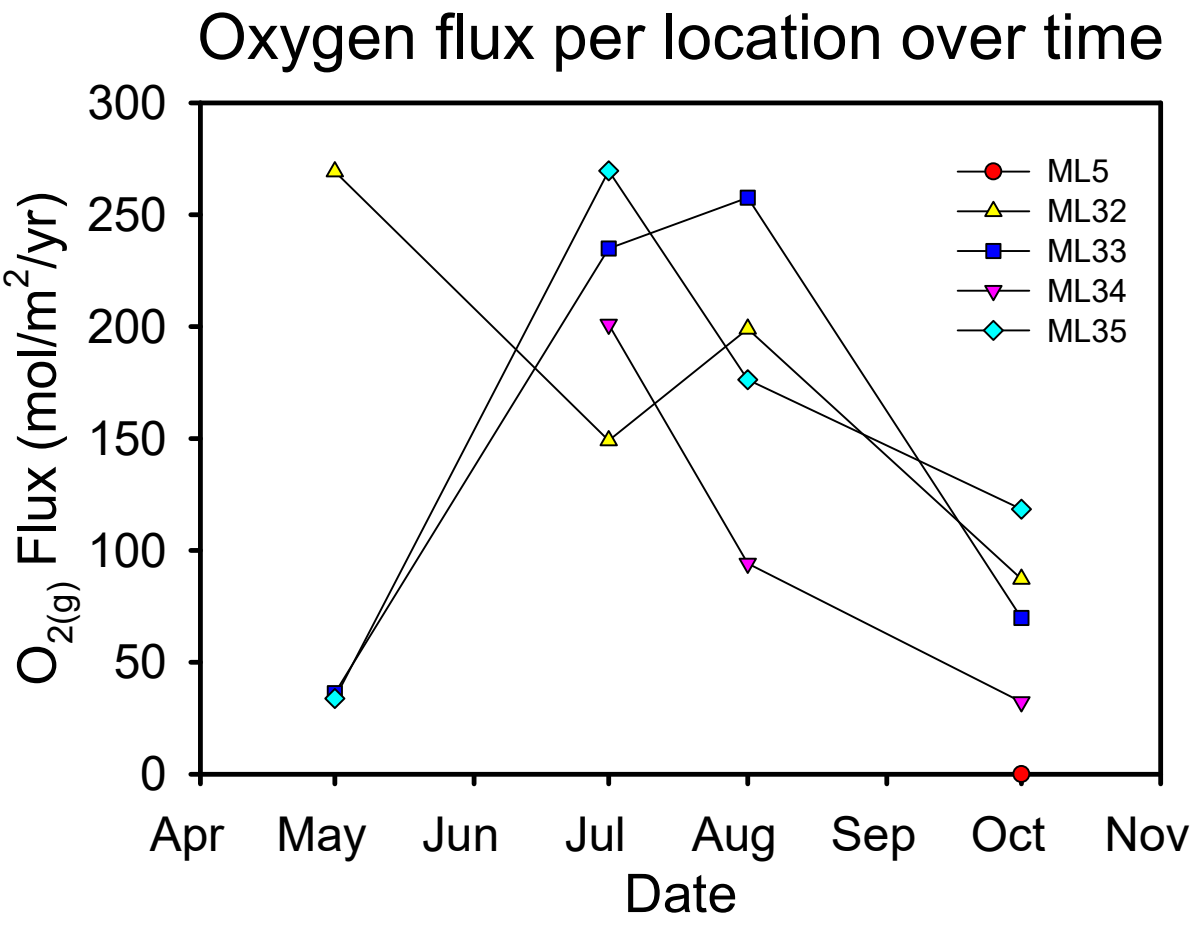

Figure B.12: Oxygen fluxes in the cover system, per location, throughout the 2019 field season. Note: ML5 has a 1-layer cover while ML32 through ML35 have a 2-layer cover system.

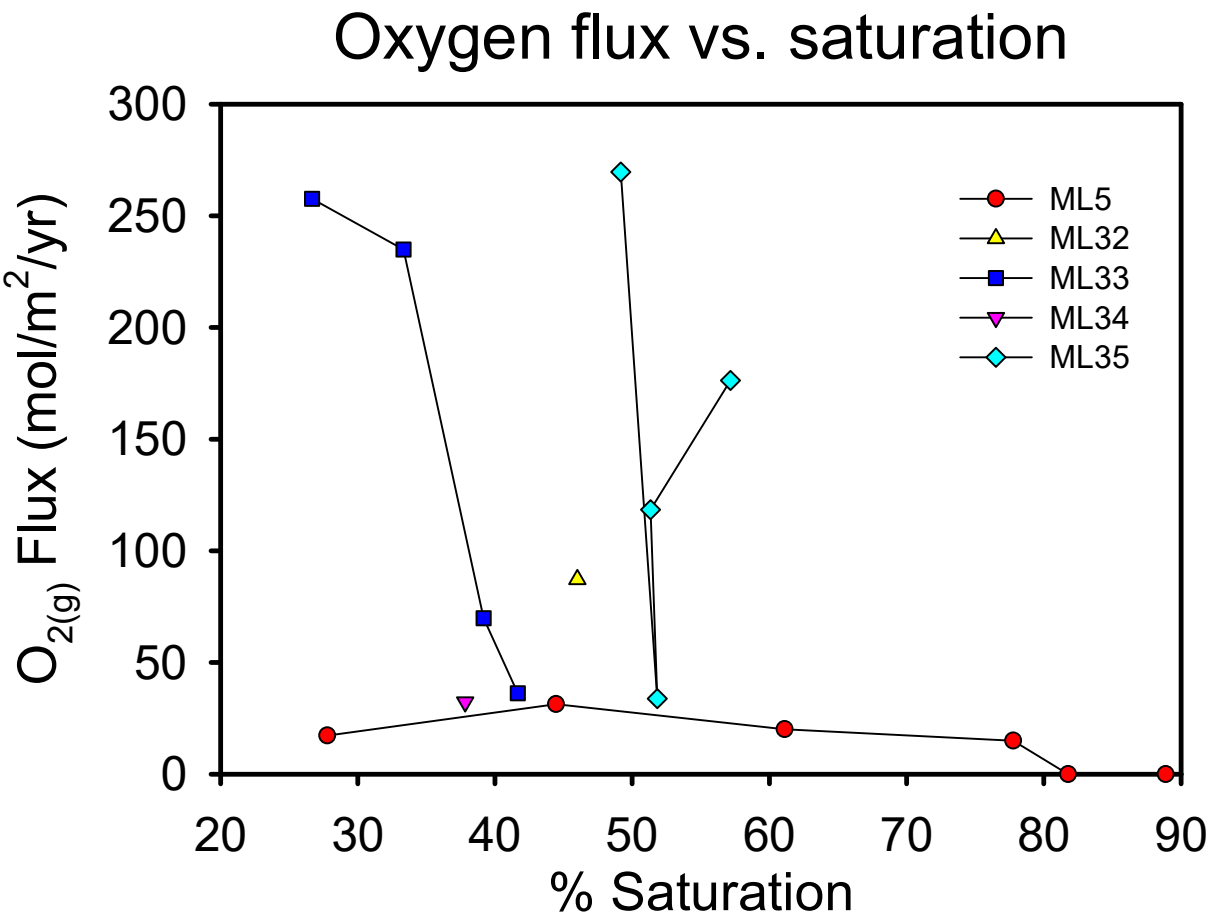

Figure B.13: Oxygen fluxes in the cover system, per location, vs. calculated saturation at the interface between the organic cover and the desulfurized tailings. ML5 has a 1-layer cover while ML32 through ML35 have a 2-layer cover system.

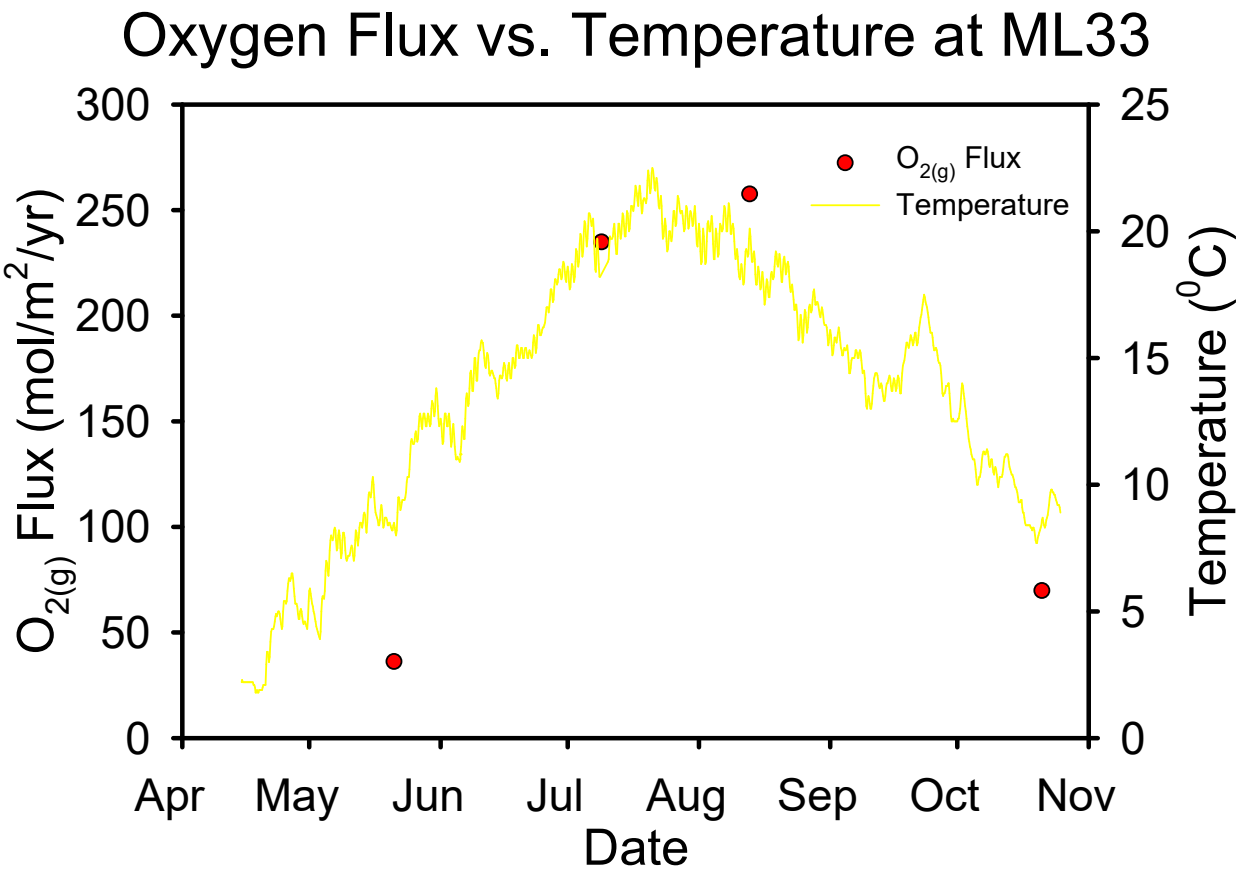

Figure B.14: Oxygen flux at ML33 vs. Temperature during the 2019 field season.

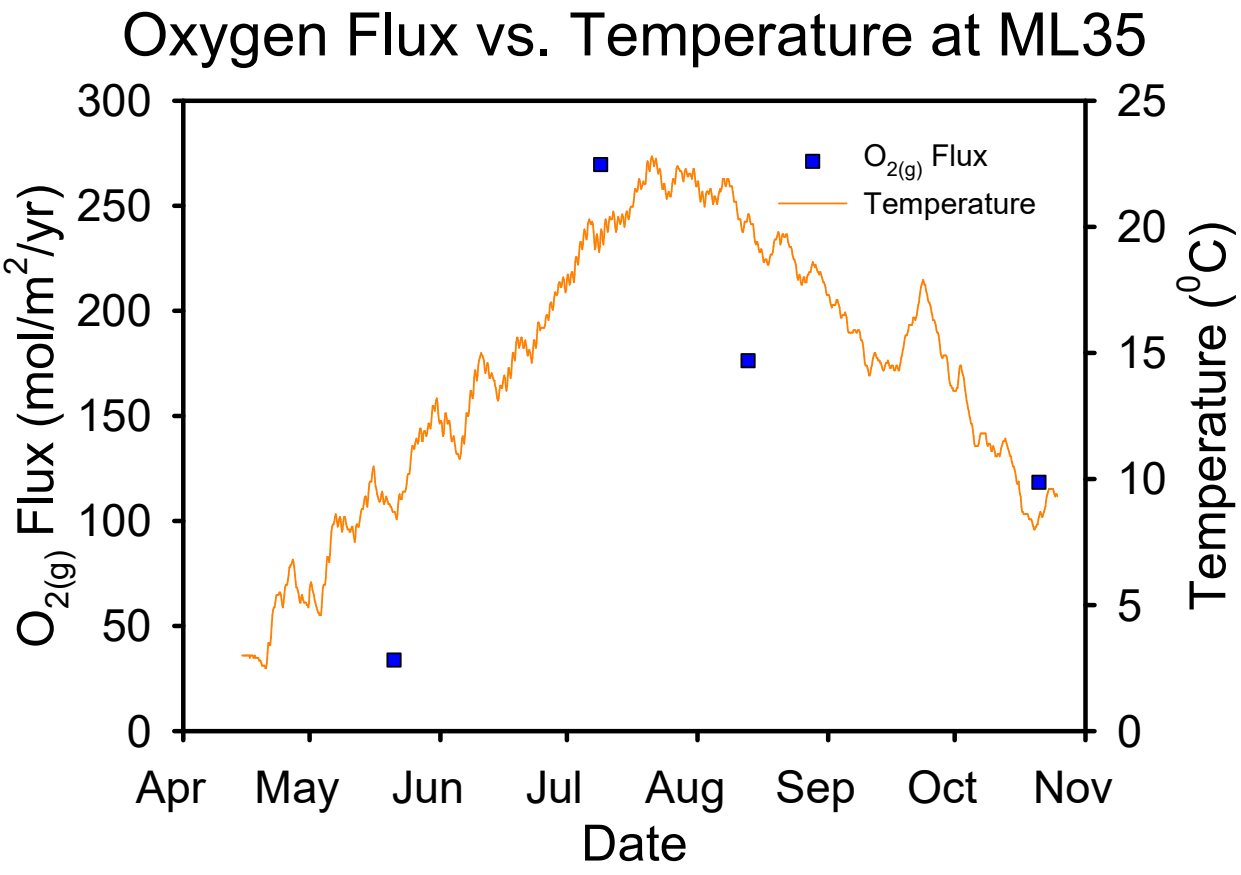

Figure B.15: Oxygen flux at ML35 vs. Temperature during the 2019 field season.

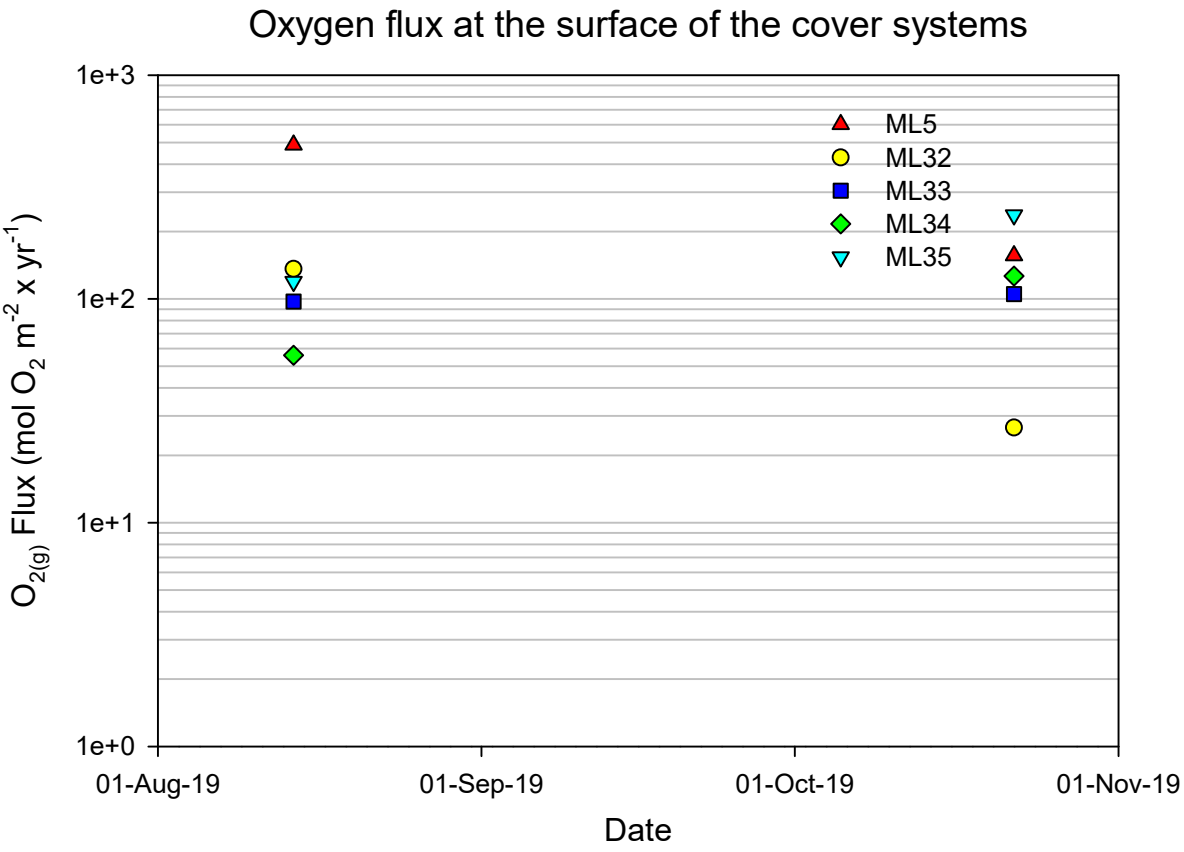

Figure B.16: Estimates of oxygen flux at the surface of the location with a 1-layer cover (ML5) and locations with a 2-layer cover system (ML32 through ML35). Calculations made using the oxygen-gradient method.

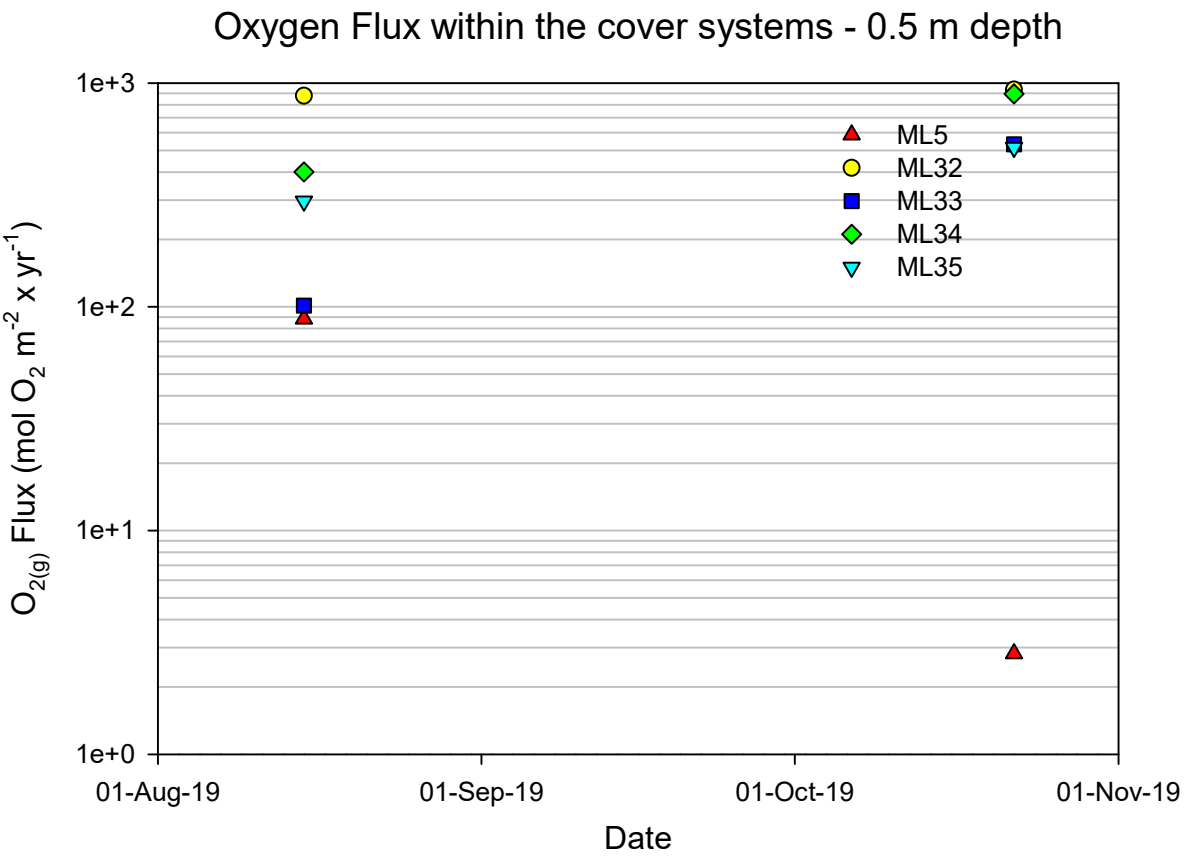

Figure B.17: Estimates of oxygen flux at a depth of 0.5 m at the location with a 1-layer cover (ML5) and locations with a 2-layer cover system (ML32 through ML35), Calculations made using the oxygen-gradient method.

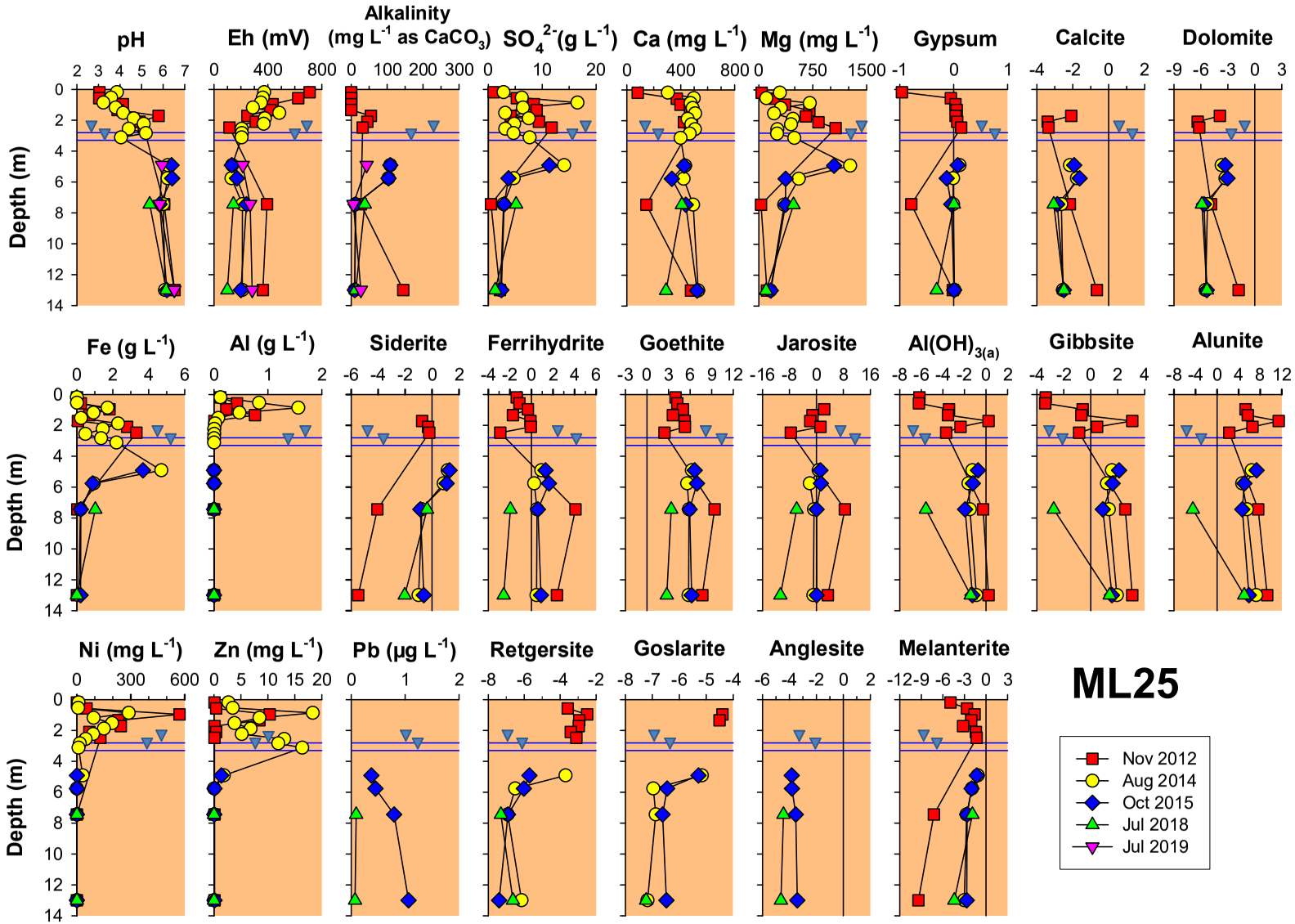

Figure B.18: Pore water chemistry results at ML25 (location without a cover) along with modelled saturation indices. Note: The blue lines, vertical lines and orange zone represent the water table, the zero SI line, and the hisotrical tailings, respectively. The two inverted blue triangles represent the highest and lowest water levels observed at this location in 2012, 2014, and 2015. Data taken from Bain and Blowes (2012) and Parigi (2020).

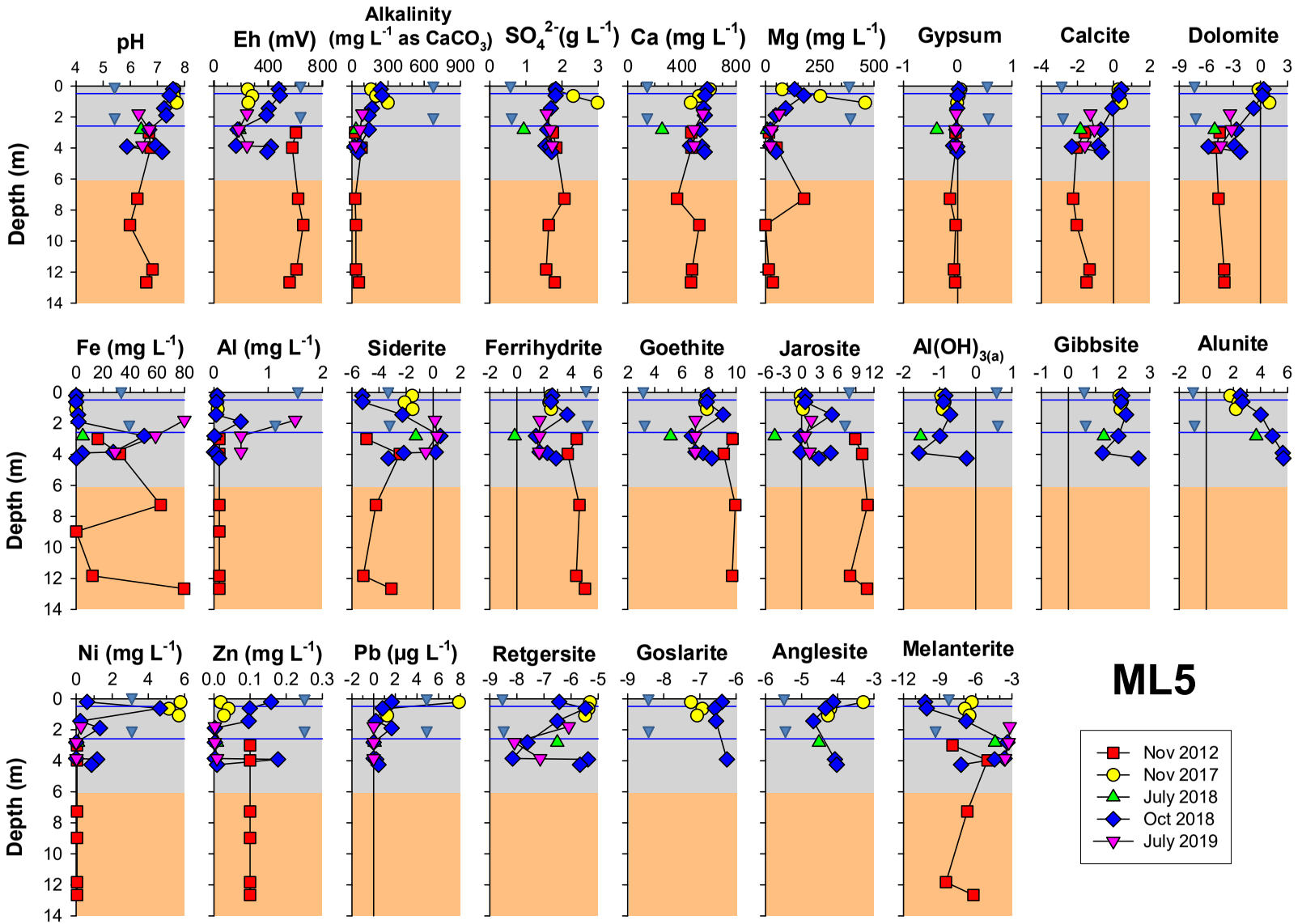

Figure B.19: Pore water chemistry results at ML5 (location with a 1-layer cover) along with modelled saturation indices. Note: the blue lines, vertical lines, grey zone, and orange zone represent the water table, zero SI line, desulfurized tailings, and historical tailings, respectively. The two inverted blue triangles represent the maximum and minimum water levels observed at this location during the study.

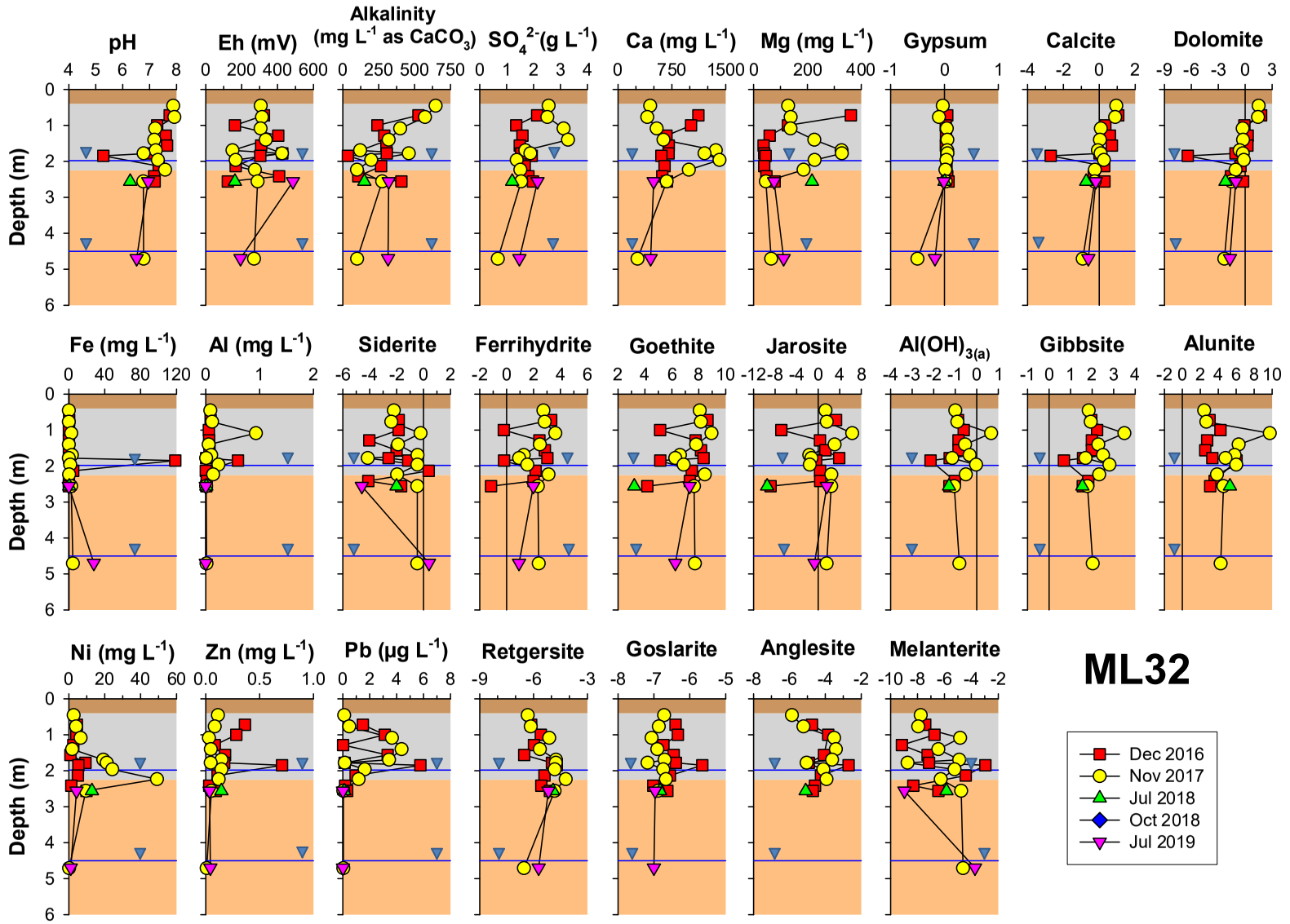

Figure B.20: Pore water chemistry results at ML32 (location with a 2-layer cover system) along with modelled saturation indices. Note: the blue lines, vertical lines, and zones of brown, grey, and orange represent the water table, zero SI line, and zones of the organic cover, desulfurized tailings, and historical tailings, respectively. The two inverted blue triangles represent the maximum and minimum water levels observed at this location during the study.

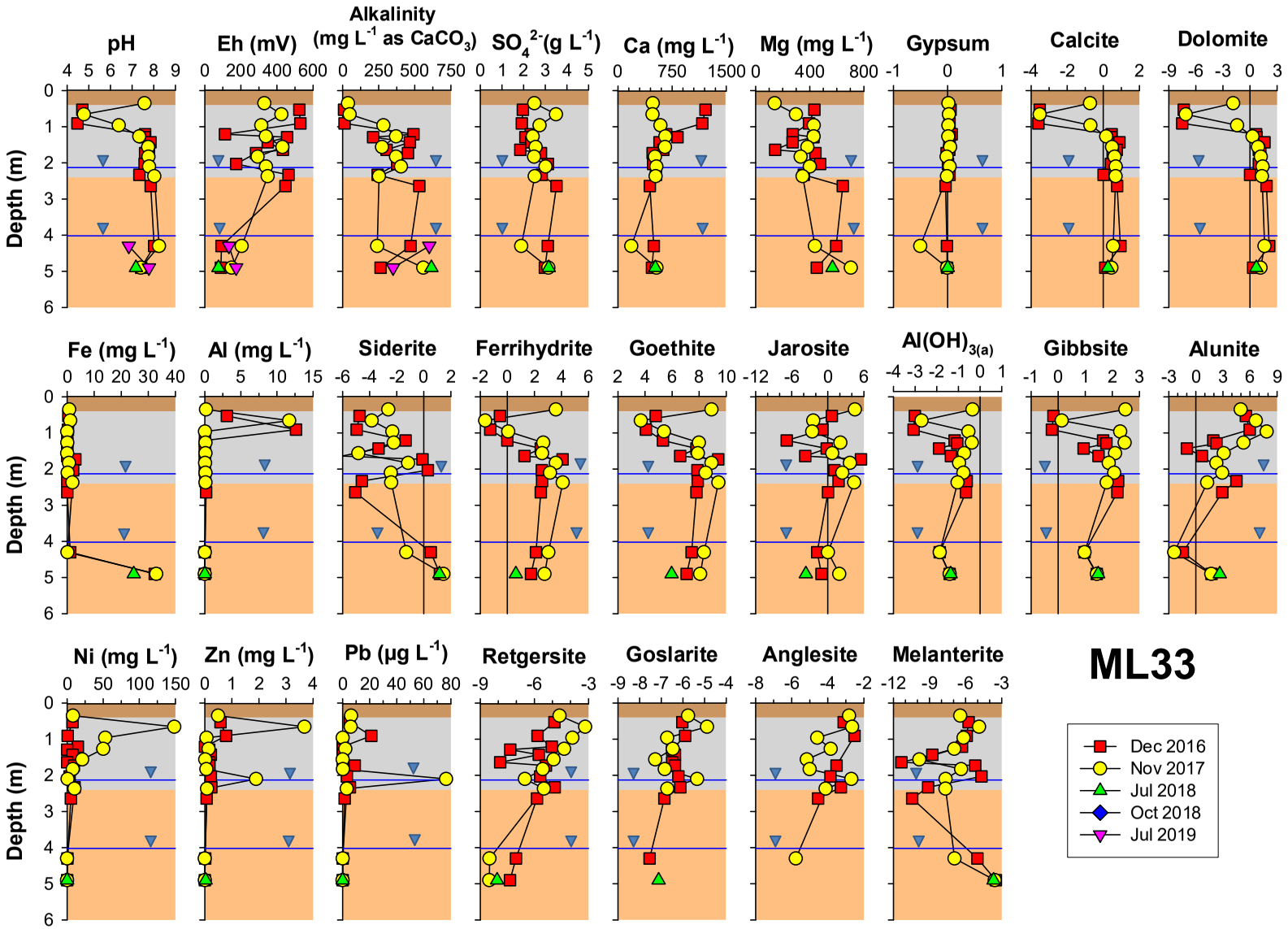

Figure B.21: Pore water chemistry results at ML33 (location with a 2-layer cover system) along with modelled saturation indices Note: the blue lines vertical lines, and zones of brown, grey and orange represent the water table, zero SI line, and the zones of the organic cover, desullfurized tailings and historical tailings, respectively. The two inverted blue triangles represent the maximum and minimum water levels observed at this location during the study.

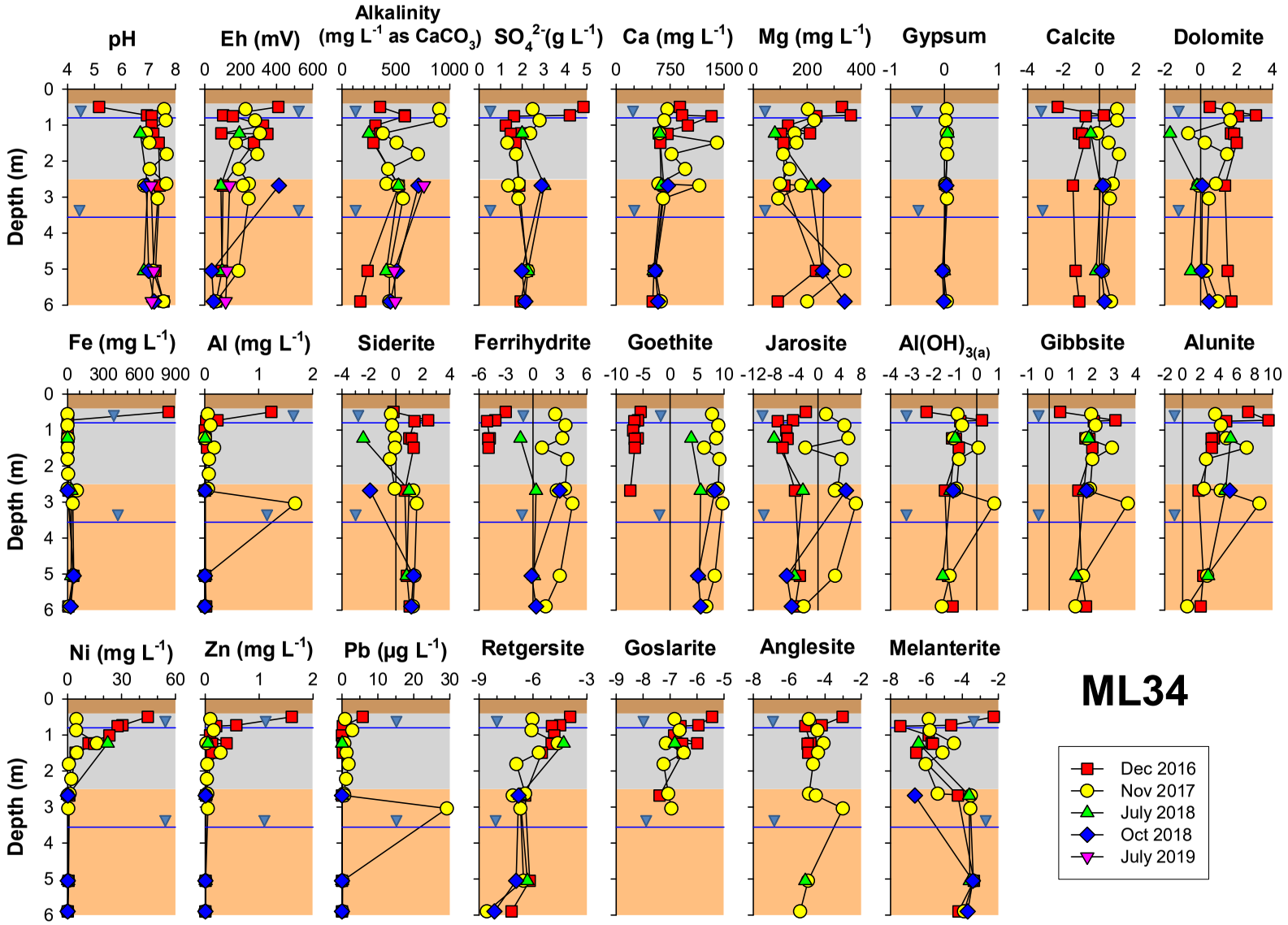

Figure B.22: Pore water chemistry results at ML34 (location with a 2-layer cover system) along with modelled saturation indices. Note: the blue lines vertical lines, and zones of brown, grey and orange represent the water table, zero SI line, and zones of the organic cover, desulfurized tailings and historical tailings, respectively. The two inverted blue triangles represent the maximum and minimum water levels observed at this location during the study.

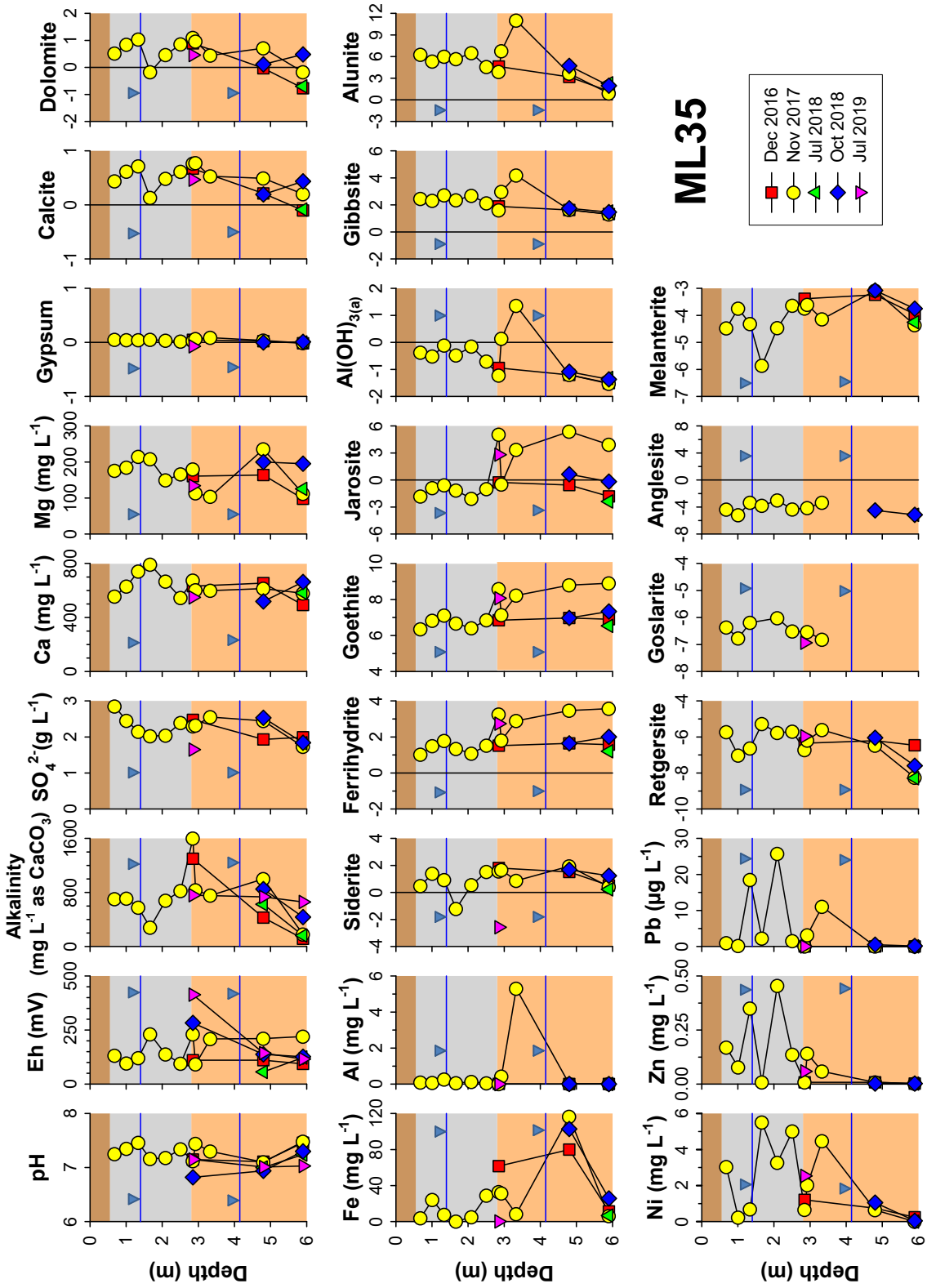

Figure B.23: Pore water chemistry results at ML35 (fully covered location) along with modelled saturation indices Note: the blue lines, vertical lines, and zones of brown, grey and orange represent the water table, zero SI line and zones of the organic layer, desulfurized tailings and historical tailings, respectively. The two inverted blue triangles represent the maximum and minimum water levels observedat this location during the study.

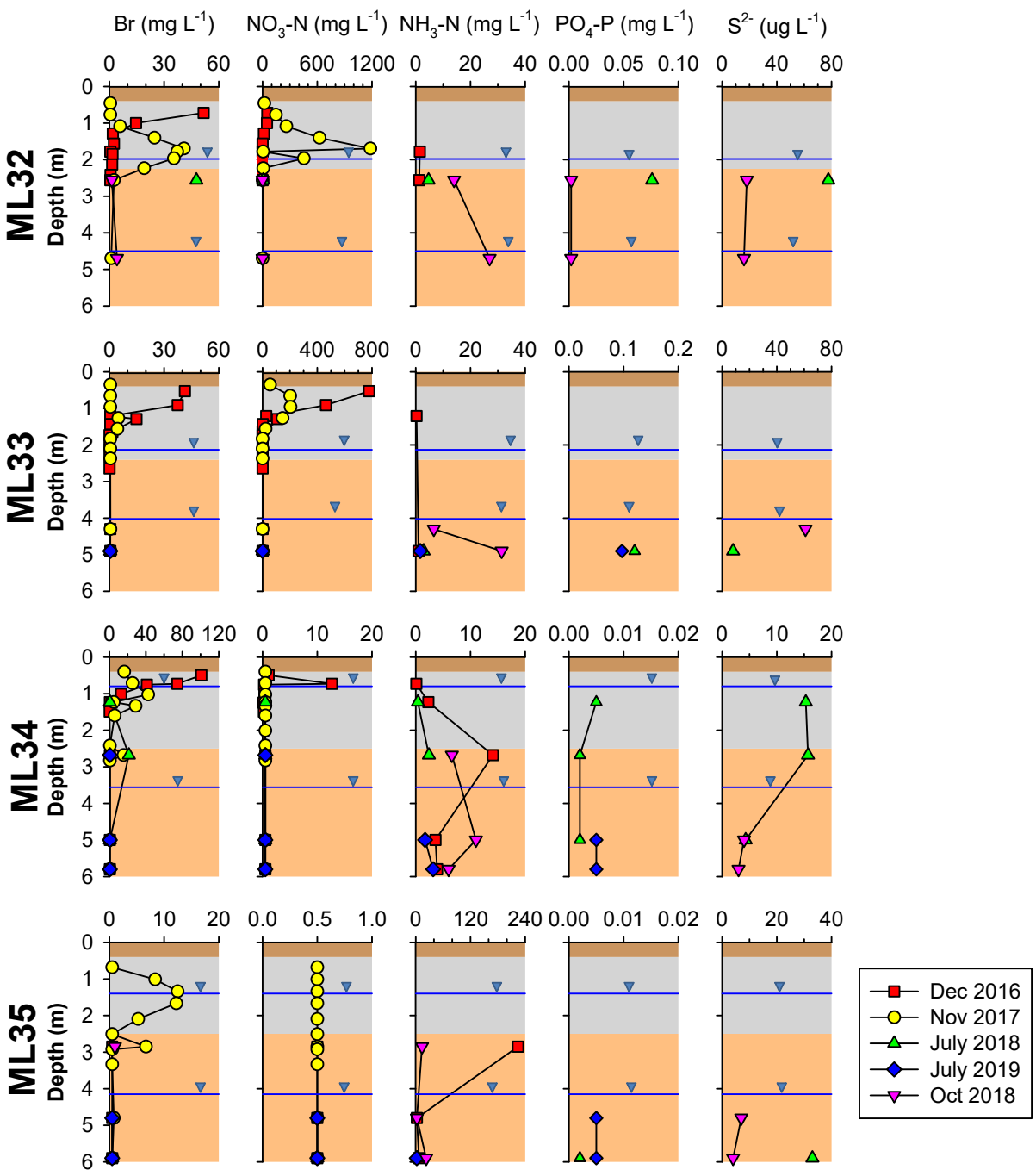

Figure B.24: Select pore water quality results, including nutrients, for all locations with a 2-layer cover system. Note: the blue lines and the brown, grey, and orange zones represent the water table, organic carbon layer, desulfurized tailings layer, and historical tailings, respectively. The two inverted blue triangles represent the highest and lowest water levels observed during the 2018 and 2019 monitoring episode.

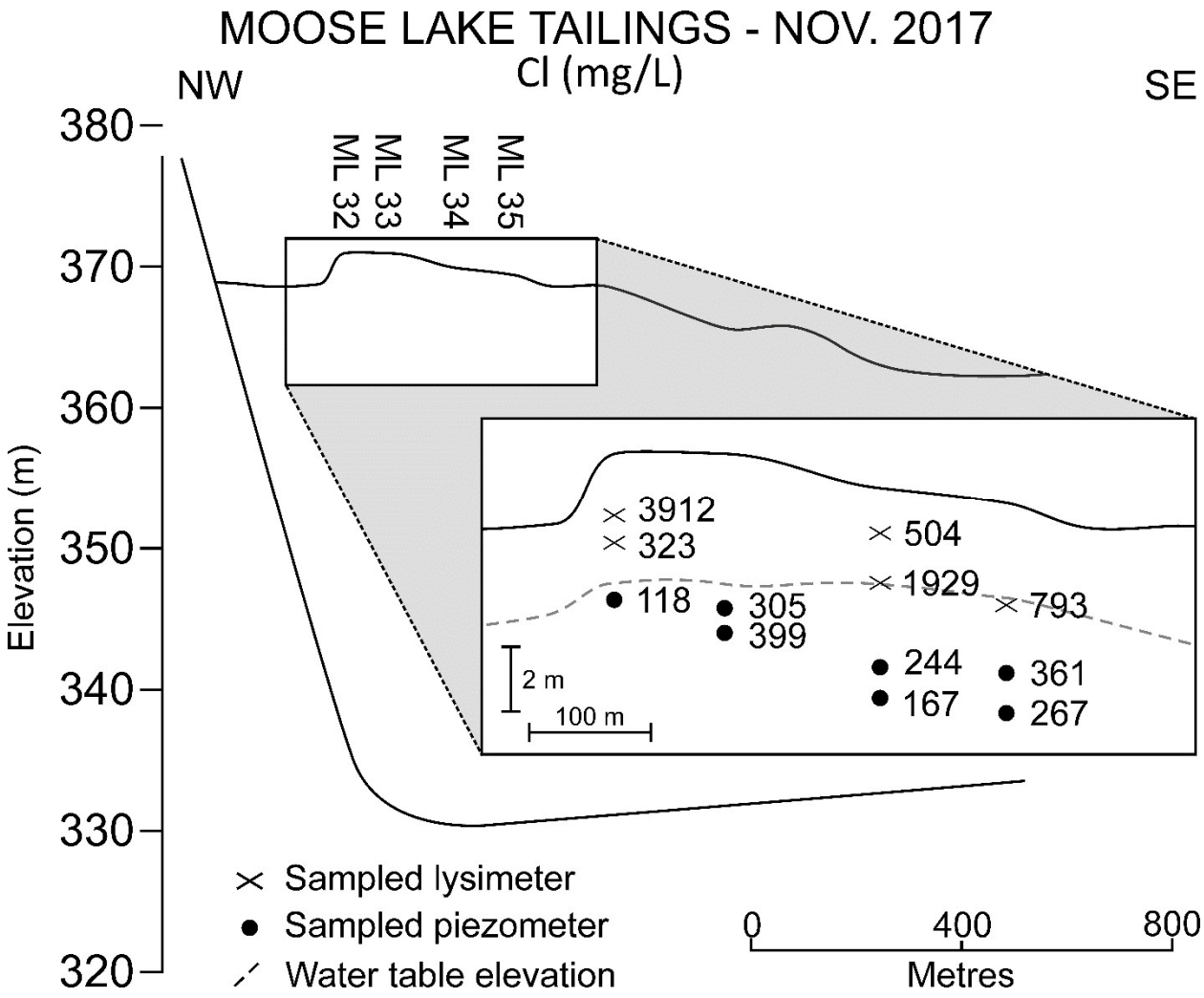

Figure B.25: Cross section of Cl concentrations at select locations in November 2017.

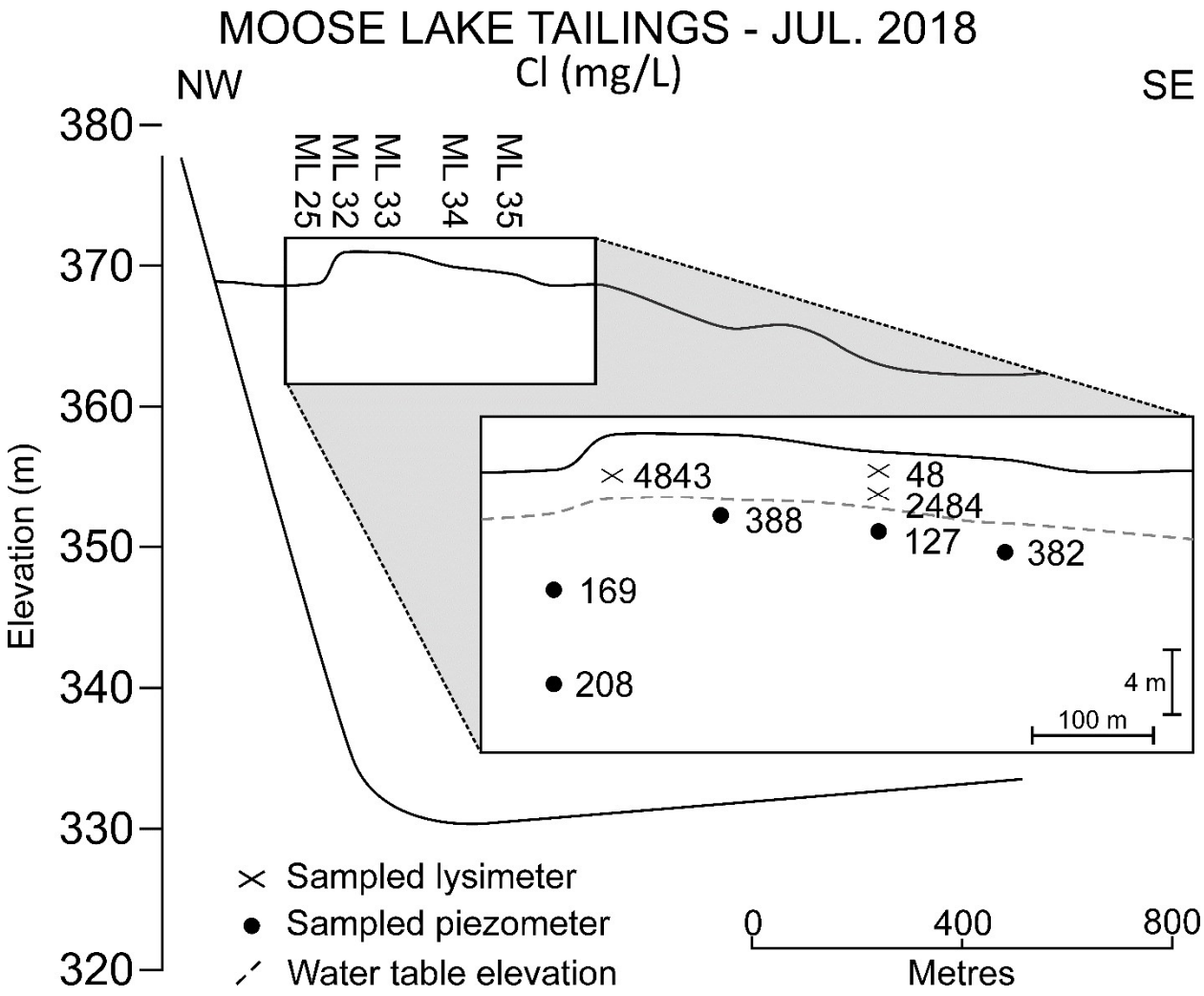

Figure B.26: Cross section of Cl concentrations at select locations in July 2018.

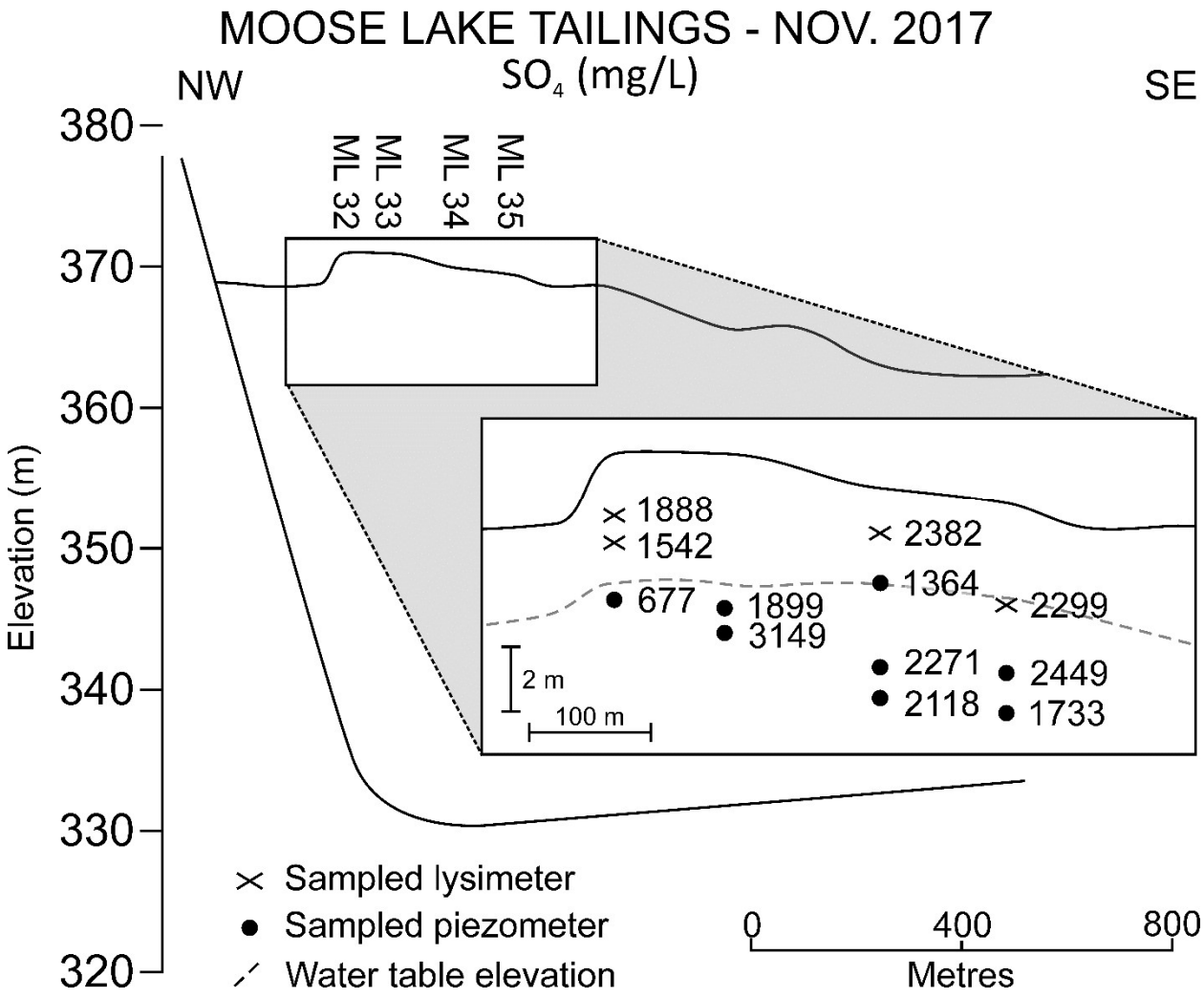

Figure B.27: Cross section of SO_4 concentrations at select locations in November 2017.

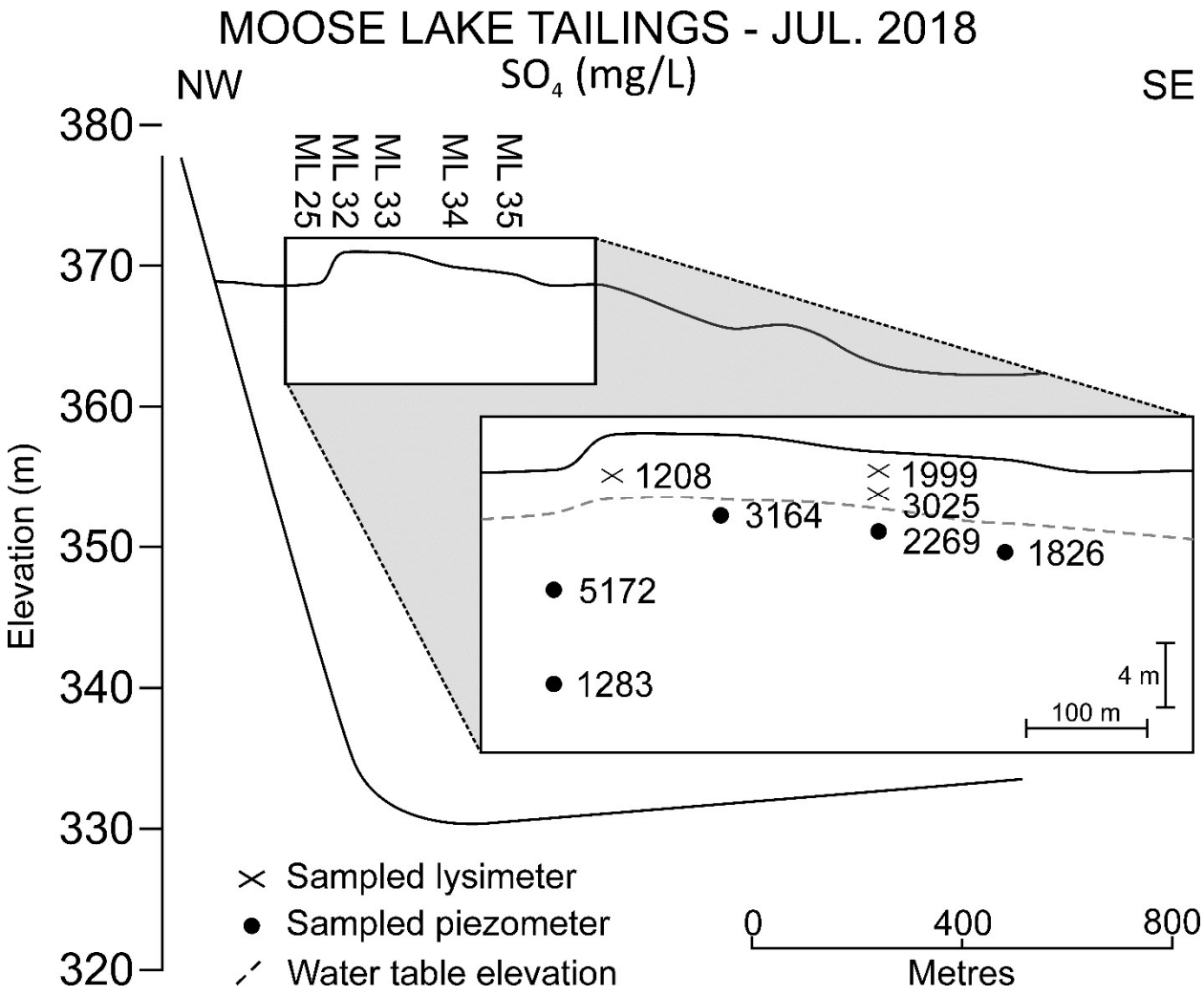

Figure B.28: Cross section of SO_4 concentrations at select locations in July 2018.

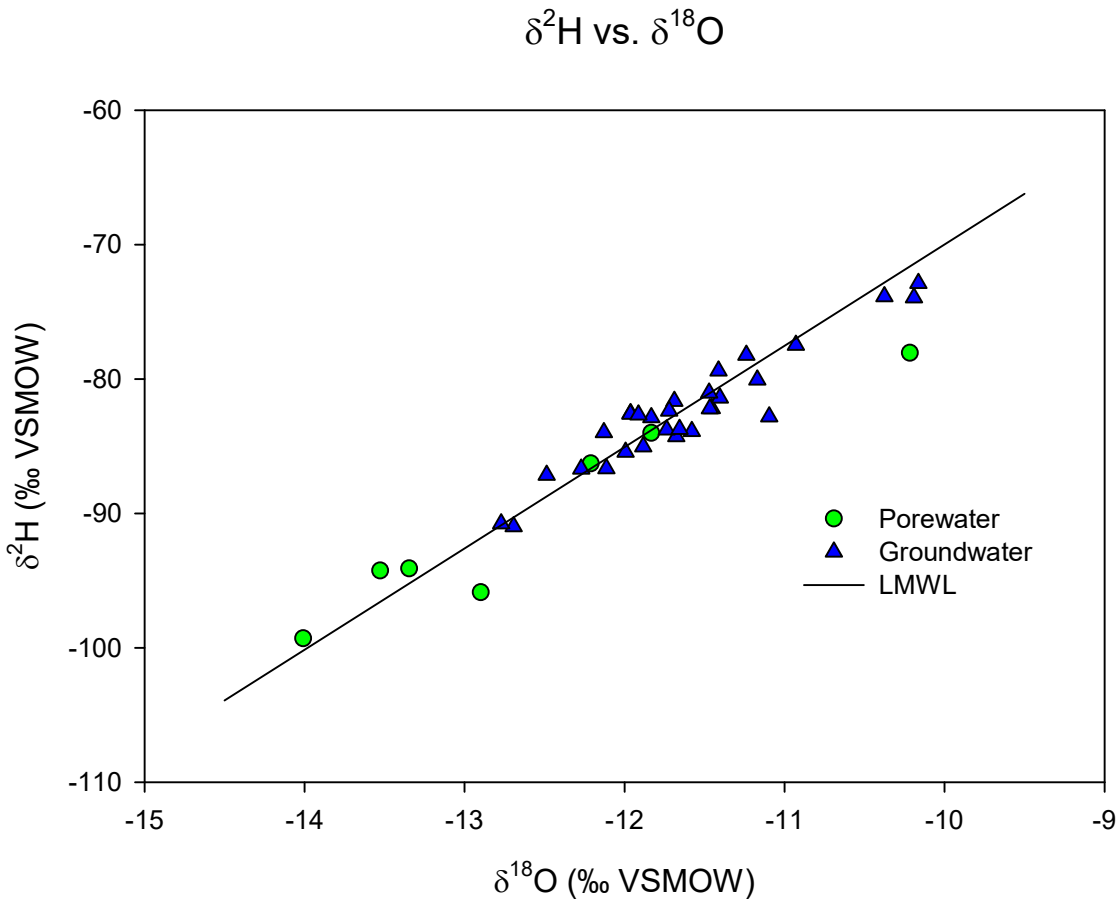

Figure B.29: Porewater and groundwater δ^2H and $\delta^{18}O$. Note: the local meteoric water line (LMWL) used is that of Bonner Lake, ON.

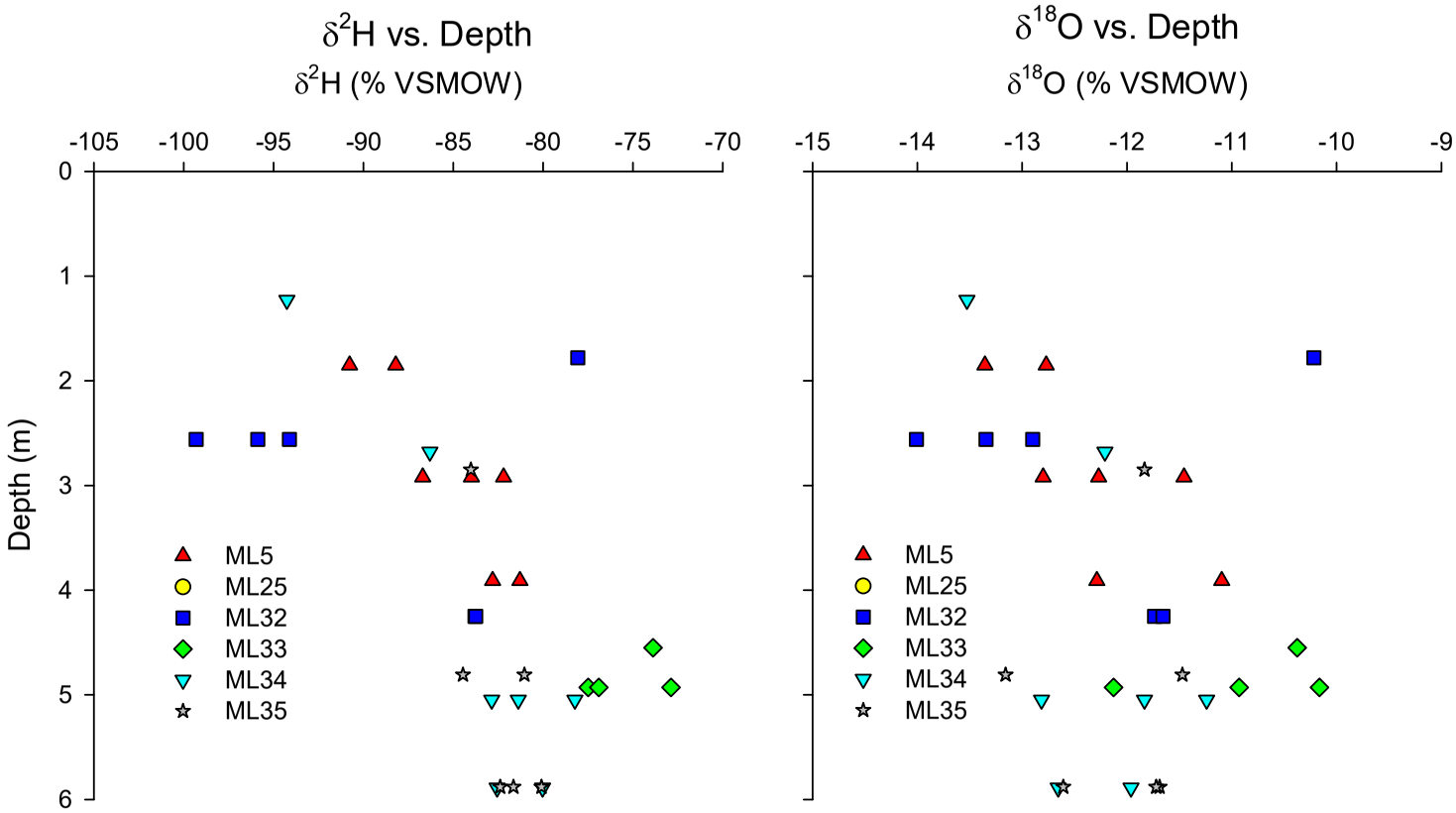

Figure B.30: pore water δ^2H and $\delta^{18}O$ vs. depth

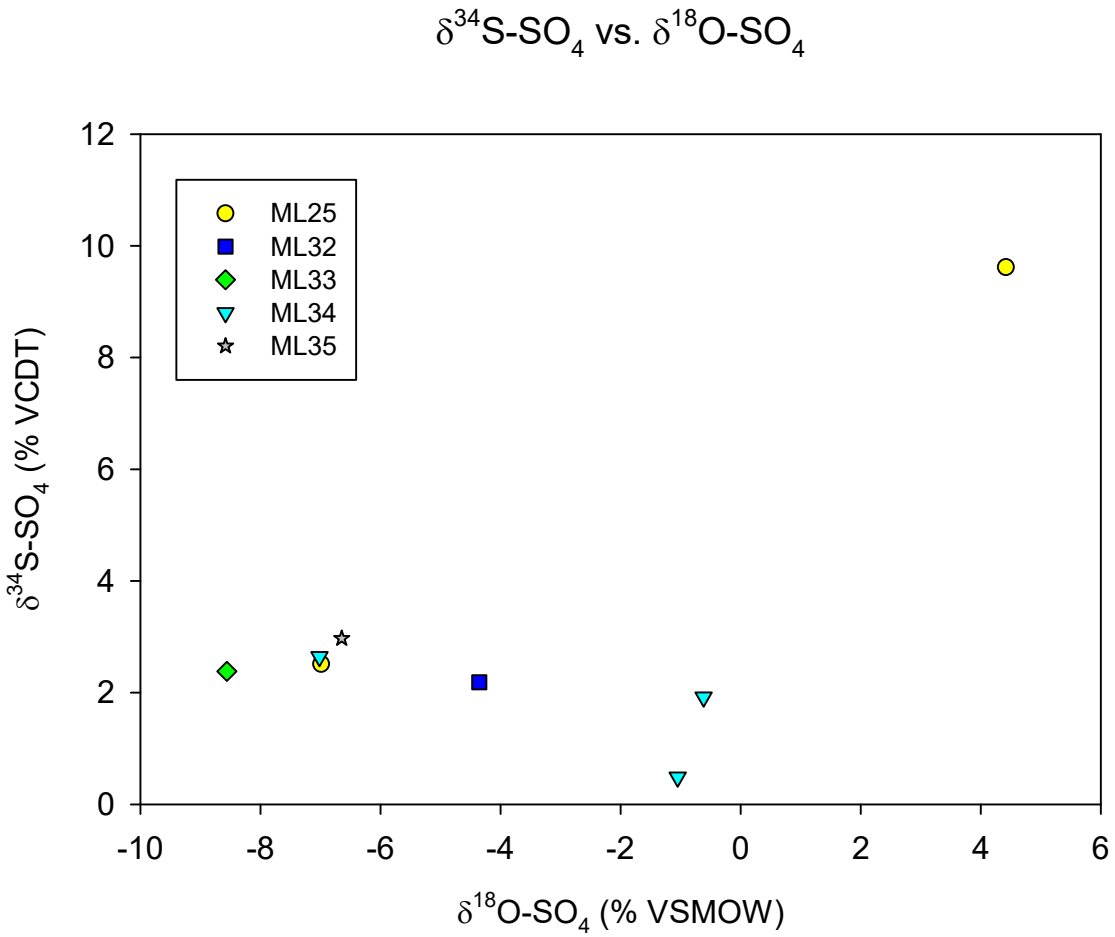

Figure B.31: Pore water $\delta^{34}S\text{-}SO_4$ vs. $\delta^{18}O\text{-}SO_4$.

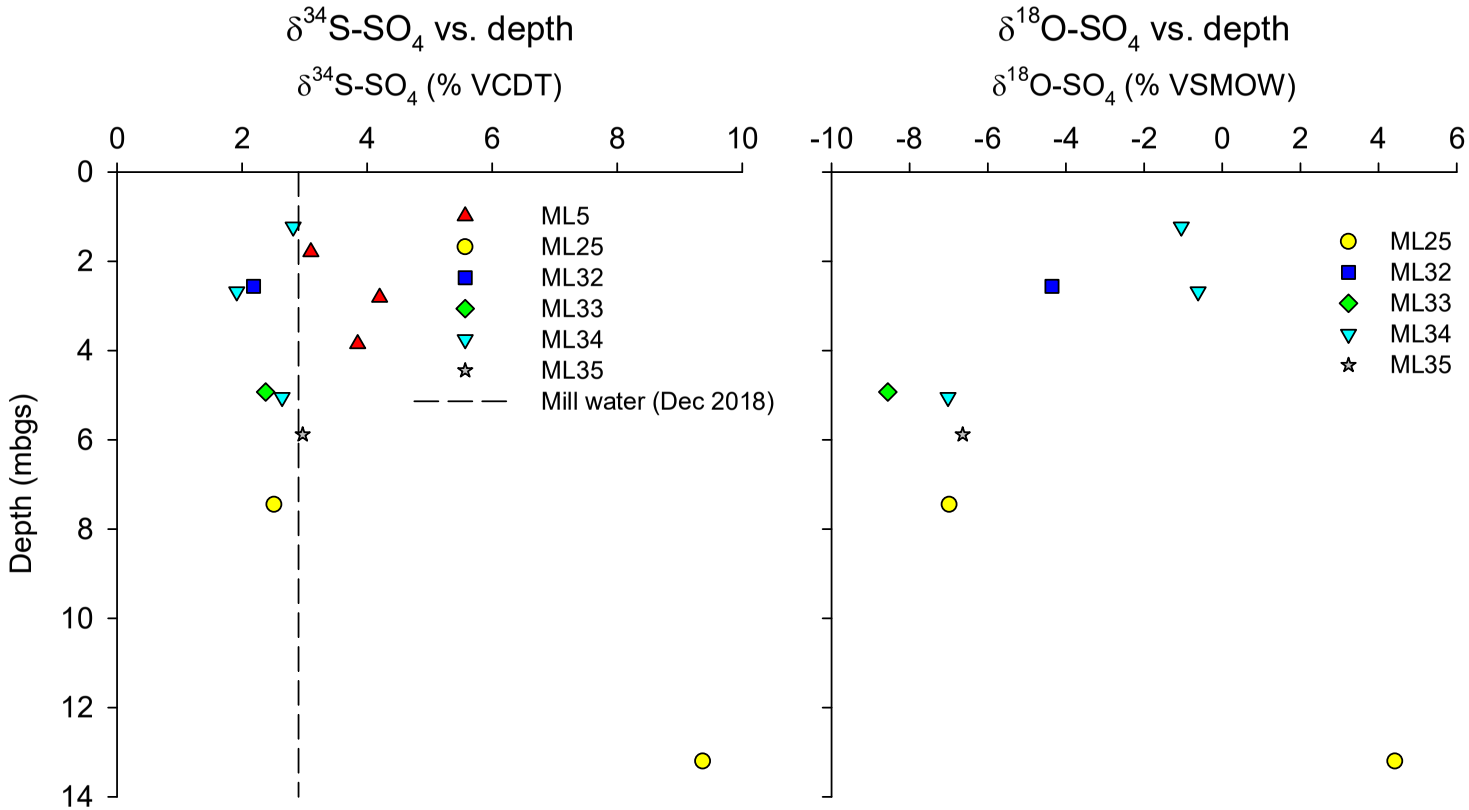

Figure B.32: pore water δ^{34}S-SO_4 and δ^{18}O-SO_4 vs. depth.

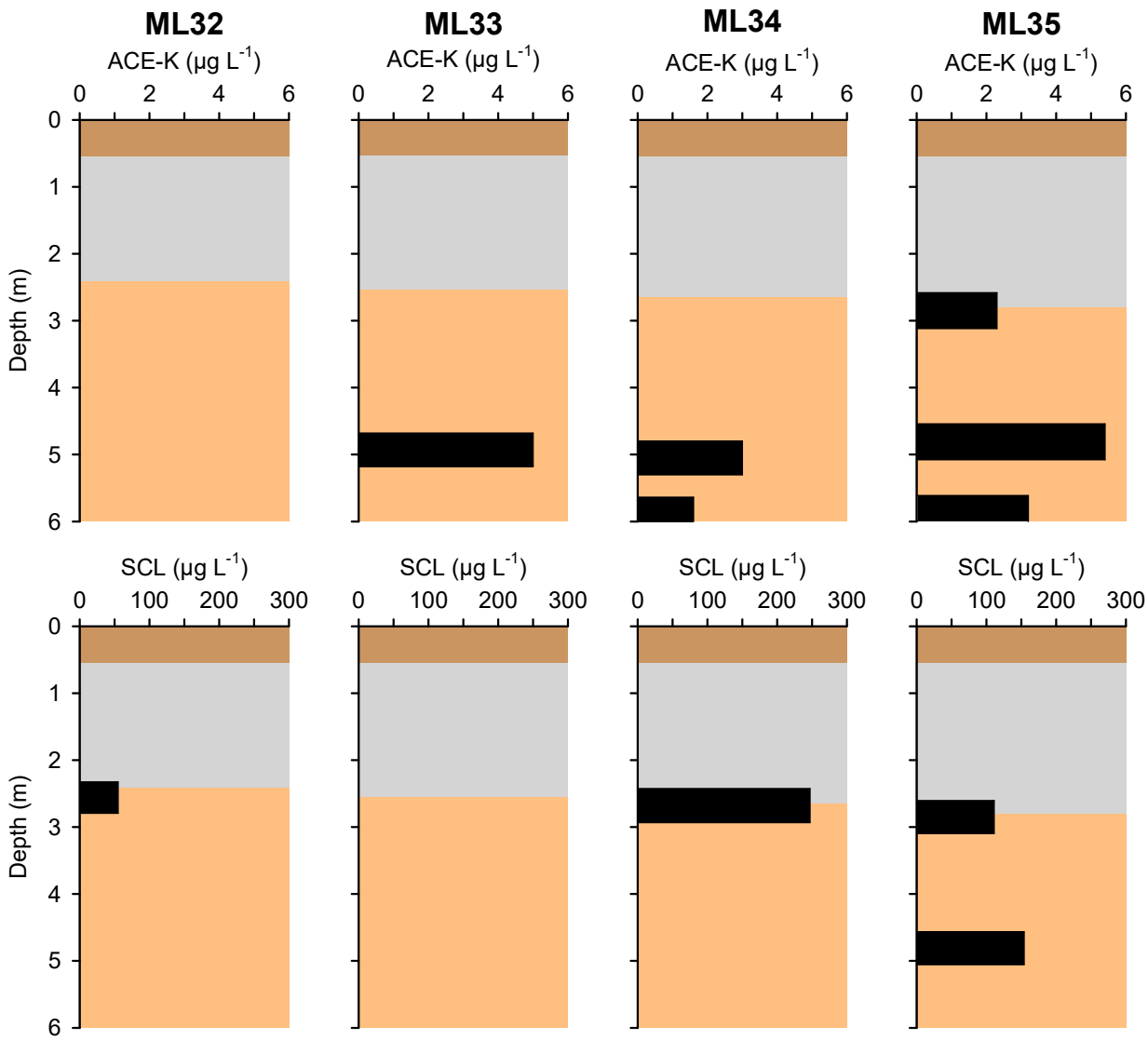

Figure B.33: Concentrations of artificial sweetener compounds with depth at the locations with a 2-layer cover system. ACE-K, and SCL stand for Acesulfame-K and Sucralose, respectively. Concentrations of Cyclamate and Saccharin were not detected.

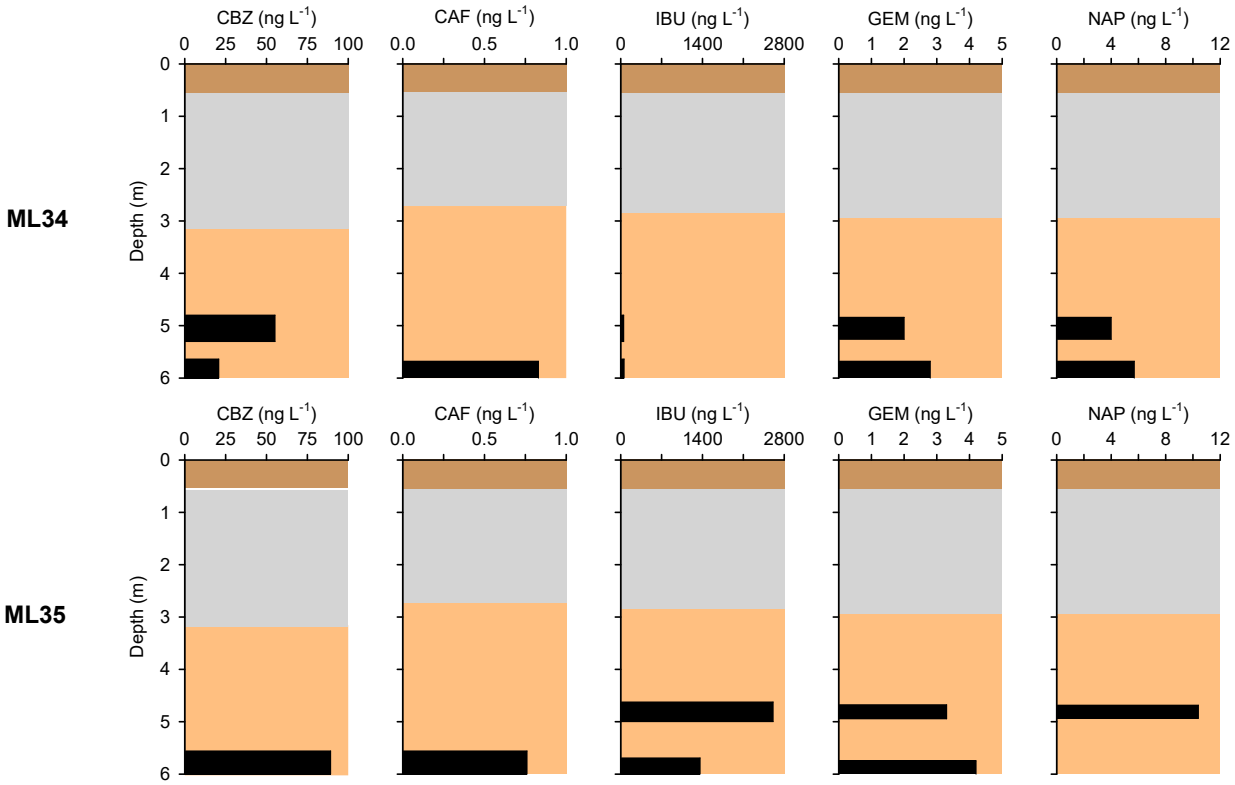

Figure B.34: Concentrations of pharmaceutical compounds with depth at ML34 and ML35. CBZ, CAF, IBU, GEM and NAP stand for Carbamazepine, Caffeine, Ibuprofen, Gemfibrozil and Naproxen, respectively.

Appendix C:

Draft Journal Article on the Microbiology of the SWWTS

Microbiology of a mine tailings impoundment covered with a multi-layer dry cover containing biosolids

Eva Pakostova[1], Mason McAlary[1], Stephanie Marshall[2], Samantha McGarry[2], Carol J. Ptacek[1], David W. Blowes[1]

[1]Department of Earth and Environmental Sciences, University of Waterloo, Waterloo, Canada.
[2]Glencore, Sudbury, Canada.

Abstract

The Ni/Cu mining and milling complex operated by Sudbury Integrated Nickel Operations is located in the City of Greater Sudbury, ON, Canada. The Strathcona Waste Water Treatment System (SWWTS), located on the property, received tailings from ore processing from 1970 to present. Demonstration-scale, multi-layer cover systems were installed at SWWTS in selected cells. The cover systems comprise an upper layer of organic carbon-rich material composed of biosolids fertilizer along with composted municipal food and yard waste, and a layer of desulfurized, fine-grained tailings. The aim of this study was to investigate microbial diversity in tailings recovered from the site and assess the impact of the organic component of the cover system four to six years after application. Organic carbon promotes microbial communities that consume O_2, thus decreasing sulfide oxidation rates. Tailings samples recovered from locations with and without organic carbon cover components were characterized by circumneutral bulk pH. Culturable sulfur-oxidizing (SOM), iron-oxidizing (IOM), iron-reducing, sulfate-reducing and aerobic heterotrophic microorganisms were enumerated. Presence of the organic cover seemed to result in elevated counts (~10^8 cell g^{-1}) of heterotrophic species at greater depth (~4 m) in the tailings profile. However, mineral-oxidizing microorganisms were also present in the tailings, with neutrophilic SOM dominating the samples (mean ~10^6 cells g^{-1}). Bacterial and archaeal communities (BACs) were investigated using high-throughput amplicon sequencing of 16S rRNA genes. No increase in richness or consistent, significant shifts in BACs in samples collected from the covered sites were observed when compared to a control. Relative abundances of SOM/IOM ranged from 0.5% to 18.3% of total reads (mean in amended tailings ~5.6%) and were not significantly affected by the organic cover.

1. Introduction

Metal mining and mineral processing generate large quantities of fine-grained gangue residue (mill tailings) that is commonly rich in iron sulfides pyrite (FeS_2) and pyrrhotite ($Fe_{(1-x)}S$). Typically, mill tailings are disposed of in impoundments at mine sites. Oxidation of sulfide minerals can lead to production of acid mine drainage (AMD), containing high concentrations of dissolved sulfate, iron and other metal(loid)s (*e.g.,* Blowes *et al.*, 2003; Johnson and Hallberg, 2003). Direct oxidation of sulfide minerals by O_2 and indirect oxidation by Fe^{3+} is greatly accelerated in the presence of iron- and sulfur-oxidizing microorganisms (Baker and Banfield, 2003; Johnson and Hallberg, 2003). Lithotrophic sulfur oxidation by taxonomically and ecologically diverse bacteria and archaea has been reviewed by Ghosh and Dam (2009). Neutrophilic sulfur-oxidizing microorganisms (nSOM; e.g. *Thiobacillus, Sulfurifustis, Sulfuricurvum,* and *Sulfuricella* spp.) and iron-oxidizing microorganisms (nIOM; e.g. *Gallionella*, *Ferrovibrio, Ferritrophicum* and *Sideroxydans* spp.) are often detected in neutral-pH mine wastes (e.g. Blowes *et al.* 1998), while acidophilic species dominate acidic mine wastes (Johnson and Hallberg, 2003; Johnson, 1998). The mesophilic, obligately chemolithotrophic *Acidithiobacillus* (*At.*) *ferrooxidans* (oxidizing sulfur, Fe^{2+} and H_2) is the most widely studied among acidophiles. *Leptospirillum* and *Acidimicrobium* spp. are acidophilic IOM (that do not oxidize sulfur) frequently detected in low-pH habitats with high metal concentrations. Several species of *Acidithiobacillus* (*At. caldus*, *At. thiooxidans* and *At. albertensis*), and other genera (e.g. *Thiomonas*) oxidize sulfur but not iron.

AMD formation can be prevented by limiting the contact between mine tailings and O_2 oxygen. The use of dry (barriers to O_2 or H_2O transport) covers is a common practice for *in situ* remediation of heavy metal-contaminated mine wastes (e.g. Anawar *et al.*, 2015; Pepper *et al.*, 2012; Cousins *et al.*, 2009; Hallberg *et al.*, 2005; Peppas *et al.*, 2000; Haering *et al.*, 2000). The incorporation of organic carbon components in cover systems promotes microbial communities to consume oxygen before it reaches tailings, thus decreasing sulfide oxidation rates. Accelerated microbial activity can improve physicochemical properties of soils disturbed by surface mining and mine wastes, such as increased water retention (Gardner *et al.*, 2010), soil pH (Alvarenga *et al.*, 2013; Brown *et al.*, 2003), reduction in metal toxicity (Alvarenga *et al.*, 2013; Brown *et al.*, 2003), and nutrient cycling (Campbell *et al.*, 2017). Enhanced soil development and improved soil quality can also promote plant growth (e.g. Campbell *et al.*, 2017; Pepper *et al.*, 2012; Brown *et al.*, 2003; Shu *et al.*, 2002). Several studies have evaluated the effect of organic carbon covers (such as biosolids,

municipal solid waste compost, or green-waste derived compost) on mill tailings; most of them focused on physicochemical properties of the soil. Others have investigated enzymatic activity (Touceda-Gonzales *et al.*, 2017; Zornoza *et al.*, 2012; de Varennes *et al.*, 2010; Perez de Mora *et al.*, 2005, 2006), microbial counts (Gardner *et al.*, 2010), phospholipid fatty acid (PLFA; Baker *et al.*, 2011), or microbial community structure in heavy metal-contaminated mine wastes (Touceda-Gonzales *et al.*, 2017; Pepper *et al.*, 2012; Perez de Mora *et al.*, 2006). Most studies investigating the effects of biosolid applications at mine tailings sites were short-term (< 5 years; Touceda-Gonzales *et al.*, 2017; Gardner *et al.*, 2012, 2010; Brown *et al.*, 2003), but fewer studies have focused on the longer-term (> 5 years) effects of organic covers on reclaimed mine wastes (Antonelli *et al.*, 2018; Nason *et al.*, 2014; Trlica and Teshima, 2011).

The Sudbury Integrated Nickel Operations (Sudbury INO) encompasses a currently operational mining and milling site owned by Glencore that is located adjacent to the community of Onaping (part of the City of Greater Sudbury, ON, Canada). The Strathcona Waste Water Treatment System (SWWTS) is one of the tailings containment and treatment areas included in the Sudbury INO. The SWWTS began receiving tailings from ore processing at the Strathcona Mill in 1968 (Blowes, 1996; Bain and Blowes, 1998; Bain and Blowes, 2013) and is one of the largest tailings containment areas in the Sudbury region (MEND, 1997). During the initial years of milling, unsegregated tailings (sulfur ~15%, mainly in the form of pyrrhotite) were deposited in the impoundment. Active deposition of tailings in Strathcona Tailings Cell 1A, 2A, and 2B concluded in 2012, and demonstration-scale, multi-layer cover systems were installed there in selected cells. These covers are composed of an upper 0.5 m layer of organic material over a thick layer (1 to 3 m) of lime-stabilized, fine-grained desulfurized mill tailings (0.4 to 1 wt.% S) deposited from 1996 until 2012 (EcoMetrix Incorporated, 2014). The Strathcona covers have been in place for up to 7 years, providing an opportunity to evaluate the impacts of the cover systems on the hydrology, water quality and microbiology within the cover and the underlying tailings.

Previous research at SWWTS was conducted prior to desulfurization in the mid-1990s in order to assess the water quality throughout the tailings (Blowes *et al.*, 1996). Oxidation rates across the impoundment were measured in the field, showing that the tailings were undergoing rapid oxidation. Later, investigations were carried out with the objective to evaluate changes in pore-water quality after 1996 (Bain *et al.*, 1998; Bain and Blowes, 2013). Covering the sulfide-rich

tailings with fine-grained, low-sulfur tailings has limited the extent of sulfide oxidation in the underlying tailings, presumably due to the low diffusion of oxygen through the low sulfur tailings layer. Sulfide oxidation was thus limited to shallow depths within the desulfurized tailings. Instrumentation installed previously remains in place, allowing for direct comparison between covered and uncovered tailings.

Although there is a general consensus that efficiency of soil remediation greatly depends on the presence and activity of microorganisms, the long-term effects of organic matter on microbial communities need further investigation. The aim of this study was to assess the diversity of bacterial and archaeal communities (BACs) in cover systems with an organic carbon component overlying a layer of desulfurized tailings, by investigating the microbiome in samples recovered from two cells including organic carbon and desulfurized tailing components and one control location without the organic carbon component. High-throughput amplicon sequencing of the 16S rRNA gene was used to analyze entire BACs, as well as to assess relative abundances of microorganisms catalyzing dissimilatory oxidation-reduction of sulfur and iron. Culturable sulfur-oxidizers, iron-oxidizers, sulfate-reducers, and heterotrophs were enumerated using a culture-dependent technique. The microbiology data were compared with results of geochemistry analyses performed within an ongoing broader study conducted by the University of Waterloo.

The layered vertical profile at the SWWTS includes a layer of desulfurized tailings overlying older (partially oxidized) sulfide-rich tailings. In Strathcona Tailings Cell 1 (Fig. 1) the desulfurized tailings were covered with a ~0.5 m organic cover (~3.5 ha ML33 in 2014, and ~0.9 ha ML34 in 2012), composed of compost mixed with a locally produced biosolids fertilizer. The compost is a product of composting 10% source-separated organics (municipal food waste); 30% leaf waste; 30% yard waste; 10% aged bark; and 10% small sticks (approximately 1.5cm x 5cm) (Tisch *et al.*, 2008). The biosolids fertilizer is a soil amendment produced from wastewater treatment residuals (biosolids) mixed with cement kiln dust and/or quicklime. Two locations within Tailings Cell 1 (ML33 and ML34; Fig. 1), as well as a control location without an organic cover (ML5 is within Tailings Cell 2a; Fig. 1) were sampled for microbiological and geochemical characterization.

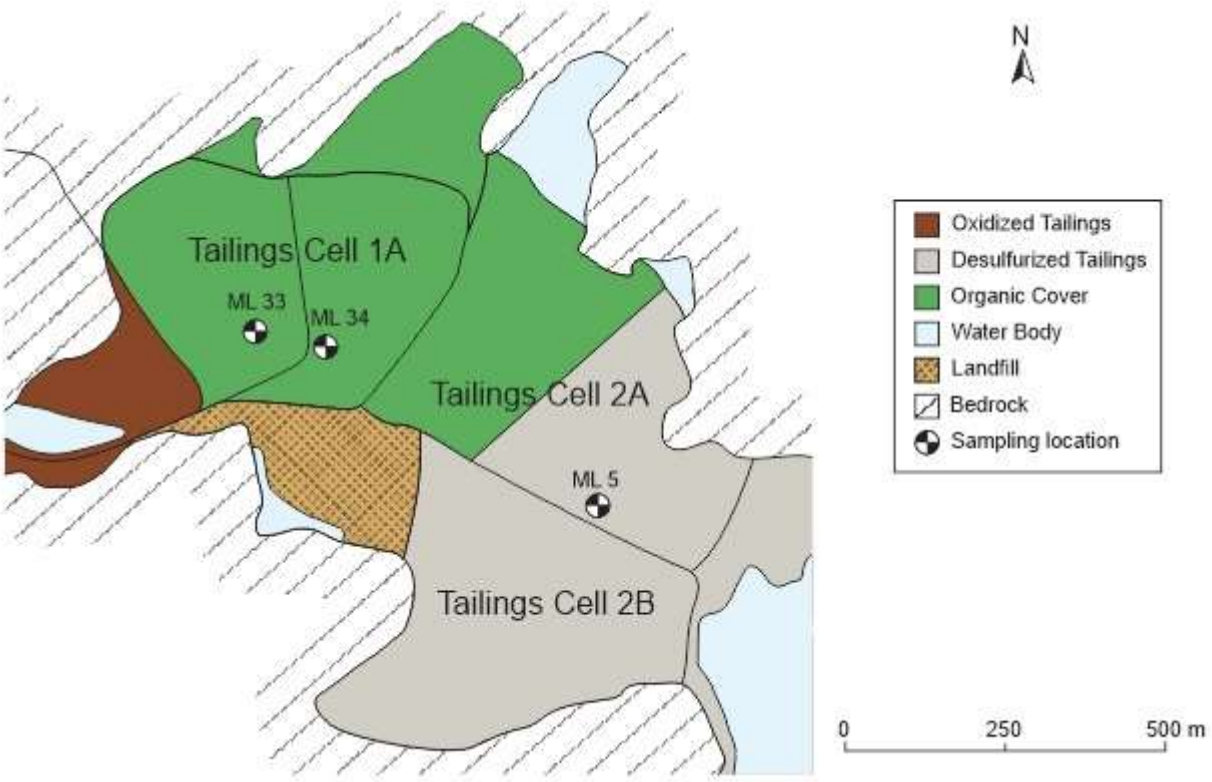

Fig. 1. Site map of the Strathcona Tailings area within the SWWTS area showing the three locations (ML33, ML34, and ML5) sampled for detailed microbiological characterization.

2. Material and methods

2.1. Site and sampling

Core samples of the tailings were collected in September 2018 to a depth of approximately 4.5 m using the method described by Starr and Ingleton (1992). The core samples were stored at 4°C and transported to the laboratory for further processing. The Al casings were cut at desired depths (Table 1) perpendicular to their long axes, thin layers of exposed materials were discarded, and subsamples from the cross-section centers were collected into sterile 50-mL centrifuge tubes, stored at 4°C, and processed for the most probable number (MPN) within 7 days after core collection. Another set of samples was frozen (-20 °C), and later used for total DNA extractions.

Table 1. Summary of environmental samples collected from three locations within SWWTS; the ML33 and ML34 sites were covered with an organic cover, while the ML5 site served as a control site (i.e. no organic cover). The microbial diversity was analyzed using high-throughput amplicon

sequencing of the 16S rRNA gene. Samples in which metabolically active groups of microorganisms were also enumerated using MPN are in bold. † m below ground surface. * cored, sub-sampled and analyzed in duplicate.

Sample type	Depth (mbgs†)		
	ML33 site	ML34 site	ML5 site
Organic cover (OC)	0.15 **0.30*** 0.40	**0.21**	n.a.
Oxidized desulfurized tailings (ODT)	**0.73***	0.40 **0.62**	**0.21**
Unoxidized desulfurized tailings (UDT)	**1.15*** 2.20*	2.00 **2.71**	**1.10** 2.20
Historical tailings (HT)	**2.80*** 3.20* **3.80**	3.20 **4.37** -	3.20 **4.28** -

2.2. Enumerations of culturable microorganisms

Groups of culturable microorganisms were enumerated using the most probable number (MPN) technique (Cochran, 1950; Garthright and Blodgett, 2003). Anaerobic cultivations were performed in triplicate. To enumerate iron-reducing microorganisms (IRM), 1 g of sample was added to 20 mL serum bottles containing 9 mL of liquid basal medium (pH ~ 7.0; supplemented with 1.5 g L^{-1} peptone as a carbon source) described by Gould *et al.* (2003). The first dilutions were serially diluted, following the MPN protocol described by Gould *et al.* A similar protocol was applied to enumerate sulfate-reducing microorganisms (SRB). SRB were cultivated in a modified Postgate C medium (pH ~ 7.5), containing 2.92 g L^{-1} Na lactate (60%) and 1.28 g L^{-1} Na acetate, and supplemented with resazurin serving as an anaerobic indicator. After a 5-week incubation period in an anaerobic chamber, SRB cultures were inspected for precipitation indicating biogenic H_2S production by sulfate reduction. Iron reduction (in IRM cultures) was determined by an addition of ferrozine reagent (Stookey, 1970), with a purple color indicating Fe^{2+} formation.

MPN enumerations of neutrophilic sulfur-oxidizers (nSOM) were performed in five replicates under aerobic conditions. Environmental sample (1 g) was added to each replicate sterile test tube, containing 9 mL of filter-sterilized basal salt medium (pH ~ 7.0) and composed of (in g L^{-1}): NH_4Cl (0.1), KH_2PO_4 (3.0), $MgCl_2 \cdot 6H_2O$ (0.2), $CaCl_2 \cdot 2H_2O$ (0.13) and $Na_2S_2O_3 \cdot 5H_2O$ (5.0). Serial

dilutions were performed and the samples were incubated for 27 days in the dark. A pH decline by ≥ 0.5 unit was considered a threshold to determine nSOM activity (Orion Combination pH Electrode, Orion Star A321 pH Portable Meter; Thermo Scientific, USA). Acidophilic oxidizers were enumerated by plating samples onto selective solid overlay media. To grow acidophilic iron-oxidizers (aIOM), serially diluted samples were streaked onto iFeo medium, described by Johnson and Hallberg (2007). Acidophilic sulfur-oxidizing microorganisms (aSOM) were enumerated on a modified overlay FeSo medium (Johnson and Hallberg, 2007), containing 500 µM Fe^{2+} (serving as a micronutrient rather than a substrate) in the overlay to eliminate growth of IOM. In order to enumerate heterotrophs, serially diluted samples were plated onto R2A agar (Sigma Aldrich, USA). Plates were incubated for 20 days for acidophiles and 5 days for heterotrophs, after which colonies were counted. Two successive dilutions that showed colony growth served as duplicates for cultivations on all solid media. All (aerobic and anaerobic) cultivations were performed at laboratory temperature (~23 °C) without agitation.

2.3. DNA extraction and Illumina MiSeq sequencing

DNeasy PowerSoil Kit (Qiagen Inc., Germany) was used to extract total genomic DNA in duplicate from solid-phase samples, following the manufacturer's protocol. As a kit control, a vial without sample was processed in a similar manner. DNA concentrations were determined using the Qubit dsDNA HS Assay Kit (Thermo Fisher Scientific, USA). Quality DNA was stored at −20 °C prior to submission for sequencing. The V4 region of 16S rRNA genes was amplified using the modified universal primers 515F/806R (Walters *et al.*, 2015), after which Illumina MiSeq sequencing of the amplicons was performed, both by Metagenom Bio Inc. (Toronto, Canada).

Sequence data were analyzed using the mothur software (v.1.39.5, updated: 3/20/2017; Schloss *et al.*, 2009), and the mothur MiSeq Standard Operating Procedure (SOP; Kozich *et al.* 2013; https://www.mothur.org/wiki/MiSeq_SOP from 15/04/2019). One out of a total 55 samples (including kit control) that contained fewer than 12,000 sequences was removed prior to duplicate merging. Chimeric sequences were discarded based on predictions by vsearch using the Silva database for 16S rRNA gene sequences (Release 132 for mothur, downloaded 18/03/2019) as a reference. After splitting into bins and clustering within each bin, sequences were clustered into operational taxonomic units (OTUs; at a 97% similarity level) by a *de novo* picking method. Taxonomic annotation of individual OTUs was based on mothur-formatted version of the Silva

reference database (details above). Several taxa (unknown, mitochondria, and eukaryotes) were not considered for further data analyses, as advised in the mothur MiSeq SOP. The SOP also recommends that *Cyanobacteria* should be removed. However, due to their possible involvement in hetero- and/or chemolitho-trophy, the group was included in further processing. To control variation resulting from an unequal number of sequences across samples, subsampling was performed for each sample after OTU generation at a rarefaction level based on the sample with the fewest number of sequences (19,200 sequences).

Good's coverage (calculated for an OTU definition of 0.03) was generated to estimate the portion of total species represented in each sample. The Gini-Simpson's diversity index and Chao1 richness estimator were chosen to assess α-diversity for each library (sites with and without organic cover components). Significance of differences in α-diversity between libraries was determined using the Wilcoxon rank sum test. Weighted UniFrac (Lozupone and Knight, 2005) was applied to investigate *β*-diversity, and 3D non-metric multidimensional scaling (3D-NMDS) was used for visualization. Diversity within groups (sites or layers) was compared using AMOVA (the analysis of molecular variance; Martin, 2002), a statistic testing the null hypothesis that genetic diversity within two populations is not significantly different from that which would result from pooling the two populations. Relative abundances of SRB, IOM, and SOM were obtained by screening the taxonomy file for prokaryotic genera (or in a few instances higher taxa when identification to the genus level was not possible) containing at least one species with the investigated metabolic trait.

2.4. Geochemical analyses

Measurements of pH were determined in pore-water samples, using an Orion Ross Ultra combination pH electrode, coupled to an Orion 3 Star pH/mV meter. Aqueous samples were filtered (0.22 μm, PVDF) and stored at 4°C prior to chemical analyses. Inductively coupled plasma-optical emission spectrometry (ICP-OES ICAP 6000, Thermo Scientific; EPA Method 6010C, 2000) and inductively coupled plasma-mass spectrometry (ICP-MS X Series II, Thermo Scientific; EPA Method 6020A, 1998) were used to determine cation concentrations (in samples preserved in HNO_3; pH < 2.0). Anions were determined by ion chromatography (Dionex IC-CO3 system; EPA Method 300.0, 1993). Aqueous samples (filtered through 0.22 μm PVDF membranes, acidified with H_2SO_4 to pH ~2.0, and stored in glass) were analyzed for dissolved organic carbon (DOC) with an Aurora 1030W TOC Analyzer (O.I Analytical - College Station,

TX), using wet oxidation with heated sodium persulfate. Inorganic carbon was removed from the sample by the instrument with the addition of 5% H_3PO_4. Levels of gaseous oxygen were determined in the field in gaseous samples collected at regular depths, using a QUANTEK 902P O_2/CO_2 analyzer. Solid-phase samples were analyzed for total carbon and total sulfur contents (ELTRA CS-2000 carbon/sulfur analyzer coupled with an induction furnace CS800).

3. Results

3.1. Overview of geochemistry data

Samples consisting of organic cover material and tailings were collected from SWWTS and have been characterized in detail within a broader initiative. Selected geochemical parameters of extracted pore-water, gaseous and solid-phase samples (corresponding to samples used for microbiological analysis) are listed in Table S1. Most samples used for microbiological analyses (Tables 1, S1) were of circum-neutral (6.4 to 7.8) or moderately acidic pH (lowest recorded pH value was ~4.8; Table S1). Dissolved sulfate concentrations ranged from 1.0 to 3.5 g L^{-1} (2.3 ± 0.6 g L^{-1}, mean ± s.d.). Total dissolved iron concentrations were low (< 5.5 mg L^{-1} in most samples, with the exception of ten samples which were all located within the historical tailings at these locations (with a maximum concentration of 51.2 mg L^{-1}). Most transition metals (e.g. Ag, Al, As, Cd, Co, Cr, Cu, Mo, Zn) were detected in mean concentrations < 2.0 mg L^{-1} except at a depth of 0.65 mbgs at ML33, where concentrations as high as 11.7 mg L^{-1} were recorded (McAlary, 2020). Only Cu, Ni and Mn were detected at elevated (> 2.0 mg L^{-1}) levels; with mean concentrations of 2.4, 10.5 and 2.5 mg L^{-1}, respectively. DOC values varied greatly across samples, ranging from 5.5 to 225 mg L^{-1}.

Total solid-phase sulfur content of the samples collected at ML33 and ML34 ranged from 0.4 in the shallow tailings, which had undergone extensive sulfide oxidation, to 1.9 wt.% in the historical tailings (Table S1). At ML5 the sulfur content ranged from 2.1 wt.% at the tailings surface to 11.6 wt.% at a depth of 4.3 m, reflecting previous deposition of a high-sulfur material within Tailings Cell 2. Total solid-phase carbon content in the tailings samples ranged from 0.05 to 0.3 wt.% (0.14 ± 0.09 wt.%, mean ± s.d.). DO data for most of the SWWTS depth profiles were not obtained. However, the available DO values, determined from measured gaseous O_2 concentrations, decreased with depth (at the ML33 and ML34 sites where more values were obtained, compared to ML5), with values ranging from 9.52 mg L^{-1} near the tailings surface to 0.05 mg L^{-1} at a depth

of 1.1 mbgs at ML5 (corresponding to gaseous O_2 concentrations decreasing from 19.7% near the tailings surface to 0.1% O_2).

3.2. Viable cell counts

Fig. 2 shows viable counts of selected metabolic groups of microorganisms at two locations with organic carbon layers in the cover system (M33 and M34) and the control site (ML5), where the cover consists of desulfurized tailings only. Variations between bacterial numbers in two duplicate cores collected at the ML33 location were negligible, and averaged values are shown in Fig. 2. Differences between the locations with covers comprising desulfurized tailings and an organic layer and the control site, with the desulfurized tailings only, were not significant; culturable neutrophilic groups of microorganisms dominated over acidophiles in all circum-neutral pH tailings samples. High numbers of nSOM (mean ~ 10^6 MPN g^{-1}, maximum of 3.3 x 10^8 MPN g^{-1}) indicated high rates of sulfur oxidation in tailings collected at all three locations. Iron-reducers were observed in greater numbers at the sites with organic carbon cover components when compared to the control site, however, the differences between the means (ML33 vs. ML5, and ML34 vs. ML5) were insignificant ($p > 0.05$). SRB enumerations indicated low abundances of sulfate reducers. Except for a complete absence of SRB in the topmost sample at ML5, numbers of SRB ranged from 2.3 x 10^1 to 4.6 x 10^2 MPN g^{-1}. However, the comparison between the SRB profiles for covered and control sites indicated that the SRB numbers increased (two orders of magnitude greater in the superficial layer of the tailings) immediately beneath the organic cover. The organic carbon present in the cover did not seem to affect the SRB population at greater depths, although greater counts of other heterotrophs were observed deeper in the tailings profiles at ML33 and ML34, compared to ML5.

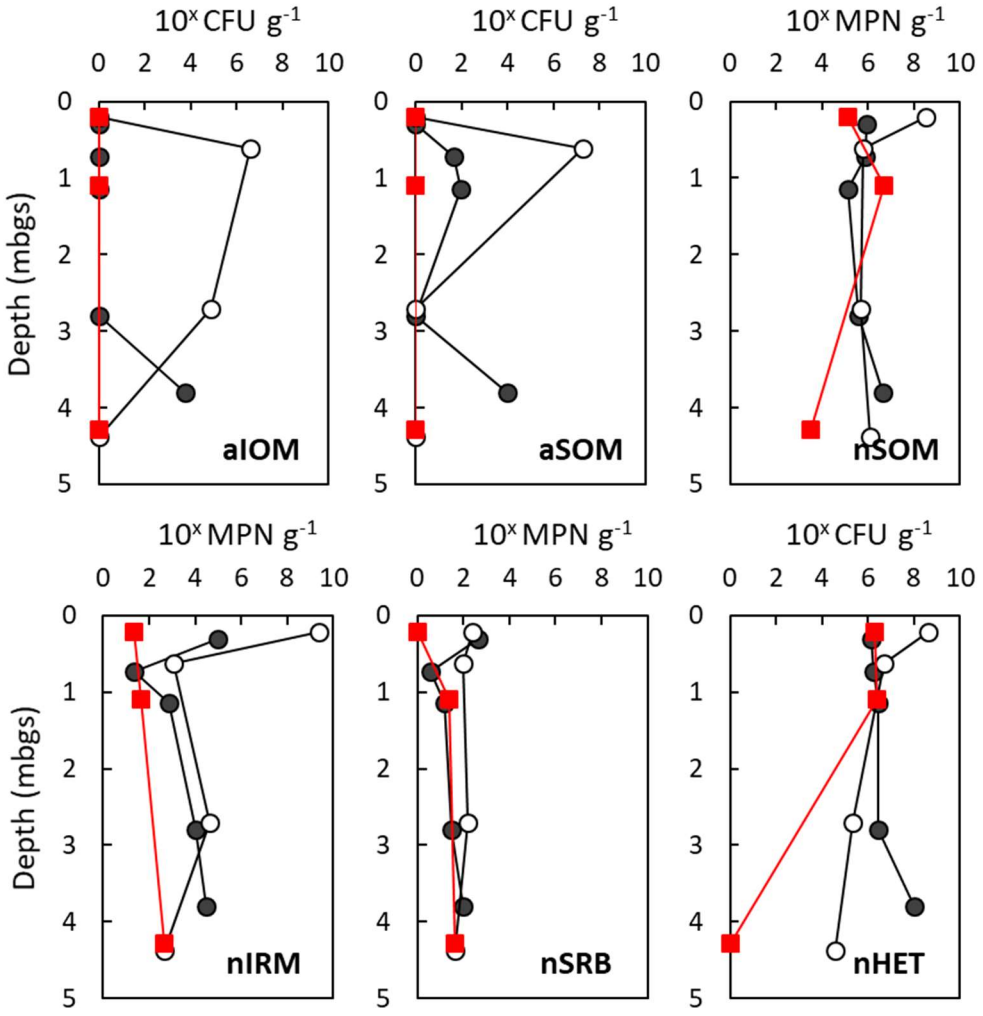

Fig. 2. Vertical profiles for microbial counts in solid-phase samples collected at SWWTS, determined by most probable number (MPN), at the (●) ML33 and (○) ML34 sites with covers including an organic carbon component, and (■) at the control site, ML5. Legend: aIOM = acidophilic iron-oxidizers, a/nSOM = acidophilic/neutrophilic sulfur-oxidizers, nIRM = neutrophilic iron-reducers, nSRB = neutrophilic sulfate-reducers, and nHET = neutrophilic heterotrophs.

3.3. 16S rRNA gene sequence data statistics

Mean values in this section refer to pooled duplicate samples sequenced in the same run. Total number of 2,205,142 raw sequences were obtained, with an average of 81,672 ± 39,906 reads per pooled sample. About 15.8% of sequences were flagged as chimeric, and another 9.4% of reads were lost to quality trimming. A total effective sequence number was 1,648,468, with 61,054 ± 32,702 reads per sample, and an average of 1,197 ± 1,118 OTUs (97% sequence similarity) per

library (Supplementary Table S2). The Good's coverage ranged from 89.3% to 99.6% (Supplementary Table S2).

3.4. Entire bacterial and archaeal populations at SWWTS

Proteobacteria were the most abundant phylum in most samples (accounting on average for 48.9% of the total amplicons), followed by *Actinobacteria* (9.7%), *Firmicutes* (6.7%), *Chloroflexi* (6.0%), *Bacteroidetes* (4.4%), and *Acidobacteria* (4.1%; Fig. 3). The phyla *Proteobacteria* and *Firmicutes* contain species known to oxidize sulfur and iron, and their abundances were slightly elevated in the ML5 samples compared to samples collected at locations with organic carbon components. However, the differences between abundances of both *Proteobacteria* and *Firmicutes* in samples from locations with and without organic carbon layers were not significant ($p > 0.05$). Mean relative proportion of unclassified bacteria was relatively low, accounting for 5.8% of total reads.

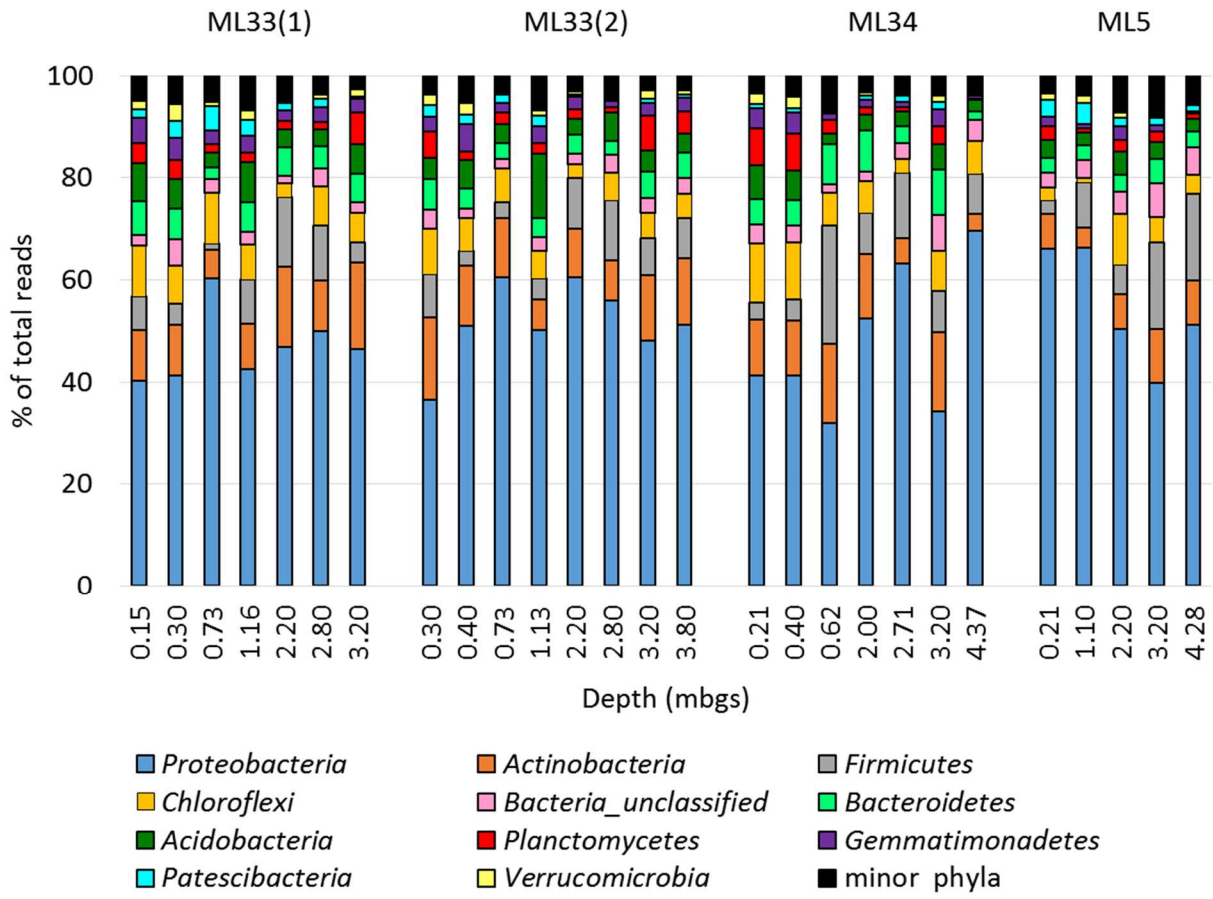

Fig. 3. Proportions of total reads of dominant major phyla (with mean relative abundance > 1% of total amplicons) at three locations (ML33 was analyzed in duplicate) at SWWTS. Minor phyla with mean relative abundance < 1% of total reads were grouped together.

Entire bacterial and archaeal communities (BACs) were also assessed on the genus level and a total 1,539 genera were detected. Major genera (or higher taxa when identification to the genus level was not possible) are shown in Supplemental Table S3. Minor genera (< 0.5% of total amplicons) were grouped together, and their sum accounted for 53.9% of total reads. Prokaryotes that were dominant in the samples use many different types of metabolic strategies and have been observed in a variety of different habitats, including plant symbionts (*Rhizobia,* 4.8%), decomposers found in soil (e.g. *Actinobacteria,* 1.7%), or human and animal pathogens (e.g. *Legionella,* 0.6%; *Clostridia,* 0.6%). *Alpha-* (3.1%), *Beta-* (6.4%) and *Gamma-proteobacteria* (5.4%) include species that are diverse in terms of their phylogenetic, ecological, and physiological properties. Among the most abundant genera were those containing species known to metabolize iron and/or sulfur (described in more detail in section 3.5. Iron- and sulfur-metabolizing genera); *Thiobacillus* (SOM) accounted for 1.3% of total reads, *Sulfurifustis* (SOM) for 0.8%, *Desulfurivibrio* (SRB) for 0.8%.

In order to determine whether presence of the organic cover affected microbial richness (number of OTUs), Chao's index was determined for two libraries representing treated and untreated samples. A pairwise comparison revealed no significant differences ($p > 0.05$) between the two values. A similar result was obtained for the Gini-Simpson's index (a metric considering OTU abundances). Fig. 4 shows an NMDS plot of weighted UniFrac comparing entire BACs (on the genus level) at different SWWTS locations. Significant differences ($p < 0.05$; AMOVA) were determined between BACs in samples collected at ML34 and ML5 (but not between ML33 and ML5). However, different results were obtained for unweighted UniFrac (data not shown); a significant difference ($p < 0.05$; AMOVA) between BACs in ML33 and ML5 samples was observed, indicating that abundance of each OTU affected the overall β-diversity.

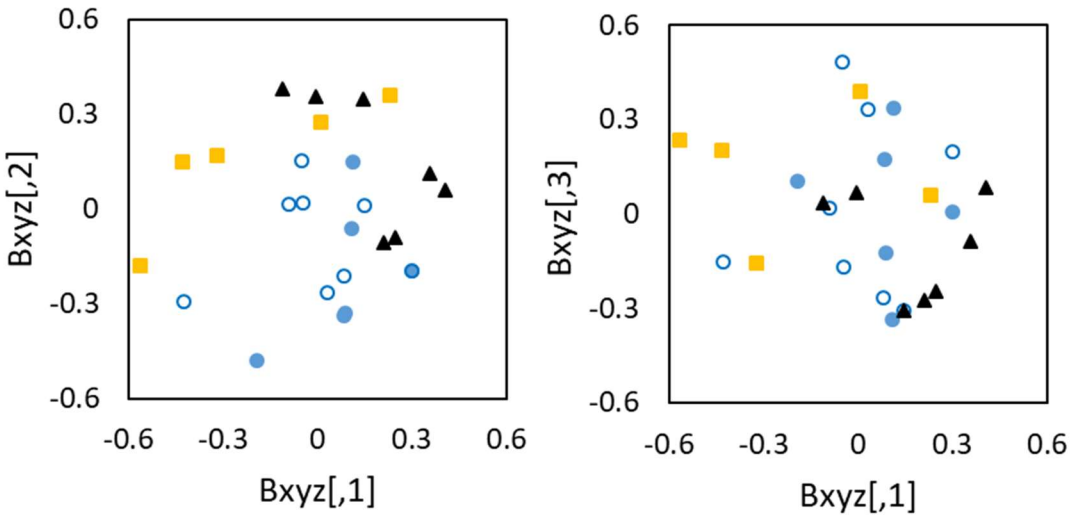

Fig. 4. Three dimensional non-metric multidimensional scaling plot (3D-NMDS, stress=0.220) of weighted UniFrac used to investigate bacterial and archaeal communities (BACs) at (●○) covered ML33 (analyzed in duplicates), (▲) covered ML34, and (■) control ML5 locations within SWWTS. The distance between any two points represents the difference between those two microbial communities.

β-diversity in layers within SWWTS vertical profile was compared using weighted UniFrac (Fig. 5). Significant differences ($p < 0.05$; AMOVA) were observed between BACs in organic cover samples and unoxidized desulfurized tailings samples, and also between BACs in organic cover and historical tailings.

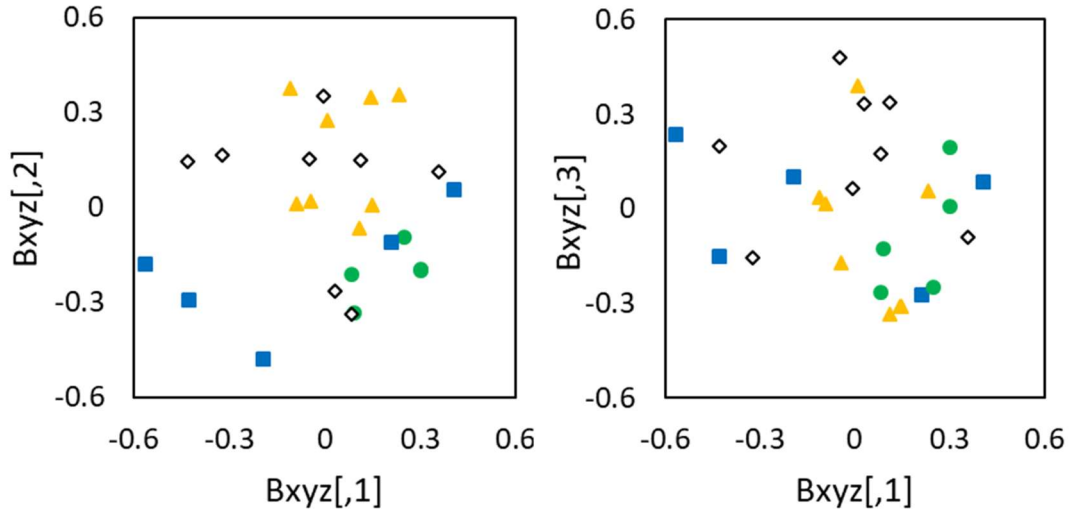

Fig. 5. 3D-NMDS plot (stress=0.220) of weighted UniFrac used to investigate BACs in (●) organic cover (OC), (■) oxidized desulfurized tailings (ODT), (◊) unoxidized desulfurized tailings (UDT), and (▲) historical tailings (HT) at SWWTS. More details about each layer can be found in Table 1.

3.5. Iron- and sulfur-metabolizing genera

Relative abundances (not considering numbers of individual genera in each sample) and physiological traits of sulfur- and/or iron-metabolizing genera detected in samples collected from SWWTS are summarized in Table 2.

Table 2. Metabolic traits of genera detected in tailings at SWWTS that are known to catalyze the dissimilatory oxido-reduction of iron and sulfur (Quatrini and Johnson, 2016). '+' indicates that at least one species of the genus has been reported to catalyze the dissimilatory reaction referred to in that column. EA=extremely acidophilic, MA=moderately acidophilic, N=neutrophilic, and A=alkaliphilic. * higher taxa that could not be identified on the genus level.

Genus	Mean % of total reads	pH preference	Sulfur oxidation	Iron oxidation	Sulfate reduction	Iron reduction[1]
Thiobacillus	1.32	N	+			
Sulfurifustis	0.81	N	+			
*Desulfuromonadales**	0.77	N			+	+
Desulfurivibrio	0.76	A			+	+
Sulfuriferula	0.37	MA (& N)	+			
*Acidimicrobiia**	0.37	EA		+		+
Acidithiobacillus	0.24	EA	+	+		+
*Desulfobulbaceae**	0.18	N			+	+
*Acidiferrobacteraceae**	0.15	EA	+	+		+
Desulfurispora	0.12	N			+	+
Dethiobacter	0.12	A			+	+
Desulfosporosinus	0.11	N & MA			+	+
*Desulfobacteraceae**	0.10	N & MA			+	+
Geobacter	0.07	N				+
*Gallionellaceae**	0.06	N (& MA)		+		
Acidibacillus	0.04	EA	+	+		+
Sulfuricurvum	0.04	N	+			

Desulfitobacterium	0.04	N & MA			+	+
Ferrovibrio	0.04	N		+		
Desulfuromonas	0.04	N			+	+
Desulfobacca	0.04	N			+	+
*Sulfuricellaceae**	0.04	N	+			
Sulfuricella	0.03	N	+			
Desulfatiglans	0.03	N			+	+
Halothiobacillus	0.03	N (& MA)	+			
Desulfotomaculum	0.02	N & A			+	+
Thiovirga	0.02	N	+			
Acidithrix	0.02	EA & MA		+		+
Ferrithrix	0.02	EA		+		+
Sulfurimonas	0.02	N	+			
Acidiphilium	0.02	EA	+			+
*Desulfobacterales**	0.02	N & MA			+	+
Desulfobulbus	0.02	N			+	+
Desulfovibrio	0.02	N & MA			+	+
Thiomonas	0.02	MA	+			
Desulfitibacter	0.01	N & A			+	+
Desulfomonile	0.01	N & MA			+	+
Acidiferrobacter	0.01	EA	+	+		+
Gallionella	0.01	N (& MA)		+		
Leptospirillum	0.01	EA		+		
Desulfatirhabdium	0.01	N			+	+
*Desulfobulbaceae**	0.01	N			+	+
*Desulfuromonadales**	0.01	N			+	+
*Halothiobacillaceae**	0.01	N (& MA)	+			
Sulfurovum	<0.01	N	+			
Dethiosulfatibacter	<0.01	N			+	+
Desulfitispora	<0.01	A			+	+
Acidicaldus	<0.01	EA	+			+
Desulfatiferula	<0.01	N			+	+
Desulfatitalea	<0.01	N			+	+
Desulfobacula	<0.01	N			+	+
Desulfococcus	<0.01	MA & N			+	+
Desulfocapsa	<0.01	N			+	+
Desulfoprunum	<0.01	N			+	+
*Desulfuromonadacea e**	<0.01	N			+	+

*Acidiferrobacteraceae**	<0.01	EA	+	+		+
Ferrovum	<0.01	EA		+		+
Sulfurisoma	<0.01	N	+			
Sulfuritalea	<0.01	N	+			
Ferritrophicum	<0.01	N (& MA)		+		
Sulfurirhabdus	<0.01	N	+			
Acidihalobacter	<0.01	EA	+	+		

[1]both direct and indirect

Similar abundances of IOM and/or SOM and SRB were observed in the duplicate samples collected at ML33 (data not shown), and therefore, means were used for further comparisons (marked with asterisks in Fig. 6). Numbers in the following paragraphs refer to weighted relative abundances (considering different numbers of genera in the samples), in contrast to numbers in Table 2. Abundances of sulfur- and/or iron-oxidizers (Fig. 6A) ranged from 0.5 to 18.3% of total reads. No significant differences ($p < 0.05$) were observed between relative abundances of IOM and/or SOM in tailings samples collected at locations with organic carbon cover components (5.5 ± 5.6% of total reads; mean ± s.d.) and ML5 (6.6 ± 4.0% of total reads). Also, the higher sulfur content in the historical Strathcona tailings compared to the desulfurized tailings did not result in significantly elevated proportions of SOM and/or IOM ($P < 0.05$), yielding 6.1 ± 6.2% of total reads (mean ± s.d.) vs. 6.7 ± 4.6% of total reads in desulfurized tailings.

SOM were far more abundant in the Strathcona tailings samples than IOM. The mean abundance of sulfur-oxidizing genera (but not iron-oxidizing) reached 4.75% of total reads in the samples (ranging from 0.1 to 16.5% of total reads), with the neutrophilic *Thiobacillus* genus identified as the most abundant SOB (mean abundance of 2.8%). Microorganisms that oxidize both sulfur and iron (SOM/IOM) accounted for 0.5% of total reads, out of which 0.3% was *Acidithiobacillus* spp. Genera that oxidize iron (but not sulfur) were detected with the mean abundance of 0.5%.

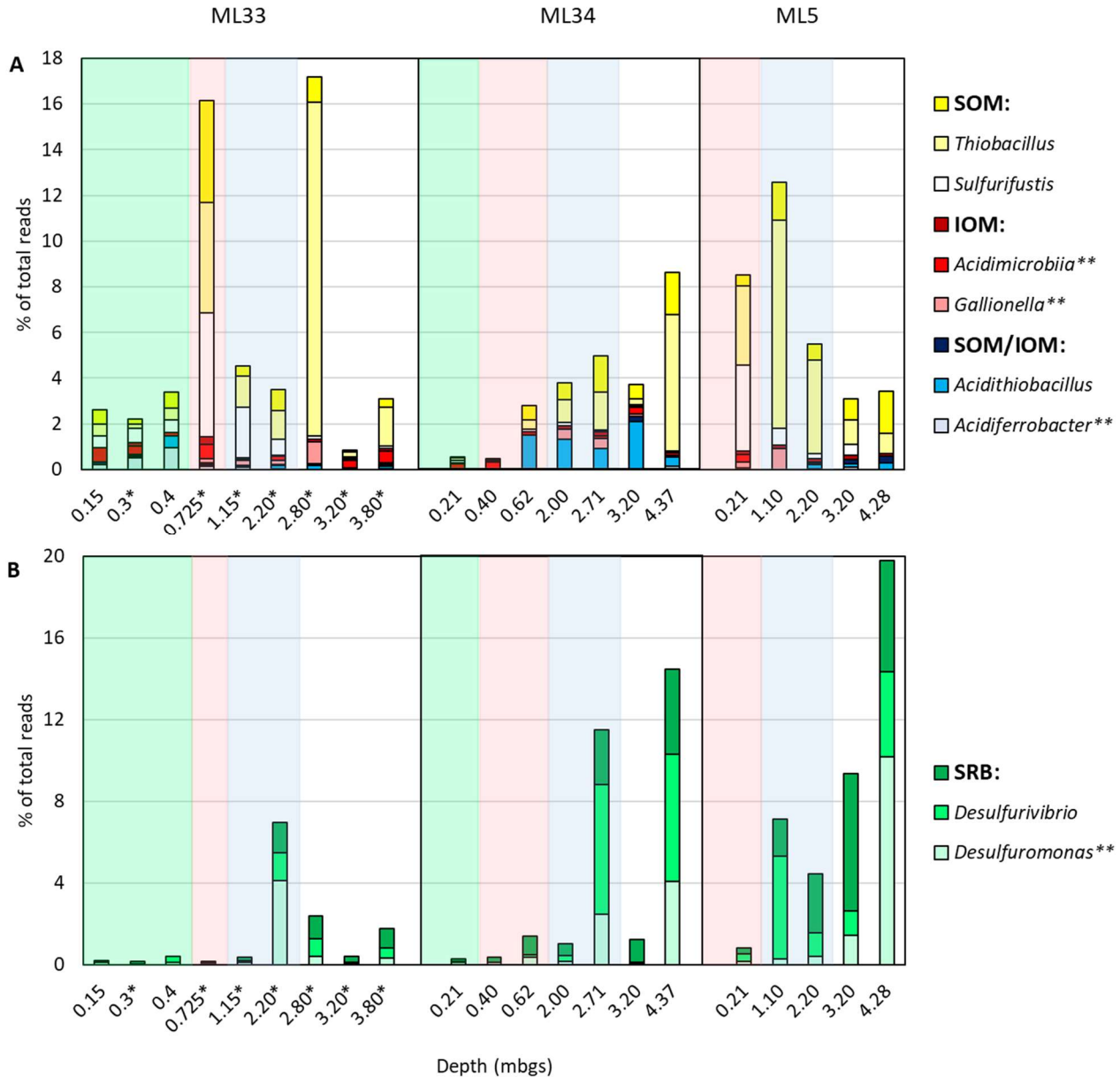

Fig. 6. Proportions of total reads of (A) sulfur- (SOM) and/or iron-oxidizers (IOM), and (B) sulfate- and/or sulfur-reducers (SRB) at three locations at SWWTS; ML33 and ML34 had been covered with an organic cover, while the untreated ML5 location served as a control site. Vertical profile layers are delineated in colored fields: organic cover (OC) in green, oxidized desulfurized tailings (ODT) in pink, unoxidized desulfurized tailings (UDT) in blue, and historical tailings (HT) in white. * averaged values. ** higher taxa that could not be identified at the genus level.

Fig. 6B shows relative abundances of sulfur- and/or sulfate-reducers in the SWWTS samples. A slightly greater relative abundance of SRB (8.3 ± 7.2% of total reads; mean ± s.d.) was observed in ML5 samples, compared to samples from the locations with organic carbon cover components (2.4 ± 3.9% of total reads). The difference was, however, insignificant ($P < 0.05$). SRB in desulfurized tailings accounted for 3.2 ± 3.8% (mean ± s.d.) and in historical tailings 5.4 ± 6.8% of total reads, difference between which was again insignificant ($P < 0.05$). The overall mean abundance of SRB constituted for 3.5% of the total reads, with *Desulfuromonas* (and higher taxa) detected as the most abundant SRB (reaching 1.1% of the total amplicons).

4. Discussion

The Strathcona impoundment was primarily constructed by depositing tailings into a portion of the former Moose Lake (now within the SWWTS). Most of the tailings initially were deposited subaqueously and remained continuously saturated, minimizing sulfide oxidation reactions in large areas of the impoundment. However, as tailings deposition progressed, parts of the impoundment became progressively elevated above the level of Moose Lake. Groundwater sampling at SWWTS in 1994, before the installation of the multi-layer cover system indicated extensive sulfide oxidation in tailings exposed on the upgradient beach at the tailings, generating high concentrations of oxidation products (up to 13 g L^{-1} Fe; 21 g L^{-1} SO_4^{2-}; 125 mg L^{-1} Ni; 1 mg L^{-1} Co, 17 mg L^{-1} Zn; and 0.8 mg L^{-1} Pb) and low pH water (< 4) (Blowes *et al.*, 1996). Between 1994 and 1996 the tailings surface was buried with 3-4 m of fresh tailings. As a means of reducing the rate of sulfide oxidation in the beached tailings areas, 2-3 m of fine-grained, high-moisture content, desulfurized and neutralized tailings were deposited over the beached tailings surfaces in 1996, after which basic pH (~7.2 to 9.5) conditions dominated the shallow layers, infiltrating through the previously exposed tailings (Bain *et al.*, 1998). The pore-water chemistry in the sulfide-rich tailings in 1996 was generally similar to that observed during 1994. At the locations where oxidation-affected pore-water was present near surface in 1994, enriched solute levels remained in 1996, except that these zones became entombed by overlying desulfurized tailings. Bain and Blowes (2013) evaluated the changes in pore-water quality that occurred at SWWTS area between 1996 and 2012, reporting that the layer of desulfurized tailings limited the ingress of oxygen to within the desulfurized tailings, therefore limiting the extent and rate of sulfide oxidation to shallow depths. Elevated concentrations of dissolved Al (25 mg L^{-1}), Co (5 mg L^{-1}), Cu (10 mg L^{-1}), Ni (184 mg L^{-1}), SO_4^{2-} (5.4 g L^{-1}) and low pH (4.25) were found at ~0.9 m depth in the

desulfurized tailings, likely caused by sulfide mineral oxidation at a time when desulfurized tailings at this depth were still exposed to the atmosphere. In the areas that had not been covered, acidic pH (3 to 4) was measured in the vadose zone, increasing to more neutral values closer to the water table. Also, high concentrations of dissolved SO_4^{2-}, Al, Co, Cu, Fe, Ni and Zn were detected in this zone due to more extensive sulfide oxidation.

Concentrations of dissolved metals in the cover system, determined in the current study, were generally low (with the exception of Mn and Ni). However, the mobility of metals (including Fe, which plays a particularly important role in mine-impacted environments) is pH-dependent, while some metals (e.g. Co, Cu and Ni) can also be limited by adsorption onto ferric oxyhydroxide and clay mineral surfaces. Despite improved pore-water quality detected in this study, dissolved SO_4^{2-} concentrations (1.0 to 3.5 g L^{-1}) and low pH values (min. ~4.8) indicated that localized sulfide oxidation occurred in the tailings since the deposition of the organic cover, although at generally low rates. Other authors have reported that the establishment of organic covers over metal-contaminated mining areas (e.g. tailings impoundments, sulfide concentrates, and contaminated soil) suppressed sulfide oxidation. Brown *et al.* (2003) reported that surface application of certain amendments including biosolids mixed with wood ash resulted in significant decreases in subsoil acidity and aqueous metal concentrations. Many studies have also demonstrated that even a single application of biosolids was sufficient to restore a plant cover to the contaminated areas (Trlica and Teshima, 2011; Brown *et al.*, 2003).

Mine wastes generally have very low soil organic matter content. The principle of organic cover application over tailings impoundments is to support plant growth, increase biodiversity, improve water holding capacity, and limit water and wind erosion to the underlying low sulfur tailings (Campbell, 2017). The organic cover also promotes heterotrophic microbial communities, whose activity facilitate the reductive physicochemical processes and changes in the mine wastes. Increased enzymatic activity in tailings as a result of a treatment with municipal waste compost and biosolids has been reported both shortly (de Vareness *et al.*, 2010; Alvarenga et a., 2008; Perez de Mora *et al.*, 2005) and several years after amendment (Touceda-Gonzales *et al.*, 2017; Zornoza *et al.*, 2012; Baker *et al.*, 2011; Perez de Mora *et al.*, 2006). Some studies detected an increase in microbial biomass (Zornoza *et al.*, 2012; Perez de Mora *et al.*, 2005,2006), or in total phospholipid fatty acid (Baker *et al.*, 2011) in mine-waste soils amended with organic matter, compared to

unamended controls. In a 3-year field study, Gardner *et al.* (2010) reported that biosolids enhanced microbial activity by increasing the numbers of total aerobic, total anaerobic, iron-reducing, sulfate-reducing and denitrifying microorganisms near the surface on an open pit Cu/Mo mine in BC, Canada. In this study, as well as in a prior report by Harris and Megharaj (2001), the total aerobic heterotroph counts declined in two years after the biosolid application. Pepper *et al.* (2012) and Seaker and Sopper (1988) observed increases in the aerobic heterotrophic bacteria population for biosolid-amended mine sites compared with those receiving chemical fertilizers. A significant increase in culturable numbers of aerobic heterotrophs due to the organic amendment application 4 to 6 years prior to sample collection was also detected in this study. No heterotrophic growth was observed in (high-sulfide) historical tailings samples collected at ~4 mbgs depth at the control site, whereas high populations (10^5 to 10^8 cells g^{-1}) were detected in samples from the sites with organic carbon cover components. The detected numbers are similar to values in undisturbed soils (1 to 34 x 10^6 cells g^{-1}; Sopper 1993).

Application of organic matter over tailings impoundments can effectively promote sulfate reduction mediated by strictly anaerobic, heterotrophic SRB (Gardner *et al.*, 2010). However, these microorganisms cannot utilize complex organic compounds and are therefore dependent on other microorganisms (e.g. fermentative bacteria) to produce short chain organic molecules. Sulfate reduction facilitates depletion of sulfate anions along with metal reduction and immobilization. Due to availability of oxygen in the surficial part of the impoundment, most organic carbon supplied to the SWWTS system seemed to be utilized by aerobes. Oxygen levels in the system decreased with depth, and subsequent measurements (Aug and Oct 2019) showed that O_2 was depleted below 1 mbgs at the control site, and between 1 and 2 mbgs at the two locations with organic carbon cover components (McAlary, 2020). The sequence data indicated a substantially higher relative abundance of SRB below historical desulfurized tailings (with maxima as high as 14.5% and 19.8% of total reads at the greatest depths at ML34 and ML5, respectively). The counts of culturable SRB, however, did not follow this trend, and stayed constant throughout the tailings vertical profile. The low numbers of culturable SRB (and to a lesser extent IRM) suggest a large proportion of SRB detected by sequencing might have been inactive. It is, however, also possible that MPN numbers were underestimated, in which case the sequence data might provide a more realistic representation. Nevertheless, the IRM cultivation data in this study were most likely

overestimated due to the capacity of many iron-metabolizing species to both oxidize and reduce iron, depending on oxygen availability.

Slow groundwater flow was previously observed in the SWWTS tailings (Blowes *et al.*, 1996); surface organic matter supply could thus sustain heterotrophic metabolism for years. Pepper at al. (2012) reported elevated counts of heterotrophs in Cu tailings 10 years after biosolids application. However, it is evident from long-term applications and field studies that organic matter used in cover designs for mine tailings remediation decomposes and may become depleted over time (Jia *et al.*, 2015), requiring re-application of the amendments in order to sustain the system. Another drawback of organic covers is the potential for dissolved organic material to act as a complexing agent for heavy metals, and thus increase concentrations of these elements of environmental concern in tailings (from where they could be mobilized) and in plant tissue (Gardner *et al.*, 2012; McBride, 2003; Sopper, 1993). Also, some bacterial strains might use organic matter to reduce Fe^{3+} to Fe^{2+} (Johnson and McGinness, 1991). Finally, insufficient hydration of the cover layers can enhance the ingress of oxygen. McAlary (2020) measured the variation in volumetric water content (saturation) in the organic cover (depths 0.2 and 0.45 mbgs) and desulfurized tailings (0.75 and 1.05 mbgs) over the 2019 field season. The desulfurized tailings maintained a higher degree of saturation than the organic cover where saturation was generally <60%. Desiccation cracks developed within the SWWTS cover systems (at both locations with and without organic cover component) during summer months of 2018 and 2019. Mbonimpa et al. (2003) reported that O_2 diffusion significantly decreases when saturation is >70%. In a laboratory experiment with municipal sewage sludge (Peppas *et al.*, 2000), the authors determined that the cover usually fails when the water content in the organic layer drops to approximately 50% v/v. Measurements of gas-phase O_2 concentrations indicate that O_2 is depleted within the desulfurized tailings component of the cover.

Oxygen availability generally supports the growth of mineral-oxidizing microorganisms. Neutrophilic SOM were more numerous in the SWWTS samples than acidophilic SOM, determined by both MPN (means ~10^2 vs. 10^6 cell g^{-1}, respectively) and high-throughput sequencing (4.4% vs. 1.3% of total reads). IOM were detected with a much lower relative abundance (0.5% of total reads). The MPN counts of acidophilic IOM could be overestimated as several sulfur-oxidizing species (e.g. *At. ferrooxidans*) also metabolize iron.

Important shifts in the entire bacterial community structure in metal-rich tailings amended with organic materials have been detected by molecular techniques. Touceda-Gonzales *et al.* (2017) reported differences between BACs in untreated and in compost-amended soils during a three-year field trial, using a DGGE analysis. Through ARDRA analyses, Perez de Mora *et al.* (2006) observed changes in structural diversity in both bacterial and fungal communities under seven different treatments (representing four different organic amendments, one inorganic treatment and two controls). Pepper *et al.* (2012) investigated 16S rRNA clone libraries obtained from community DNA in Cu mine tailings, reporting significant shifts in dominant bacterial populations 10 years after biosolid application. When entire BACs and proportions of sulfur- and iron-metabolizing genera detected in this study were compared, no consistent, significant differences were found between the sites amended with organic carbon and the control site. However, elevated numbers of heterotrophs at greater depth at locations with organic carbon layers indicate there is a potential benefit in using organic covers for mine waste remediation. However, increased amendments with the biosolids mixture (and/or their application frequency) might be considered for the Strathcona site.

5. Conclusion

The combination of subaqueous disposal of high-sulfide tailings, and covering exposed tailings with a layer of partly saturated, fine-grained, desulfurized tailings has been previously reported to reduce rates of sulfide oxidation. Addition of organic materials is an effective method for amending closed tailings storage facilities that are no longer active, while providing the nutrients to establish a vegetative cover over the impacted area. Our data indicate that the application of an organic cover consisting of a mixture of biosolids and composted municipal waste in conjunction with the desulfurized tailings layer can be beneficial for the reclamation of sulfide-rich tailings.

Acknowledgement: Funding for this research was provided by the NSERC TERRE-NET program (grant NETGP 479708-15). The authors gratefully acknowledge financial and logistical support provided by Glencore. In addition, the authors thank Robert Mellow for his assistance on this project. J. Bain, L. Groza and W.D. Gould (University of Waterloo, UW), and J. McBeth (University of Saskatchewan) provided technical assistance.

Abbreviations

(a)IOM	(acidophilic) iron-oxidizing microorganisms
(a/n)SOM	(acidophilic/neutrophilic) sulfur-oxidizing microorganisms
AMD	acid mine drainage
AMOVA	analysis of molecular variance
BAC	bacterial and archaeal community
DGGE	denaturing gradient gel electrophoresis
INO	Integrated Nickel Operations
IRM	iron-reducing microorganisms
mbgs	meters below ground surface
MPN	most probable number
NMDS	non-metric multidimensional scaling
OC	organic cover
ODT	oxidized desulfurized tailings
HT	historical tailings
OTU	operational taxonomic unit
SRB	sulfate-reducing bacteria
SWWTS	Strathcona Waste Water Treatment System
UDT	unoxidized desulfurized tailings
3D-NMDS	three dimensional non-metric multidimensional scaling

References

Alvarenga P., Palma P., Goncalves A.P., Baiao N., Fernandes R.M., de Varennes A., Vallini G., Duarte E., Cunha-Queda A.C. 2008. Assessment of chemical, biochemical and ecotoxicological aspects in a mine soil amended with sludge of either urban or industrial origin. Chemosphere 72: 1774-1781.

Alvarenga P., de Varennes A., Cunha-Queda A.C. 2013. The effect of compost treatments and a plant cover with *Agrostis tenuis* on the immobilization/mobilization of trace elements in a mine-contaminated soil. International Journal of Phytoremediation 16: 138-154.

Anawar H.M., Akter F., Solaiman Z.M., Strezov V. 2015. Biochar: An emerging panacea for remediation of soil contaminants from mining, industry and sewage wastes. Pedosphere 25: 654-665.

Antonelli P.M., Fraser L.H., Gardner W.C., Broersma K., Karakatsoulis J., Phillips M.E. 2018. Long term carbon sequestration potential of biosolids-amended copper and molybdenum mine tailings following mine site reclamation. Ecological Engineering 117: 38-49.

Bain J., Blowes D.W., Robertson W.D. 1998. 1996-1997 Groundwater Quality Strathcona (Moose Lake) Tailings Area, University of Waterloo Report presented to Joe Fyfe and Falconbridge Ltd.

Bain J., Blowes D.W. 2013 Water Chemistry at the Strathcona Waste Water Treatment System, University of Waterloo Report presented to Joe Fyfe and Xstrata Nickel.

Baker B.J., Banfield J.F. 2003. Microbial communities in acid mine drainage. FEMS Microbiology Ecology 44: 139-152.

Baker L.R., White P.M., Peirzynski G.M. 2011. Changes in microbial properties after manure, lime, and bentonite application to a heavy metal-contaminated mine waste. Applied Soil Ecology 48: 1-10.

Beak International Incorporated (BEAK). 1998. Oxygen Consumption Measurements to Monitor Oxidation Rates in Tailings at the Strathcona Tailings Impoundment. Report submitted to Falconbridge Ltd.

Blowes D.W., Robertson W.D., Hanton-Fong C.J. 1996. Groundwater Conditions in the Area of the Fecunis and Moose Lake Tailings Impoundments. Institute of Groundwater Research, University of Waterloo Report presented to Falconbridge Ltd.

Blowes D.W., Jambor J.L., Hanton-Fong C.J., Lortie L., Gould W.D. 1998. Geochemical, mineralogical and microbiological characterization of a sulphide-bearing carbonate-rich gold-mine tailings impoundment, Joutel, Quebec. Applied Geochemistry 113: 687-705.

Blowes D.W., Ptacek C.J., Jambor J.L., Weisener C.G. 2003. The geochemistry of acid mine drainage. In: Lollar B.S. (Ed.), Holland H.D., Turekian K.K. (Exec. Eds.), Treatise on Geochemistry, vol. 9, Elsevier-Pergamon, Oxford, p. 149-204.

Brown S.L., Henry C.L., Chaney R.L., Compton H., DeVolder P. 2003. Using municipal biosolids in combination with other residuals to restore metal-contaminated mining areas. Plant Soil 249: 203–215.

Campbell D., Stewart K., Spiers G., Beckett P. 2017. Growth and metal uptake of canola and sunflower along a thickness gradient of organic-rich covers over metal mine tailings. Ecological Engineering 109: 133-139.

Cochran W.G. 1950. Estimation of bacterial densities by means of the “Most Probable Number“. Biometrics 6: 105-116.

Cousins C., Penner G.H., Liu B., Beckett P., Spiers G. 2009. Organic matter degradation in paper sludge amendments over gold mine tailings. Applied Geochemistry 24: 2293-2300.

de Vareness A., Cunha-Queda C., Qu G. 2010. Amendment of an acid mine soil with compost and polyacrylate polymers enhances enzymatic activities but may change the distribution of plant pecies. Water, Air, & Soil Pollution 208: 91-100.

EcoMetrix Incorporated. 2014. Field Investigation of a Tailings Cover at the Strathcona Impoundment. Report submitted to Sudbury Integrated Nickel Operations, Glencore Company.

Gardner W.C., Broersma K., Naeth A., Chanasyk D., Jobson A. 2010. Influence of biosolids and fertilizer amendments on physical, chemical and microbiological properties of copper mine tailings. Canadian Journal of Soil Science 90: 571-583.

Gardner W.C., Naeth M.A., Broersma K., Chanasyk D.S., Jobson A.M. 2012. Influence of biosolids and fertilizer amendments on element concentrations and revegetation of copper mine tailings. Canadian Journal of Soil Science 92: 89-102.

Garthright W.E., Blodgett R.J. 2003. FDA's preferred MPN methods for Standard, large or unusual tests, with a spreadsheet. Food Microbiology 20: 439-445.

Ghosh W., Dam B. 2009. Biochemistry and molecular biology of lithotrophic sulfur oxidation by taxonomically and ecologically diverse bacteria and archaea. FEMS Microbiology Review 33: 999-1043.

Gould WD, Stitchbury M, Francis M, Lortie L, Blowes DW. 2003. An MPN method for the enumeration of iron-reducing bacteria. In Mining and the Environment III. Laurentian University, Sudbury, Ontario, Canada.

Haering K.C., Daniels W.L., Feagly S.E. 2000. Reclaiming mined lands with biosolids, manures and papermill sludges. In R. Barnhisel (Ed.), Reclamation of drastically disturbed lands (pp. 615–644). Madison: Soil Science Society of America, Inc.

Hallberg R.O., Granhagen J.R., Liljemark A. 2005. A fly ash/biosludge dry cover for the mitigation of AMD at the Falun mine. Chemie der Erde 65 SI: 43-63.

Harris M.A., Megharaj M. 2001. The effects of sludge and green manure on hydraulic conductivity and aggregation in pyritic mine tailings materials. Environmental Geology 41: 285-296.

Jia Y., Nason P., Maurice C., Alakangas L., Ohlander B. 2015. Investigation of biosolids degradation under flooded environments for use in underwater cover designs for mine tailing remediation. Environmental Science and Pollution Research 22: 10047-10057.

Johnson D.B., McGinness S. 1991. Ferric iron reduction by acidophilic heterotrophic bacteria. Applied and Environmental Microbiology 57: 207-211.

Johnson D.B. 1998. Biodiversity and ecology of acidophilic microorganisms. FEMS Microbiology Ecology 27: 307-317.

Johnson D.B., Hallberg K.B. 2007. Techniques for detecting and identifying acidophilic mineral-oxidising microorganisms. In: Rawlings D.E., Johnson D.B. (Eds.), Biomining. Springer-Verlag, Heidelberg, pp. 237–262.

Kozich J.J., Westcott S.L., Baxter N.T., Highlander S.K., Schloss P.D. 2013. Development of a dual-index sequencing strategy and curation pipeline for analyzing amplicon sequence data on the MiSeq Illumina sequencing platform. Applied and Environmental Microbiology 79: 5112-20.

MEND Project PCA-2. 1997. Subaqueous Deposition of Tailings in the Strathcona Tailings Treatment System. Prepared by Lakefield Research Limited Environmental Services (Report # 7777-111, 1996).

Lozupone C., Knight R. 2005. UniFrac: A new phylogenetic method for comparing microbial communities. Applied and Environmental Microbiology 71: 8228-8235.

Martin A.P. 2002. Phylogenetic approaches for describing and comparing thy diversity of microbial communities. Applied and Environmental Microbiology 68: 3673-3682.

Mbonimpa M, Aubertin M, Aachib M, Bussière B. 2003. Diffusion and consumption of oxygen in unsaturated cover materials. Canadian Geotechnical Journal 40: 916-932.

McBride MB. 2003. Toxic metals in sewage sludge-amended soils: has promotion of beneficial use discounted the risks? Advances in Environmental Research 8: 5-19.

McAlary M. 2020. Effectiveness of Organic Carbon Cover Systems on Sulfide-rich Tailings (Master thesis). University of Waterloo, Waterloo, ON, Canada.

Nason P., Johnson R.H., Neuschutz C., Alakangas L., Ohlander B. 2014. Alternative waste residue materials for passive in situ preventionof sulfide-mine tailings oxidation: A field evaluation. Journal of Hazardous Materials 267: 245-254.

Peppas A., Komnitsas K., Halikia I. 2000. Use of organic covers for acid mine drainage control. Minerals Engineering 13: 563-574.

Pepper I.L., Zerzghi H.G., Bengson S.A., Iker B.C., Banerjee M.J., Brooks J.P. 2012. Bacterial populations within copper mine tailings: Long-term effects of amendment with Class A biosolids. Journal of Applied Microbiology 113: 569-577.

Perez-de-Mora A., Ortega-Calvo J.J., Cabrera F., Madejon E. 2005. Changes in enzyme activities and microbial biomass after ‘‘in situ’’ remediation of a heavy metal-contaminated soil. Applied Soil Ecology 28: 125-137.

Perez-de-Mora A., Burgos P., Majedon E., Cabrera F., Jaeckel P., Schloter M. 2006. Microbial community structure and function in a soil contaminated by heavy metals: Effects of plant growth and different amendments. Soil Biology & Biochemistry 38: 327-341.

Quatrini R., Johnson D.B. (eds.). 2016. Acidophiles: Life in Extremely Acidic Environments. Caistor Academic Press, Haverhill, UK, pp. 310.

Schloss P.D., Westcott S.L., Ryabin R., Hall J.R., Hartmann M., Hollister E.B., Lesniewski R.A., Oakley B.B., Parks D.H., Robinson C.J., Sahl J.W., Stres B., Thallinger G.G., Van Horn D.J., Weber C.F. 2009. Introducing mothur: Open-source, platform-independent, community-supported software for describing and comparing microbial communities. *Applied and Environmental Microbiology 75:* 7537-7541.

Seaker M., Sopper W.E. 1988. Municipal sludge for minespoil reclamation: I. Effects on Microbial Populations and Activity. Journal of Environmental Quality 17: 591-597.

Shu W.S., Xia H.P., Zhang Z.Q., Lan C.Y., Wong M.H. 2006. Use of Vetiver and three other grasses for revegetation of Pb/Zn mine tailings: Field experiment. International Journal of Phytoremediation 4: 47-57.

Sopper W.E. 1993. Municipal Sludge use in Land Reclamation. Lewis Publishers, Boca Raton, FL, pp. 163.

Starr R.C., Ingleton R.A. 1992. A new method for collecting core samples without a drill rig. Groundwater Monitoring & Remediation 12: 91-95.

Stookey L.L. 1970. Ferrozine – a new spectrophotometric reagent for iron. Analytical Chemistry 42: 779–781.

Tisch B., Hargreaves J., Beckett P., Lock A., Spiers G. 2008. Post-mining agriculture for biofuels on mine tailings: an overview of results from the Green Mines Green Energy (GMGE) initiative. 32nd Annual British Columbia Mine Reclamation Symposium. Kamloops, BC, Canada. Sept 15-18.

Touceda-Gonzalez M., Alvarez-Lopez V., Prieto-Fernandez A., Rodriguez-Garrido B., Trasar-Cepeda C., Mench M., Puschenreiter M., Quintela-Sabaris C., Macias-Garcia F., Kidd P.S. 2017. Aided phytostabilisation reduces metal toxicity, improves soil fertility and enhances microbial activity in Cu-rich mine tailings. Journal of Environmental Management 186: 301-313.

Trlica A., Teshima M. 2011. Assessing soil carbon storage and climate change mitigation in biosolids mine reclamation projects. In: Fourie A., Tibbett M (Eds.), Post-closure Monitoring and Responsibilities, vol. 2, proceedings of the 6th International Mine Closure Conference, Sept 18-21, Lake Louise, Alberta, Canada.

Walters W., Hyde E.R., Berg-Lyons D., Ackermann G., Humphrey G., Parada A., Gilbert J.A., Jansson J.K., Caporaso J.G., Fuhrman J.A., Apprill A., Knight R. 2015. Improved bacterial 16S rRNA gene (V4 and V4-5) and fungal internal transcribed spacer marker gene primers for microbial community surveys. mSystems 1: 1-10.

Zornoza R., Faz A., Carmona D.M., Kabas S., Martinez-Martinez S., Acosta J.A. 2012. Plant cover and soil biochemical properties in a mine tailing pond five years after application of marble wastes and organic amendments. Pedosphere 22: 22–32.

1. Supplementary materials

Table S1. Selected physicochemical characteristics of samples collected at SWWTS that were used for microbiological analysis, determined in pore-water, gaseous (*) or solid-phase samples (**). Legend: mbgs = m below ground surface, DO = dissolved oxygen, DOC = dissolved organic carbon, OC = organic cover, ODT = oxidized desulfurized tailings, UDT= unoxidized desulfurized tailings, and HT = historical tailings.

Site	Sample	Depth (mbgs)	pH	S^{2-} (wt.%)	Fe (mg L^{-1})	SO_4^{2-} (g L^{-1})	DOC (mg L^{-1})	DO*$^{\Delta}$ (mg L^{-1})	S** (wt.%)	C** (wt.%)
	OC	0.15	n.a.	n.a.	n.a.	n.a.	n.a.	8.68 (8.77)	n.a.	n.a.
	OC	0.3	6.39	n.a.	0.80	2.50	68.1	8.55 (8.55)	n.a.	n.a.
	OC	0.4	6.39	n.a.	0.80	2.50	68.1	8.55 (8.33)	n.a.	n.a.
	ODT	0.73	4.78	0.22	1.20	3.51	41.4	8.20 (7.03)	0.73	0.18
ML33	UDT	1.13	7.34	n.a.	0.13	2.42	28.1	7.05 (n.a.)	n.a.	n.a
	UDT	2.2	7.79	0.36	0.25	3.02	100.5	n.a.	0.45	0.06
	HT	2.8	n.a.	1.80	n.a.	n.a.	n.a.	n.a.	1.94	0.16
	HT	3.2	n.a.	1.80	n.a.	n.a.	n.a.	n.a.	1.94	0.16
	HT	3.8	n.a.	0.22	n.a.	n.a.	n.a.	n.a.	0.37	0.31
	OC	0.21	n.a.	n.a.	n.a.	n.a.	n.a.	8.60 (9.52)	n.a.	n.a.
	ODT	0.4	n.a.	0.03	n.a.	n.a.	n.a.	7.58 (6.33)	1.32	0.13
	ODT	0.62	7.59	0.03	0.29	2.49	n.a.	5.33 (2.16)	1.32	0.13
ML34	UDT	2	n.a.	0.09	n.a.	n.a.	n.a.	n.a.	0.65	0.11
	UDT	2.71	7.67	0.89	1.26	1.84	n.a.	n.a.	1.03	0.05
	HT	3.2	7.35	0.14	44.3	1.83	154.5	n.a.	0.46	0.32
	HT	4.37	n.a.	n.a.	n.a.	n.a.	n.a.	n.a.	n.a.	n.a.
	ODT	0.21	7.58	n.a.	0.08	1.83	28.2	7.01 (4.82)	n.a.	n.a.
	UDT	1.1	7.55	n.a.	0.04	1.83	8.5	0.44 (0.05)	n.a.	n.a.
ML5	UDT	2.2	n.a.	1.51	n.a.	n.a.	n.a.	n.a	2.12	0.07
	HT	3.2	n.a.	5.25	n.a.	n.a.	n.a.	n.a	5.49	0.05
	HT	4.28	7.18	11.94	0.23	1.71	n.a.	n.a	11.55	0.06

$^{\Delta}$ values refer to DO in samples collected in August 2019 (and in October 2019).

Table S2. Total numbers of raw and effective sequences, OTU (operational taxonomic unit) counts, and Good's coverage in SWWTS samples. Legend: mbgs = m below ground surface.

Site	Sample	Depth (mbgs)	Total raw sequences	Effective sequences for analysis	OTU counts	Good's coverage
ML33(1)	OC	0.15	47,157	34,148	792	0.988
	OC	0.30	71,352	44,294	1,877	0.945
	ODT	0.73	137,770	112,781	467	0.987
	UDT	1.16	75,696	55,569	915	0.980
	UDT	2.20	42,717	35,055	349	0.994
	OT	2.80	127,299	108,952	294	0.990
	OT	3.20	37,969	23,480	3,477	0.903
ML33(2)	OC	0.30	50,248	32,728	3,005	0.913
	OC	0.40	57,898	41,683	571	0.989
	ODT	0.73	132,296	86,813	555	0.986
	UDT	1.13	49,872	36,547	550	0.986
	UDT	2.20	148,666	112,225	580	0.982
	OT	2.80	141,356	121,883	165	0.996
	OT	3.20	53,096	32,483	3,528	0.893
	OT	3.80	47,363	29,634	2,725	0.915
ML34	OC	0.21	30,031	19,207	3,210	0.914
	ODT	0.40	31,499	21,949	2,958	0.924
	ODT	0.62	33,307	25,526	736	0.989
	UDT	2.00	57,771	45,142	523	0.991
	UDT	2.71	111,519	86,245	477	0.985
	OT	3.20	83,753	64,048	923	0.971
	OT	4.37	121,276	92,736	523	0.984
ML5	ODT	0.21	148,935	99,895	879	0.972
	UDT	1.10	85,174	66,014	341	0.992
	UDT	2.20	89,465	68,105	891	0.972
	OT	3.20	77,274	57,009	659	0.983
	OT	4.28	114,383	94,317	342	0.991

Table S3. Mean proportions of total reads of major bacterial genera (mean relative abundance > 0.5% of total amplicons), and sum of minor genera (< 0.5%) determined in SWWTS samples. * higher taxa that could not be identified on the genus level.

Genus	Mean % of total reads				
	all locations	ML33(1)	ML33(2)	ML34	ML5
minor genera	53.9	66.8	60.0	67.6	58.7
*Betaproteobacteriales**	6.36	3.61	6.99	4.52	10.1
*Bacteria**	5.75	2.55	2.77	3.57	4.56
*Gammaproteobacteria**	5.37	3.35	4.06	2.59	3.23
*Rhizobiales**	4.25	1.53	2.14	1.00	0.46
*Alphaproteobacteria**	3.05	1.53	1.72	1.70	0.91
Subgroup_6_ge	1.67	2.41	2.60	1.47	1.14
Thiobacillus	1.32	3.10	3.21	1.35	3.72
*Burkholderiaceae**	1.25	0.80	1.40	2.58	1.87
*Proteobacteria**	1.21	0.36	0.57	0.69	0.99
*Actinobacteria**	1.70	0.74	0.99	1.11	0.56
uncultured	1.08	1.84	1.49	0.78	0.71
*Xanthobacteraceae**	0.98	0.88	0.82	0.80	0.33
*Micrococcales**	0.95	0.39	0.56	0.44	0.32
*Sphingomonadaceae**	0.84	0.57	0.39	0.68	0.63
Sulfurifustis	0.81	1.68	0.77	0.08	1.04
*Desulfuromonadales**	0.77	0.39	0.67	0.84	2.30
Desulfurivibrio	0.76	0.26	0.46	1.87	2.37
*Deltaproteobacteria**	0.72	0.14	0.30	0.42	1.16
*Microbacteriaceae**	0.69	0.54	0.90	0.45	0.30
*Bacillales**	0.67	0.36	0.63	0.48	0.17
*Parcubacteria**	0.65	0.89	0.41	0.23	0.77
A4b_ge	0.64	0.80	0.61	0.61	0.14
*Hydrogenophilaceae**	0.64	0.85	1.27	0.50	1.39
Legionella	0.61	0.62	1.03	0.71	0.62
*Bacillaceae**	0.61	0.58	0.70	0.44	0.17
*Rhizobiaceae**	0.59	0.55	0.72	0.52	0.34
*Chloroflexi**	0.56	0.37	0.24	0.39	0.17
KD4-96_ge	0.55	0.86	0.67	0.81	0.51
*Pirellulaceae**	0.52	0.17	0.29	0.29	0.10
uncultured	0.52	0.42	0.62	0.54	0.26